

Descent into the Cryogenian: secular
trends in seawater chemistry offer insights
into pre-Sturtian paleoenvironments

Thesis submitted in accordance with the requirements of the University of Adelaide for an
Honours Degree in Geology

Caleb Michael Brian Bishop
November 2018

Word Count: 7843



Descent into the Cryogenian; secular trends in seawater chemistry offer insights into pre-Sturtian paleoenvironments.

ABSTRACT

The Tonian was a remarkable period in Earth's history, experiencing dramatic changes in the Earth system that resulted in a series of global climatic catastrophes, ultimately leading to marked changes in the biosphere. The break-up of the supercontinent Rodinia is thought to have had a profound impact on the Earth system during the Tonian, ultimately resulting in the ~58 million-year deep freeze of the Sturtian glaciation. Increased continental margins and the weathering of vast continental flood basalts, promoting high levels of primary productivity, were large players in the drawdown of atmospheric CO₂, the chemical implications of which resonate through Tonian ocean chemistry.

The laterally extensive Skillogalee and Myrtle Springs Formations, within the Burra Group sediments of South Australia, span a pre-Sturtian carbonate succession that offer further insights into late Tonian paleo-environments. High resolution geochemical trends throughout the Skillogalee and Myrtle Springs Formations display evidence of a shift from a restricted to a more open marine setting, that was met with a flux of hydrothermally influenced waters. A hydrothermal flux through underlying basalts likely accounts for the enigmatic widespread deposition of sedimentary magnesites throughout the Skillogalee Formation. The longevity and regional reproducibility of significant europium anomalies suggests that a mafic mantle flux endured throughout Burra Group sedimentation. Cerium anomalies, supported by Zn/Fe ratios, evince open marine seawaters were largely dysoxic throughout the late Tonian, constraining Neoproterozoic oxygenation to post-Sturtian. Neodymium isotopes in Burra Group marine waters display a rise towards primitive endmembers, reflecting a mafic weathering flux, induced, no doubt, by the break-up of Rodinia. High levels of organic carbon burial are coupled

with pronounced mafic weathering, detailing a mass drawdown of CO₂ throughout Burra Group sedimentation during the late Tonian, hereby also holding important ramifications for the instatement of the Cryogenian glaciations.

1 TABLE OF CONTENTS

<i>Abstract</i>	<i>i</i>
<i>Introduction</i>	1
Background to ocean redox proxies.....	3
Background to the use of REY in carbonates.....	4
Regional geology.....	6
<i>Methods</i>	8
Carbonate sample collection.....	8
Carbonate sample powder preparation.....	8
Carbon isotope analytical procedure	8
Carbonate leaching analytical procedure.....	9
Solution ICP sample preparation	9
X-ray diffraction (XRD) preparation	9
Sr isotope analytical procedure	10
Sm-Nd analytical procedure.....	10
<i>Results</i>	12
Carbonate Element Concentrations	12
Carbon Isotopes and Organic Carbon Burial	13
Strontium isotopes	17
Samarium-Neodymium Isotopes	19
<i>Discussion</i>	20
Chemostratigraphy	20
Chemostratigraphy of the Skillogalee Formation – Termination Hill	20
Chemostratigraphy of the Gammon Ranges	21
Chemostratigraphy of the Willouran Ranges – Copley.....	23
Sedimentology.....	25
Magnesite Facies.....	25
Dolomitic Facies.....	27
Facies Distribution.....	29
Paleo-Redox Proxies.....	31
Paleo-redox of the Skillogalee Formation	31
A Late Tonian Paleo-Redox Model	35
REY interpretation for the Burra Group’s marine setting.....	36
Marine setting of the Skillogalee Formation	36
Marine Setting of the Myrtle Springs Formation - Copley.....	39
Implications of a hydrothermal flux through Burra Group marine waters.....	40
Overwhelming influence of rifting on marine waters	42
Global and Local Variations in Organic Carbon Burial.....	44
<i>Conclusion</i>	45
<i>Appendix</i>	47

References.....	87
------------------------	-----------

LIST OF FIGURES AND TABLES

Figure 1: Northern Adelaide Rift Complex sediments distribution.....	7
Figure 2: Chemostratigraphy of the Skillogalee Formation at Termination Hill S.A.....	20
Figure 3: Chemostratigraphy of the Skillogalee Formation in the Gammon Ranges S.A.....	23
Figure 4: $\delta^{13}\text{C}$ as a function of stratigraphic position for the Myrtle Springs Formation at Copley, S.A.....	24
Figure 5: Magnesite facies sedimentary features.....	26
Figure 6: Dolomite facies sedimentary features.....	28
Figure 7: Stratigraphic profiles of the Skillogalee Formation at Termination Hill (Willouran Ranges) and the Gammon Ranges, and the Myrtle Springs Formation at Copley, S.A.....	30
Figure 8: $\delta^{13}\text{C}$, Ce/Ce* and Zn/Fe molar ratios for Willouran Ranges' Termination Hill Skillogalee carbonates, and Gammon Ranges Skillogalee carbonates.....	33
Figure 9: $\delta^{13}\text{C}$, Ce/Ce* and Zn/Fe molar ratios for Willouran Ranges Myrtle Springs Formation at Copley.....	34
Figure 10: left; cross plot of Ce/Ce* and Pr/Pr* data. Right; KDE index for Ce/Ce* Pr/Pr* cross plot data.....	35
Figure 11: Rare earth element trends through the Skillogalee Formation.....	37
Figure 12: Rare earth element trends through the Myrtle Springs Formation.....	40
Figure 13: Relative abundance of Large Igneous Province abundances through time.....	41
Figure 14: εNd throughout Termination Hill Skillogalee carbonates and the global mudstones	43
Figure 15: Organic carbon burial (f_{org}) for Burra Group sediments.....	45
Table 1: Summary of $\delta^{13}\text{C}$, $\delta^{18}\text{O}$ and f_{org} data for the Skillogalee Formation.....	13
Table 2: Summary of $\delta^{13}\text{C}$, $\delta^{18}\text{O}$ and f_{org} data for the Myrtle Springs Formation in the Willouran Ranges, Copley, S.A.....	17
Table 3: Summary of new $^{87}\text{Sr}/^{86}\text{Sr}$ results for the Skillogalee Formation.....	18
Table 4: Summary of Sm-Nd isotope data founded in this study.....	19

1 INTRODUCTION

The Cryogenian was a time that displayed marked changes in paleo-environments and global seawater chemistry. Rigorous isotopic constraints link secular changes in marine chemistry to major tectonic and paleoclimatic events (Kaufman & Knoll, 1995). The Tonian shows numerous pronounced global isotopic shifts, with a notable rise in $^{87}\text{Sr}/^{86}\text{Sr}$ isotopic ratios, concurrent with a global increase in εNd values observed throughout multiple basins in Australia and South China (Barovich & Foden, 2000; Cox et al., 2016; Rooney et al., 2014; Turner, Foden, Sandiford, & Bruce, 1993; Wade et al., 2005). Isotopic trends also provide a biogeochemical framework for our comprehension of the emergence and radiation of eukaryotic primary producers, stratigraphically associated, perhaps causally, with a global increase in organic carbon burial (f_{org}) and concomitant rise of O_2 (Kaufman & Knoll, 1995). Global tectonic implications, associated with the break-up of the supercontinent Rodinia, were followed by a ~58 million-year deep freeze; the so called “Snowball Earth” hypothesis (Cox et al., 2016; Hoffman et al., 2017; Hoffman, Kaufman, Halverson, & Schrag, 1998; Kirschvink, 1992). These events impeded on a plethora of chemical cycles and global ocean chemistry, orchestrating marked changes in the global Earth system.

Throughout the Late Proterozoic, intracratonic and marginal cratonic syn-rift sediments were deposited through much of Central Australia (Powell, Preiss, Gatehouse, Krapez, & Li, 1994; Preiss & Forbes, 1981; Preiss, 2000). In particular, the Adelaide Rift Complex of South Australia hosts a suite of Neoproterozoic to Cambrian rift basin sediments, recording evidence of at least five major rift cycles, associated with the breakup of the Rodinian supercontinent (Preiss, 2000). Discord exists surrounding the finer details of the tectonic and paleogeographic evolution of the Adelaide Rift Complex, particularly towards the Burra Group sediments. The Skillogalee and Myrtle Springs Formations are widespread, stromatolitic carbonate units within the Burra Group,

with the Skillogalee in particular noted for its laterally persistent sedimentary intraclastic magnesite beds. Previous interpretations owe this phenomena to the presence of marginal alkaline lagoons, in a setting analogous to the modern Coorong lakes of South Australia (Borch & Lock, 1979), and the ascribed cyclicity to minor marine transgressive-regressive flooding events. Earlier interpretation rendered the Burra Group as non-marine, suggesting a large inland sea, or a playalacustrine setting (Murrell, 1977; Uppill, 1980; Von der Borch, 1980). The specifics of the Burra Group's facies development and associated paleogeographic setting, are pertinent to the overall tectonostratigraphic interpretation of the Adelaide Rift Complex (Belperio, 1990).

Primary marine carbonates document the chemical conditions of their marine environment, preserving an archive of geochemical signatures (Schier, Bau, Münker, Beukes, & Viehmann, 2018). Rare earth element and Yttrium (REY) data from ancient carbonates serve as good tracers of water mass mixing on a local scale, and secular evolution of seawater chemistry on a global scale (Nothdurft, Webb, & Kamber, 2004). The Skillogalee and Myrtle Springs Formations' carbonate geochemical records track secular changes in seawater chemistry through time. Here we use trace metal and rare earth element abundances together with carbon, strontium and neodymium isotopes to constrain the evolution of the Burra Group marine environments, offering a more open marine interpretation with a hydrothermal source accounting for the widespread deposition of sedimentary magnesite. In addition, Burra Group carbonates couple primitive neodymium isotopes with high levels of organic carbon burial (f_{org}), detailing two large players that contributed to the mass drawdown of CO₂ during the late Tonian.

The Neoproterozoic displays marked enrichments in atmospheric oxygen, although the relative timing, magnitude and continuity remain uncertain (Lyons, Reinhard, & Planavsky, 2014). A variety of opinion revolves around the timing of Neoproterozoic oxygenation. Chromium

isotope ratios in shales suggest ages as early as ca. 800 Ma (Cole et al., 2016), whilst a distinct rise in the concentration of phosphorus in fine-grained sediments offers an age of post ca. 720 Ma (Reinhard et al., 2016). Later dates, such as an Ediacaran age of ca. 580 Ma have been proposed based on marked enrichments in Mo concentrations in black shales (Scott et al., 2008), whilst large iron speciation and concomitant rise of eukaryotes argues for minor Ediacaran oxygenation, followed by significant oxygenation in the Ordovician (Canfield, Poulton, & Narbonne, 2007; Lenton, Boyle, Poulton, Shields-Zhou, & Butterfield, 2014). Using REY and trace metal abundances, the Burra Group offers insights into the onset of early Neoproterozoic oxygenation, constraining paleo-redox to dysoxic conditions.

Rigorous paleoenvironmental constraints on the Skillogalee and Myrtle Springs Formation's marine settings imply phases of communication with open water environments. Late Tonian paleoenvironmental interpretation may therefore be extended to regional, or perhaps even global, contexts.

1.1 Background to ocean redox proxies

Rare earth elements plus yttrium (REY), provide valuable insights into the nature of marine-carbonate hosted environments including the redox state, marine setting, and relative inputs from any reducing hydrothermal fluids (Tostevin et al., 2016). Redox sensitive Ce is unique to REY in that oxic conditions result in the oxidation of Ce from Ce^{3+} to Ce^{4+} and subsequent binding of Ce^{4+} to insoluble Fe-Mn oxyhydroxides (German & Elderfield, 1990; Nakada, Takahashi, & Tanimizu, 2013), resulting in a preferential loss of Ce from the water column. An oxygenated water body thus produces a negative (<1) Ce anomaly (Ce/Ce^*). There are limitations to this redox proxy with Ce/Ce^* showing values that trend towards 1 with closer proximity to

marginal marine settings, approaching shale normalised REY distribution patterns that reflect flatter “continental like” trends due to the concentrated influence of aeolian input (Elderfield, Upstill-Goddard, & Sholkovitz, 1990). Increased productivity in shallow marine environments also drives Ce anomalies towards more positive values (Dilek & Furnes, 2013; Elderfield et al., 1990; German & Elderfield, 1990; Tostevin et al., 2016). Ce/Ce* greater than 1.05 and less than 0.95 confidently distinguish anoxic from oxic water bodies in carbonate successions (Holser, 1997; Shields, Stille, Brasier, & Atudorei, 1997).

Zn/Fe relationships have also been used to constrain surface redox evolution through time, with Fe²⁺ precipitating out of the water column when oxidised to Fe³⁺, whilst Zn remains in its soluble divalent state and thus is incorporated into carbonates (Liu et al., 2014). Large Zn/Fe ratios, therefore, infer greater free oxygen content throughout a water body. For implications on the use of Ce/Ce* and Zn/Fe ratios, see appendix.

1.2 Background to the use of REY in carbonates

The distribution of rare earth element and Yttrium (REY) patterns present diagnostic trends that hint at the relative flux contributions from mantle, riverine and aeolian sources in a waterbody, herein providing insights towards marine setting (Lawrence & Kamber, 2006; Tostevin et al., 2016). Yttrium (Y) is commonly included alongside the REEs as it contains a similar valence charge and ionic radii to Holmium (Ho) (Tostevin et al., 2016). REY are supplied to the ocean through hydrothermal, aeolian sources and through sediment in river discharge (Byrne & Kim, 1990; Douville et al., 1999; Elderfield et al., 1990). REY’s chemical properties are extremely alike, and therefore behave coherently, producing smooth, predictable distributions when normalised to post Archean Australian Shale (PAAS), given as an average composition for the upper crust

(Pourmand, Dauphas, & Ireland, 2012). Riverine waters and nearshore environments, carry flatter, more enriched “continental type” REE shale normalised patterns, though marginal marine settings also display mild enrichments in heavy rare earth elements (HREE) (Elderfield et al., 1990; Tostevin et al., 2016). Open seawater displays an enrichment of HREEs to light rare earth elements (LREEs), reflecting competition between solution and surface complexation reactions. In seawater, preferential adsorption of LREEs onto organic surfaces, as well as onto a number of inorganic surface types, results in a HREE enrichment in the residual pool (Byrne & Kim, 1990). Complexation of REEs by mono and di-carbonate ions in solution are an important implication for REY distribution patterns, preferentially stabilising HREEs in solution and consequently yielding REE patterns that approach PAAS normalised seawater (Byrne & Kim, 1990; Koeppenkastrop & De Carlo, 1992; Koeppenkastrop & De Carlo, 1993; Quinn, Byrne, & Schijf, 2004).

Fluids with a large contribution of hydrothermal input display flat or HREE depleted REY patterns, with large positive europium anomalies (Eu/Eu^*). Eu is redox sensitive and (partially) reduces in high temperature ($>250^\circ\text{C}$) conditions (Douville et al., 1999). Reducing high temperature hydrothermal fluids, therefore, promote the decoupling of Eu^{2+} into solution, that upon entering a waterbody, provide a net enrichment in Eu. Chemical input from a hydrothermal fluid reservoir can therefore be detected by a positive anomaly in stromatolitic and authigenic carbonates (Bau & Dulski, 1996; Douville et al., 1999).

The mass ratio of Y to Ho (Y anomalies) is also a useful indicator of marine setting, with large Y anomalies (40-80) typical of open marine seawater-type settings, and smaller Y anomalies (33-40) typical of marginal marine or restricted settings (Bau & Dulski, 1996; Bau, Möller, & Dulski, 1997; H. J. De Baar, Bacon, Brewer, & Bruland, 1985; H. J. W. De Baar, Brewer, & Bacon, 1985).

1.3 Regional geology

The Adelaide Rift Complex (ARC) is composed of extensive, deeply subsided sedimentary successions hosting Neoproterozoic to Early Cambrian sediments (Jenkins, 1990) documenting evidence of at least five major rift cycles, associated with the breakup of the Neoproterozoic Rodinian supercontinent (Preiss, 2000). Northern exposures throughout the ARC incorporate a wide range of Neoproterozoic rift-related successions. In order of decreasing age, Callana Group sediments are composed of basal quartzites, overlain by dolomitic marbles and evaporites, with additional input from basalts, rhyolites and tuffs (Preiss, 1987). The lower to middle Burra Group contains interbedded sands, silts and carbonaceous dolomite and magnesite, whilst the upper Burra group reflects a transgressive sea-level rise hosting silty dolomites, quartzites and fine-grained shales (Paul et al., 1999). Sturtian glacial sediments of the lower Umberatana Group predominantly consist of glaciomarine diamictite, laminated siltstone, quartzite and minor turbiditic sequences, (Preiss, 1987). As a result of pronounced glaciation, the base of the Umberatana group (Fitton Formation) marks an erosional surface with underlying Adelaidean sequences.

Early Willouran rift phases are expressed through mafic basalt deposits; most notably the Wooltana basalts in the Arkaroola Subgroup (Preiss, 2000). The Emeroo Subgroup, at the base of the Burra Group, documents evidence of mostly mafic volcanism (Parker, Cowley, & Thomson, 1990) with basalts interbedded with the Rhynie Sandstone, associated with the final gasps of Willouran rift-related eruption. Burra Group sediments were deposited over an area greater than the underlying Callana Group sediments, suggestive of a widening rift zone throughout the late Tonian (Preiss, 2000). The Burra Group's Skillogalee and Myrtle Springs Formations are carbonate-dominated sequences, with the Skillogalee characterised by sedimentary magnesites

occurring predominantly as beds of reworked intraclasts. By analogy with the Coorong in South Australia, current explanations suggest a nearby lagoonal environment produced the sedimentary magnesites, that were reworked and deposited through repeated flooding events, induced by minor relative sea-level changes. Sediments directly overlying the Skillogalee Formation reflect more open marine character, inferring a relative sea-level rise between the Emeroo and Myrtle Springs deposits. The dolomite horizons throughout all three sections are laterally continuous and display striking non-recessive weathering horizons. Burra Group carbonates were sampled across both eastern and western provinces of the Adelaide rift complex; sites specifically at Termination Hill, Gammon Ranges and the Willouran Ranges exposure at Copley, S.A.

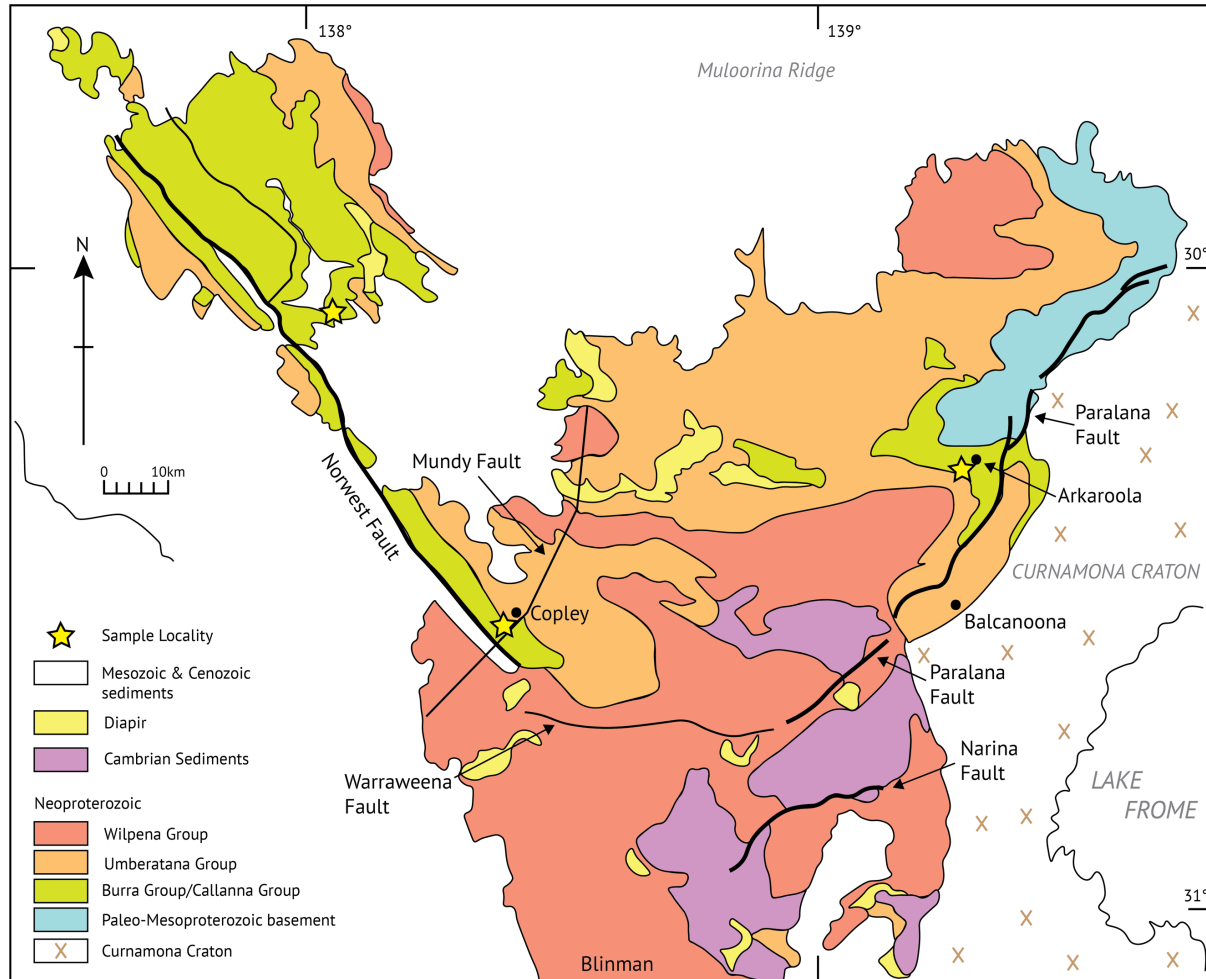


Figure 1: Northern Adelaide Rift Complex sediments distribution. Modified from (Paul, Flöttmann, & Sandiford, 1999).

2 METHODS

2.1 Carbonate sample collection

Hand samples were collected from a total of three sites throughout the northern sections of the Adelaide Rift Complex (*Fig. 1*), through the Skillogalee Formation and overlying lower Myrtle Springs and Fitton Formations. Samples were collected at ~1.5m resolution using a Jacob staff clinometer. Limited exposures restricted some sections to coarser resolutions.

2.2 Carbonate sample powder preparation

Sample powders were drilled from carbonate hand samples, drilling along laminations and targeting the carbonate matrix in conglomeritic samples. Fractures, weathered surfaces, heterogeneities and clasts were avoided.

2.3 Carbon isotope analytical procedure

A Nu Perspective dual-inlet isotope ratio mass spectrometer connected to a NuCarb carbonate preparation system measured carbon and oxygen isotopes at McGill University Stable Isotope Laboratory in Montreal, Canada. Approximately 30-150 µg of sample powder was weighed into glass vials and heated for 1 hour at 90°C. The sample powders were individually reacted with H₃PO₄ releasing CO₂ which was collected through cryogenic extraction. Isotope ratios were measured against an in-house reference gas in dual inlet mode, correcting for fractionation effects. The samples were calibrated to VPDB (Vienna Pee Dee Belemnite) using house standards. Both δ¹³C and δ¹⁸O errors are approximately 0.05‰ (1σ).

2.4 Carbonate leaching analytical procedure

The leaching procedure of sample powders is modified from (Liu, Wang, Raub, Macdonald, & Evans, 2014). Approximately 75 mg of each sample was weighed into 15 ml centrifuge tubes. Sample powders were initially leached with 2.7 ml of 1M ammonium acetate solution for one hour, with sample tubes then sonicated for 20 minutes. The insoluble carbonate-bearing fraction was then separated from the acetate supernate by 10 minutes of centrifugation at 4000 rpm. This supernatant was disposed. Samples were then leached twice with 2.7 ml of 0.2M ultrapure acetic acid (seastar) for one hour. Subsequent to the acetic acid leaches, all sample tubes were sonicated in a bath for 30 minutes and centrifuged at 4000 rpm for 10 minutes. The supernatants from the final leach were retrieved and dried in teflon vials.

2.5 Solution ICP sample preparation

The carbonate mass component was calculated for each sample and diluted accordingly with 2% HNO₃. Calibration solutions were diluted from 0 to 1000 ppb range, diluting also with 2% HNO₃. Potential contaminants were monitored by procedural system and acid blanks (see appendix for full results), with results also being measured against standard JDo-1. Calibration curves were generated from 10 ppm mixed element solutions.

2.6 X-ray diffraction (XRD) preparation

Primary carbonate precipitates were targeted for XRD analysis. Weathered surfaces were removed from each sample before being powdered in a ring mill for 3 minutes. Sample powders were loaded onto disk mounts, whilst avoiding smoothing, chipping or fracturing of the sample

powders that might otherwise place bias on mineral orientations. Samples were run on an Bruker D8 X-ray Diffraction system.

2.7 Sr isotope analytical procedure

Samples for Sr isotope analyses were pre-screened based on their Sr, Rb and Al concentrations, retrieved from the ICP-MS results of the carbonate leaching procedure (see above). Approximately 16 - 52 mg of sample powder was first leached in 1M ammonium acetate. The carbonate fraction of the samples was then dissolved in 0.2M acetic acid, which was then separated from the insoluble fraction by centrifugation, dried down, and taken up in 3M HNO₃. Sr was separated from the matrix following standard Sr chromatography procedures (Krabbenhöft et al., 2010) using EICHROM Sr Spec™ resin. ⁸⁸Sr/⁸⁶Sr samples were double spiked with a ratio of 12 µl double spike per 500 ng sample.

Approximately 500 ng Sr were loaded onto Re outgassed filaments. Strontium isotope ratios were measured on an Isotopix thermal ionization mass spectrometer (TIMS) at the University of Adelaide. Procedural blanks recorded values <0.1%, yielding values of approximately 300 pg. Internal mass bias was corrected based on the ratio ⁸⁶Sr/⁸⁸Sr = 0.1194. For the period of this study analysis of NBS SRM 987 yielded an average of 0.710243, whilst the long-term average yields 0.710245, compared to the accepted value of 0.710248. No correction, therefore, was made to sample data.

2.8 Sm-Nd analytical procedure

Samples for Sm-Nd isotope analyses were pre-screened based on their Rb, Zr and Al concentrations, retrieved from the ICP-MS results (see appendix) of the carbonate leaching procedure (see above). Sample leachates were dried and equilibrated in 1 ml of 2M HCl (single

distilled) before undergoing 5 minutes of centrifugation at 13,200 rpm. The Sm and Nd fractions were extracted using a two-stage procedure. In the first stage Sr and Sm-Nd were extracted from the matrix through standard Sr and Sm-Nd chromatography procedures (Foden, Turner, & Morrison, 1990) using 200 mg of 200 – 400 mesh AG 50W-X8 cation exchange resin. The Sr fraction was removed and underwent standard Sr chromatography separation with the other Sr samples (see method above). In the second stage the Sm-Nd bearing fractions were passed through 1 ml of EICHROM Ln resin, using standard Sm-Nd chromatography procedures (Foden et al., 1990).

The $^{143}\text{Nd}/^{144}\text{Nd}$ and $^{147}\text{Sm}/^{144}\text{Nd}$ ratios reported were measured on an Isotopix thermal ionization mass spectrometer (TIMS) at the University of Adelaide, South Australia. Sm and Nd were analysed using Re outgassed filaments in a triple filament array, using an outer filament to load the samples, whilst an inner filament (parallel) and centre filament (parallel with 90° rotation) further controlled ionization. Approximately 20-60 ng of Nd, and 4-15 ng of Sm were loaded and were run manually, measuring in dynamic mode using $e^{12} \Omega$ resistors. Procedural blanks recorded values <0.1% of, recording values of less than 20 pg.

The reported $^{143}\text{Nd}/^{144}\text{Nd}$ and $^{147}\text{Sm}/^{144}\text{Nd}$ ratios have less than 0.5% error, corresponding to less than 0.5% error in ϵNd . Mass fractionation of $^{146}\text{Nd}/^{144}\text{Nd}$ was corrected by normalising to 0.7219. For the period of this study standard JNd_i-1 yielded an average value of 0.512085 ± 33 (n=10), whilst the long-term average measurement of standard JNd_i-1 on $e^{12} \Omega$ resistors yielded a value of $^{143}\text{Nd}/^{144}\text{Nd} = 0.512101 \pm 39$ (n=10). These values are within error of the referenced value of $^{143}\text{Nd}/^{144}\text{Nd} = 0.512115 \pm 7$ (Tanaka et al., 2000). The chondritic reference value of $^{143}\text{Nd}/^{144}\text{Nd}_{\text{CHUR}} = 0.512638$ and $^{147}\text{Sm}/^{144}\text{Nd}_{\text{CHUR}} = 0.1966$ was adopted for calculating ϵNd .

(Goldstein, O'Nions, & Hamilton, 1984). The ^{147}Sm decay constant was assumed to be $6.54 \times 10^{12} \text{ a}^{-1}$.

3 RESULTS

3.1 Carbonate Element Concentrations

A combined total of 208 samples were leached from both dolomite and magnesite phases throughout the Skillogalee and Myrtle Springs Formations. High concentrations of Al, Zr or Rb were used to screen samples from any clastic influence. Further screening was also done through cross plotting REY against Zr as a tracer for silicates, Ni a tracer for oxides and Sc a tracer for sulphides (see Appendix for cross plots). Samples from the Myrtle Springs Formation at Copley display minor contamination from a sulphide phase, reflected by Y/Ho ratios yielding a correlation coefficient (R^2) value of 0.6027 with Sc, whilst Eu/Eu* also displays minor correlation with an R^2 value of 0.2747 against Sc. This relationship, however, does not extend to the Gammon Ranges and Termination Hill sections.

Alteration products were identified through correlation with $\delta^{18}\text{O}$, though only the lower exposures of the Gammon Ranges Skillogalee Formation display signs of alteration yielding a statistically significant relationship with an R^2 value of 0.302. Cross relationships between $\delta^{18}\text{O}$ with REY abundances shows no significant correlation, inferring no obvious alteration effects on REY abundances.

Molar Mg/Ca ratios reveal a predominance of dolomite, with some magnesites also present. Dolomite was inferred from Ca/Mg ratios <2 , whilst magnesites were inferred from values ≥ 2 , though most magnesites show clear enrichment of Mg, with Mg/Ca ratios of up to 125.9. Ce/Ce* display the appropriate negative correlation with Pr/Pr*, here showing no effects from positive

lanthanum anomalies (La/La^*). Molar Zn/Fe ratios broadly mirror Ce/Ce* throughout Termination Hill Skillogalee carbonates.

For a full table list of element concentrations as well as cross plots with contamination and alteration proxies see Appendix.

3.2 Carbon Isotopes and Organic Carbon Burial

$\delta^{13}\text{C}$ and $\delta^{18}\text{O}$ display significant variation, in some cases displaying $>8\text{\textperthousand}$ shifts, though typically trend isotopically heavy, characteristic of Neoproterozoic seawaters (Halverson, Wade, Hurtgen, & Barovich, 2010). Correlation with the globally recognised Bitter Springs Anomaly constrains Skillogalee and Myrtle Springs sedimentation to approximately ca. 811 Ma (see discussion) (Halverson, Maloof, Schrag, Dudás, & Hurtgen, 2007; Halverson et al., 2010). Calculated f_{org} yields high values, recognising the contribution from dominantly enriched $\delta^{13}\text{C}$ throughout the Neoproterozoic. Standard deviations of f_{org} yield modest values, crediting a biogenically driven interpretation of long-lived $\delta^{13}\text{C}$ and f_{org} , with only minor fractionation effects (Hayes et al., 1999). Summary of $\delta^{13}\text{C}$, $\delta^{18}\text{O}$ and f_{org} data for all samples may be found in the table below.

Table 1: Summary of $\delta^{13}\text{C}$, $\delta^{18}\text{O}$ and f_{org} data for the Skillogalee Formation. Estimated ages are derived from correlation of $\delta^{13}\text{C}$ with the global seawater curve (Halverson, 2006; Halverson et al., 2005). Samples with ID's beginning with "THM" are from Termination Hill in the Willouran Ranges, whereas samples with ID's starting with "Gr" are sourced from the Gammon Ranges.

Sample ID	Est. Age (Ma)	$\delta^{13}\text{C}$	$\delta^{18}\text{O}$	f_{org}	std.
THM 401	820.0	7.06	-2.07	0.45	0.029
THM 402	819.0	5.90	-2.26	0.41	0.029
THM 403	818.1	5.69	-1.85	0.40	0.029
THM 404	816.4	5.43	-1.62	0.39	0.029
THM 405	814.9	6.47	-1.39	0.43	0.029
THM 406	813.0	6.05	-0.75	0.41	0.029
THM 407	810.9	4.99	-1.06	0.38	0.029

Sample ID	Est. Age (Ma)	$\delta^{13}\text{C}$	$\delta^{18}\text{O}$	f_{org}	std.
THM 408	808.2	5.83	-0.80	0.41	0.029
THM 409	806.9	3.98	-0.78	0.35	0.029
THM 410	806.5	4.01	-0.84	0.35	0.029
THM 411	804.7	4.25	-0.89	0.36	0.029
THM 201	803.1	3.82	-0.82	0.34	0.029
THM 202	803.0	-5.88	-2.03	0.02	0.029
THM 203	803.0	3.91	-1.32	0.35	0.029
THM 204	803.0	4.23	-4.42	0.36	0.029
THM 205	803.0	0.48	-4.15	0.23	0.029
THM 206	802.9	-1.53	-3.25	0.17	0.029
THM 207	802.9	2.59	-0.97	0.30	0.029
THM 208	802.9	4.91	-1.84	0.38	0.029
THM 412	802.8	4.12	-2.65	0.35	0.029
THM 209	802.6	5.78	0.21	0.41	0.029
THM 210	802.6	6.98	-0.17	0.45	0.029
THM 211	802.5	6.81	-1.53	0.44	0.029
THM 212	802.5	6.08	-1.84	0.42	0.029
THM 213	801.7	5.67	-1.67	0.41	0.029
THM 214	801.7	6.69	-1.21	0.44	0.029
THM 215	801.5	5.37	-2.07	0.40	0.029
THM 216	801.4	6.54	-1.90	0.44	0.029
THM 217	801.2	6.59	-2.27	0.44	0.029
THM 218	801.0	5.61	-4.28	0.40	0.029
THM 219	800.6	5.57	-4.53	0.40	0.029
THM 220	800.6	6.43	-0.65	0.43	0.029
THM 221	800.5	6.87	-0.27	0.45	0.029
THM 222	800.4	5.74	-0.68	0.41	0.029
THM 223	799.8	4.62	-5.46	0.37	0.029
THM 224	799.6	5.57	-0.77	0.40	0.029
THM 225	799.6	5.80	-1.44	0.41	0.029
THM 226	799.2	5.37	-0.60	0.40	0.029
THM 227	799.0	5.25	-0.97	0.39	0.029
THM 228	798.9	5.21	-2.08	0.39	0.029
THM 229	798.8	5.66	-1.44	0.41	0.029
THM 230	798.7	5.32	-1.15	0.39	0.029
THM 231	798.6	5.63	-1.54	0.40	0.029
THM 232	798.4	5.22	-3.70	0.39	0.029
THM 233	798.2	5.07	-0.89	0.39	0.029
THM 234	798.2	4.99	-3.05	0.38	0.029
THM 235	798.1	5.40	-0.95	0.40	0.029
THM 236	798.0	4.40	-1.88	0.36	0.029
THM 237	797.9	4.90	-0.80	0.38	0.029
THM 238	797.9	5.30	-2.16	0.39	0.029
THM 239	797.7	4.39	-1.72	0.36	0.029
THM 240	797.5	4.72	-0.37	0.37	0.029
THM 241	797.4	4.03	-2.66	0.35	0.029
THM 242	796.5	2.51	-1.82	0.30	0.029
THM 243	796.0	2.31	-0.67	0.29	0.029
THM 244	795.9	4.93	-0.41	0.38	0.029
THM 245	795.8	4.19	-2.19	0.36	0.029
THM 246	795.6	3.30	-1.56	0.33	0.029
THM 247	795.5	3.14	-0.60	0.32	0.029
THM 248	795.3	5.12	-0.89	0.39	0.029
THM 249	795.1	4.72	-0.41	0.37	0.029

Sample ID	Est. Age (Ma)	$\delta^{13}\text{C}$	$\delta^{18}\text{O}$	f_{org}	std.
THM 250	795.0	2.94	-1.06	0.31	0.029
THM 251	794.9	1.67	-2.02	0.27	0.029
THM 413	792.0	5.50	-1.98	0.40	0.029
THM 101	783.0	4.47	-1.17	0.37	0.029
THM 102	783.0	5.64	-0.67	0.40	0.029
THM 103	782.9	5.31	-0.70	0.39	0.029
THM 104	782.9	4.86	-1.09	0.38	0.029
THM 105	782.8	4.04	-1.08	0.35	0.029
THM 106	782.8	4.53	-0.89	0.37	0.029
THM 107	782.8	4.44	-1.28	0.37	0.029
THM 108	782.7	4.41	-1.09	0.36	0.029
THM 109	782.7	3.95	-2.67	0.35	0.029
THM 110	782.6	5.03	-0.92	0.38	0.029
THM 111	782.5	3.98	-1.98	0.35	0.029
THM 112	782.5	4.63	-1.37	0.37	0.029
THM 112b	782.5	4.77	-1.26	0.38	0.029
THM 113	782.5	4.81	-1.91	0.38	0.029
THM 114	782.4	3.59	-0.72	0.34	0.029
THM 414	782.2	5.45	-1.65	0.40	0.029
THM 120	780.8	3.06	-0.12	0.32	0.029
THM 121	779.4	5.63	-0.88	0.40	0.029
THM 122	778.7	5.72	0.18	0.41	0.029
THM 123	777.7	5.49	-1.31	0.40	0.029
THM 124	777.1	4.86	-2.18	0.38	0.029
THM 125	774.0	5.73	-0.35	0.41	0.029
THM 126	773.9	4.86	-2.45	0.38	0.029
THM 127	773.6	4.29	-3.38	0.36	0.029
THM 128	773.6	4.73	-3.00	0.37	0.029
THM 129	773.5	4.60	-2.73	0.37	0.029
THM 130	773.4	4.07	-1.95	0.35	0.029
THM 131	773.2	4.54	-3.46	0.37	0.029
THM 132	773.1	4.30	-1.42	0.36	0.029
THM 133	773.0	3.42	-2.70	0.33	0.029
THM 134	773.0	3.84	-2.81	0.34	0.029
THM 135	772.9	2.83	-1.42	0.31	0.029
THM 136	772.9	2.90	-1.17	0.31	0.029
THM 137	772.8	2.26	-0.95	0.29	0.029
THM 138	772.8	2.58	-0.34	0.30	0.029
THM 139	772.7	3.43	-1.81	0.33	0.029
THM 140	772.6	1.70	-0.85	0.27	0.029
Gr201	821.0	-3.29	-2.59	0.107	0.029
Gr202	820.8	-1.52	-4.36	0.166	0.029
Gr203	820.5	1.55	-5.30	0.268	0.029
Gr205	820.0	-4.04	-2.07	0.082	0.029
Gr206	819.8	-0.47	-3.69	0.201	0.029
Gr207	819.5	-1.14	-3.54	0.179	0.029
Gr208	819.3	3.27	-6.04	0.326	0.029
Gr209	818.8	4.75	-5.36	0.375	0.029
Gr210	818.5	1.55	-3.32	0.268	0.029
Gr211	818.3	0.11	-2.55	0.220	0.029
Gr212	818.1	-1.57	-3.14	0.165	0.029
Gr213	817.8	-0.89	-3.17	0.187	0.029
Gr214	817.6	-0.01	-3.41	0.216	0.029
Gr216	817.1	0.99	-4.27	0.250	0.029

Sample ID	Est. Age (Ma)	$\delta^{13}\text{C}$	$\delta^{18}\text{O}$	f_{org}	std.
Gr217	816.8	-1.10	-3.30	0.180	0.029
Gr218	816.6	1.93	-4.18	0.281	0.029
Gr219	816.3	3.03	-5.15	0.318	0.029
Gr222	815.6	-0.44	-3.47	0.202	0.029
Gr223	815.4	0.69	-3.71	0.240	0.029
Gr224	815.1	0.61	-4.15	0.237	0.029
Gr225	814.9	-1.36	-1.59	0.171	0.029
Gr227	814.4	-0.86	-1.67	0.188	0.029
Gr228	814.1	2.53	-4.49	0.301	0.029
Gr229	813.9	1.51	-4.63	0.267	0.029
Gr230	813.6	2.08	-4.87	0.286	0.029
Gr231	813.4	6.04	-3.62	0.418	0.029
Gr232	812.9	4.07	-5.55	0.352	0.029
Gr233	811.4	7.60	-2.19	0.470	0.029
Gr235	810.7	-1.54	-3.36	0.165	0.029
Gr236	810.4	0.36	-4.46	0.229	0.029
Gr237	810.2	-0.46	-3.64	0.201	0.029
Gr238	810.0	-5.77	-1.66	0.024	0.029
Gr239	809.7	-0.53	-2.05	0.199	0.029
Gr240	809.5	-2.44	-2.74	0.135	0.029
Gr241	809.2	-1.90	-3.28	0.153	0.029
Gr101	799.9	3.33	-7.72	0.328	0.029
Gr102	799.4	2.42	-6.58	0.298	0.029
Gr104	796.6	3.04	-1.82	0.318	0.029
Gr105	795.9	2.99	-8.64	0.316	0.029
Gr106	793.6	2.63	-6.03	0.304	0.029
Gr109	788.3	3.93	-9.44	0.348	0.029
Gr111	783.7	5.28	-8.94	0.393	0.029
Gr112	783.3	2.18	-8.24	0.289	0.029
Gr113	782.5	3.05	-8.96	0.319	0.029
Gr114	781.7	3.06	-9.28	0.319	0.029
Gr115	774.5	3.09	-6.90	0.320	0.029
Gr116	774.0	1.99	-4.86	0.283	0.029
Gr117	772.4	3.11	-7.68	0.320	0.029
Gr118	759.8	1.89	-7.71	0.280	0.029
Gr120	759.4	2.81	-7.49	0.310	0.029
Gr121	759.3	1.96	-6.87	0.282	0.029
Gr122	759.3	2.52	-7.41	0.301	0.029
Gr123	758.8	2.36	-7.30	0.295	0.029
Gr124	758.7	2.87	-7.48	0.312	0.029
Gr125	783.1	2.66	-6.66	0.305	0.029
Gr126	758.2	2.67	-7.14	0.306	0.029
Gr127	757.8	2.75	-7.55	0.309	0.029
Gr128	757.4	2.99	-7.44	0.316	0.029
Gr129	757.2	2.26	-7.34	0.292	0.029
Gr130	756.8	1.99	-7.40	0.283	0.029
Gr131	756.3	2.14	-7.80	0.288	0.029
Gr132	755.7	2.79	-7.21	0.310	0.029
Gr133	755.4	3.73	-4.94	0.341	0.029
Gr134	755.0	4.93	-6.93	0.381	0.029
Gr135	753.7	3.12	-7.03	0.321	0.029
Gr136	753.3	3.39	-7.15	0.330	0.029
Gr137	752.5	3.11	-7.16	0.320	0.029
Gr138	751.8	2.71	-7.67	0.307	0.029

Sample ID	Est. Age (Ma)	$\delta^{13}\text{C}$	$\delta^{18}\text{O}$	f_{org}	std.
Gr140	741.5	-0.12	-12.48	0.21	0.029
Gr141	740.0	-0.18	-11.52	0.21	0.029

Table 2: Summary of $\delta^{13}\text{C}$, $\delta^{18}\text{O}$ and f_{org} data for the Myrtle Springs Formation in the Willouran Ranges, Copley, S.A.

Sample ID	Stratigraphic Position (m)	$\delta^{13}\text{C}$	$\delta^{18}\text{O}$	f_{org}	std.
WR 102	20.82	3.62	-5.61	0.34	0.029
WR 103	79.51	4.56	-5.35	0.37	0.029
WR 104	250.01	-3.63	-6.75	0.10	0.029
WR 106	319.72	-2.00	-5.25	0.15	0.029
WR 107	367.31	0.52	-4.32	0.23	0.029
WR 108	472.91	-0.25	-0.83	0.21	0.029
WR 109	524.51	-0.11	-1.80	0.21	0.029
WR 111	613.91	-1.67	-0.82	0.16	0.029
WR 112	709.62	-0.59	-4.72	0.20	0.029
WR 113	771.3	-0.47	-1.83	0.20	0.029
WR 115	1089.66	1.62	-7.30	0.27	0.029
WR 117	1291.29	2.14	-2.10	0.29	0.029
WR 118	1343.09	-0.85	0.00	0.19	0.029

3.3 Strontium isotopes

26 primary dolomitic carbonates were selected for isotopic analysis of radiogenic Sr. $^{87}\text{Sr}/^{86}\text{Sr}$ ratios were derived, taking the mean and standard deviation from 100 ratios, yielding errors of less than 0.5%. Relative to mean seawater during the late Tonian, $^{87}\text{Sr}/^{86}\text{Sr}$ ratios are relatively evolved, though still depict a coeval trend with the global record (see discussion). The reported $^{87}\text{Sr}/^{86}\text{Sr}$ ratios are consistent with former studies that also show evolved $^{87}\text{Sr}/^{86}\text{Sr}$ ratios, yielding values between 0.70905 and 0.71168 for the Skillogalee Formation, outcropped at Depot Creek in South Australia (Veizer & Compston, 1976). $^{87}\text{Sr}/^{86}\text{Sr}$ ratios for the Skillogalee Formation show an apparent increase towards the eastern margin of the ARC. A summary of new $^{87}\text{Sr}/^{86}\text{Sr}$ results for the Skillogalee Formation is described below. See appendix for Sr blank summary.

Table 3: Summary of new $^{87}\text{Sr}/^{86}\text{Sr}$ results for the Skillogalee Formation. Samples with ID's beginning with "THM" are from Termination Hill in the Willouran Ranges, whereas samples with ID's starting with "Gr" are sourced from the Gammon Ranges.

Sample ID	Locality	Est. Age (Ma)	[Rb] ppm	[Sr] ppm	$^{87}\text{Sr}/^{86}\text{Sr}$	2 std. error
THM 201	Termination Hill	803.1	BDL	292.8072	0.707670	.000003
THM 203	Termination Hill	803.0	BDL	389.4564	0.707660	.000003
THM 207	Termination Hill	802.9	BDL	465.8082	0.708865	.000003
THM 210	Termination Hill	802.6	BDL	291.3717	0.708332	.000003
THM 223	Termination Hill	799.8	BDL	270.2532	0.707810	.000004
THM 232	Termination Hill	798.4	BDL	293.8754	0.707857	.000004
THM 241	Termination Hill	797.4	BDL	476.6130	0.707943	.000003
THM 250	Termination Hill	795.0	0.1141	246.4932	0.707823	.000004
THM 103	Termination Hill	783.0	BDL	254.4099	0.709011	.000003
THM 112b	Termination Hill	782.5	BDL	576.3241	0.708426	.000004
THM 113	Termination Hill	782.5	0.2271	498.7809	0.708132	.000004
THM 122	Termination Hill	778.7	0.1260	332.4310	0.709126	.000003
Gr203	Gammon Ranges	820.5	0.1846	371.9139	0.710216	.000003
Gr213	Gammon Ranges	817.9	0.6767	409.1964	0.716176	.000004
Gr217	Gammon Ranges	816.9	0.9646	604.7286	0.717154	.000003
Gr222	Gammon Ranges	815.7	0.7399	499.6788	0.714380	.000003
Gr226	Gammon Ranges	814.8	0.5185	436.4450	0.712661	.000003
Gr234	Gammon Ranges	811.4	2.2903	409.6718	0.709135	.000003
Gr237	Gammon Ranges	810.5	0.5346	318.0059	0.713415	.000004
Gr101	Gammon Ranges	800.4	3.3945	442.3141	0.709577	.000003
Gr109	Gammon Ranges	789.1	4.3950	360.3826	0.713404	.000003
Gr118	Gammon Ranges	761.3	9.7357	420.7471	0.711634	.000003
Gr126	Gammon Ranges	759.7	5.2053	442.9598	0.710409	.000003
Gr129	Gammon Ranges	758.8	4.4504	364.1131	0.710796	.000003
Gr133	Gammon Ranges	757.1	3.8378	462.9441	0.711559	.000003

Sample ID	Locality	Est. Age (Ma)	[Rb] ppm	[Sr] ppm	$^{87}\text{Sr}/^{86}\text{Sr}$	2 std. error
Gr137	Gammon Ranges	754.2	0.0509	257.1847	0.710947	.000003
JDo1			0.01429	61.5485	0.708007	.000003

3.4 Samarium-Neodymium Isotopes

8 dolomitic carbonates from the Skillogalee Formation were chosen for Sm-Nd isotopic analysis. Ages used in εNd calculations were derived from $\delta^{13}\text{C}$ correlated age constraints founded in this study. The global compilation of εNd (*Fig. 14*) was derived from published data that included mudstones, iron formations and matrices from glacial diamictite, sourced from Australia, North America, Svalbard and South China (Barovich & Foden, 2000; Chen & Jahn, 1998; Cox et al., 2016; Li & McCulloch, 1996; Wade et al., 2005; Wang et al., 2011; Zhao et al., 1992). Studies with ≥ 4 samples per age were converted to a bootstrapped average (n=10000). Both the global compilation and local carbonate sources display a marked increase in εNd towards primitive endmembers throughout the late Tonian (*Fig. 14*). Though εNd in mudstones vary somewhat, εNd in Skillogalee carbonate phases display a strong correlation with the linear average of the global compilation. See appendix for Nd blank summary.

Table 4: Summary of Sm-Nd isotope data founded in this study. Samples with ID's beginning with "THM" are from Termination Hill in the Willouran Ranges, whereas samples with ID's starting with "Gr" are sourced from the Gammon Ranges.

Sample ID	Est. Age	[Nd] ppm	[Sm] ppm	$^{147}\text{Sm}/^{144}\text{Nd}$	$^{143}\text{Nd}/^{144}\text{Nd}$	No. Ratios	2 std. error	$\varepsilon\text{Nd}(0)$	$\varepsilon\text{Nd}(t)$
THM 203	803	0.7073	0.1490	0.1161	0.511346	118	.000007	-13.28	-5.021
THM 241	797	0.7744	0.1526	0.1171	0.511307	134	.000006	-14.01	-5.916
THM 112b	782	0.7895	0.1572	0.1278	0.511379	77	.000009	-11.77	-4.890
THM 122	778	0.7852	0.1924	0.1387	0.511381	100	.000007	-10.71	-4.949
GR 217	816	2.2344	0.4701	0.1169	0.511298	115	.000010	-13.93	-5.609
GR 234	811	2.4787	0.5781	0.1375	0.511235	155	.000006	-13.09	-6.972
GR 109	789	3.1477	0.7992	0.1583	0.511303	192	.000004	-10.06	-6.211
GR 129	758	2.0238	0.4884	0.1386	0.511490	178	.000017	-8.95	-3.327
JDo-1		1.8353	0.2899	0.1056	0.512244	198	.000007	-7.68	
JNDi-1					0.512102	10	.000007		
JNDi-1					0.512069	10	.000012		
JNDi-1					0.512085	10	.000007		

4 DISCUSSION

4.1 Chemostratigraphy

4.1.1 CHEMOSTRATIGRAPHY OF THE SKILLOGALEE FORMATION – TERMINATION HILL

Chemostratigraphic correlation with the global seawater $\delta^{13}\text{C}$ record (Halverson, 2006; Halverson et al., 2005) constrains the upper Skillogalee Formation to an age interval between ca. 803 Ma and ca. 771 Ma. Ages ca. 821 Ma through to approximately 803 Ma are interpolated from a constant sedimentation rate, though stray from the global seawater $\delta^{13}\text{C}$ record, rendering their

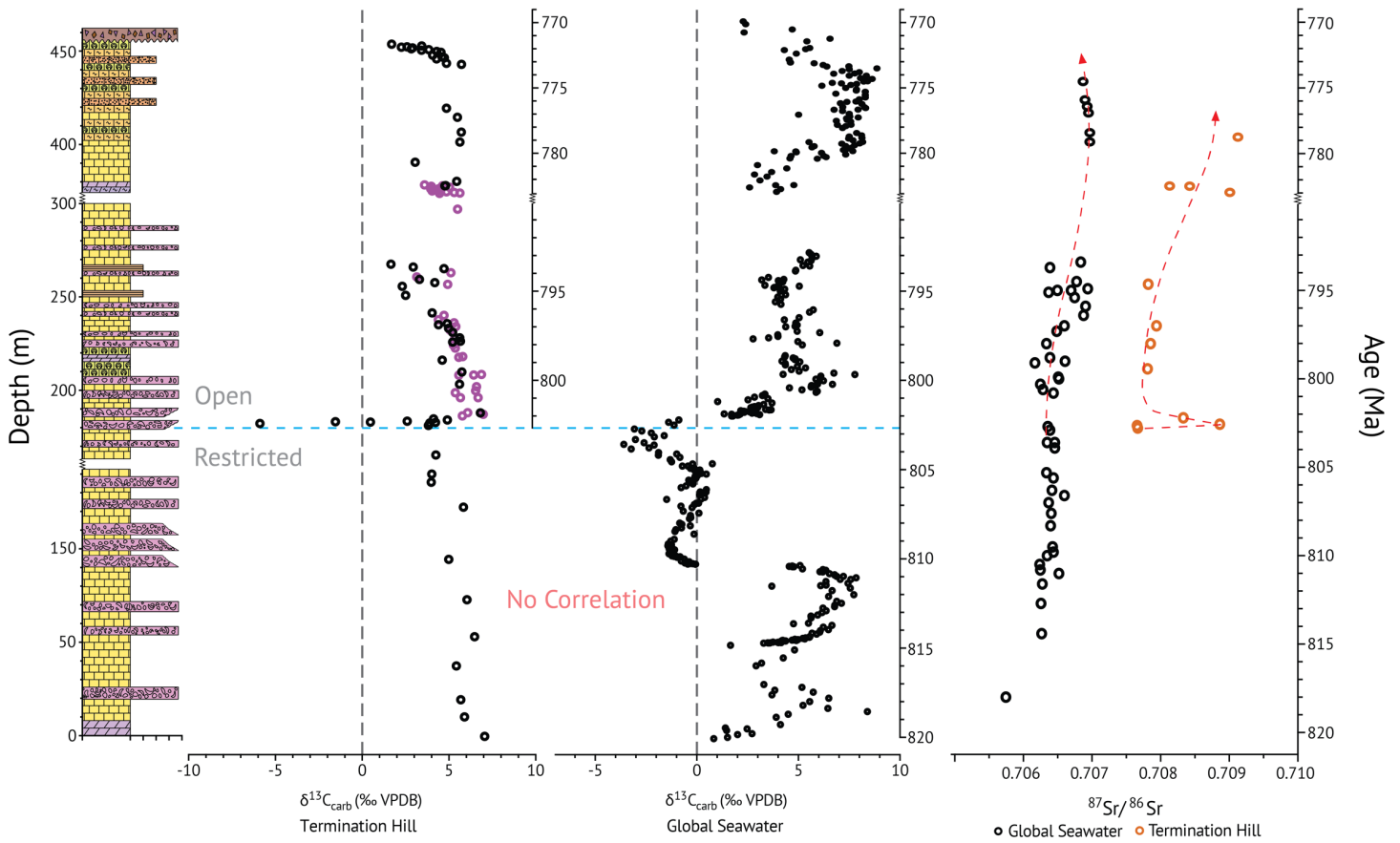


Figure 2: Chemostratigraphic correlation of the Skillogalee Formation, exposure at Termination Hill S.A. Purple data points in the $\delta^{13}\text{C}$ plots correspond to magnesite samples whereas black data points correspond to dolomite samples. The dashed blue line is representative of a proposed shift from a restricted marine to a more open marine setting. The dashed red line follows the general trend of ${}^{87}\text{Sr}/{}^{86}\text{Sr}$ isotope data through time. The stratigraphic profile can be viewed in greater detail below. Global seawater $\delta^{13}\text{C}$ data compiled from (Halverson, 2006; Halverson et al., 2005). Global seawater ${}^{87}\text{Sr}/{}^{86}\text{Sr}$ data compiled from (Cox et al., 2016; Fairchild et al., 2000; Halverson, Dudás, et al., 2007; Rooney et al., 2014).

ages indeterminant. Non-coherent $\delta^{13}\text{C}$ values trend isotopically heavy, likely suggesting an evaporative setting. From ca. 803 Ma through to ca. 771 Ma $\delta^{13}\text{C}$ trends are coherent with the global seawater record, suggestive of a more open marine environment. This is broadly consistent with the Rook Tuff constraining the maximum age of Burra Group deposition to 802 ± 10 Ma (Fanning, Ludwig, Forbes, & Preiss, 1986), whilst the Boucaut Volcanics constrain the minimum age of Burra Group deposition to ca. 777 ± 7 Ma (B. G. Forbes, 1977). $^{87}\text{Sr}/^{86}\text{Sr}$ ratios through the Skillogalee Formation at Termination Hill, display evolved values, accounted for by the weathering of surrounding cratonic material. 1.51 Ga to 2 Ga zircons from both the Gawler Craton and Curnamona Province are reported throughout the Belair Subgroup, Uppalinna Subgroup and the Rhynie Sandstone (Gehrels, Butler, & Bazard, 1996; Ireland, Flottmann, Fanning, Gibson, & Preiss, 1998) exemplifying a contribution of highly evolved cratonic crustal material into the rift basin.

The Bitter Springs Excursion recorded in the Amadeus Basin is associated with an abrupt lithofacies change from a restricted marine to alkaline lacustrine and playa settings that record contrasting $\delta^{13}\text{C}$ values (Klaebe, Kennedy, Jarrett, & Brocks, 2016). Termination Hill Skillogalee carbonates also document this trend, thus providing an inter-basinal correlation, suggestive of a regional change in environment. The reproducibility of the Bitter Springs Anomaly on a global scale is strong evidence of a global perturbation in the carbon cycle. The Skillogalee Formation is no exception.

4.1.2 CHEMOSTRATIGRAPHY OF THE SKILLOGALEE FORMATION - GAMMON RANGES

The Gammon Ranges exposure of the Skillogalee Formation records coherent $\delta^{13}\text{C}$ values that correlate well with the global seawater record; surprising, given coeval evolved $^{87}\text{Sr}/^{86}\text{Sr}$

signatures are typical of a restricted environment where evaporation effects may be considered more likely to drive the residual $\delta^{13}\text{C}$ pool isotopically heavy (Hayes et al., 1999). The basal 50 m of the Skillogalee Formation throughout the Gammon Ranges display minor perturbations from the global curve yielding values that are isotopically lighter by $\sim 2\text{--}4\text{\textperthousand}$. This shift in $\delta^{13}\text{C}$ may be a minor alteration product of decarbonation reactions during dolomitization, since such processes have been shown to yield a decrease in $\delta^{13}\text{C}$ whilst maintaining overarching trends in isotopic compositions (Kaufman, Hayes, Knoll, & Germs, 1991). Negative correlation between $\delta^{13}\text{C}$ and $\delta^{18}\text{O}$ (see appendix), yielding an R^2 value of 0.302, accounts for this alteration, as does the presence of low-grade metamorphic minerals including talc, phlogopite, albite and tremolite, detected through XRD analysis (see appendix). Correlation with $\delta^{13}\text{C}$ constrains the Skillogalee Formation in the Gammon Ranges to an age interval between ca. 821 Ma through to ca. 740 Ma, somewhat discordant with previously mentioned constraints. Samples, therefore, may include the Fitton Formation, which contains an erosional surface with underlying Burra Group strata (Preiss, 1987; Preiss, 2000). Alternatively, the apparent correlation with global $\delta^{13}\text{C}$ may be false, with values trending isotopically heavy due to a restricted marine setting (Hayes et al., 1999). Similar to Termination Hill, the Skillogalee Formation throughout the Gammon Ranges display significantly evolved $^{87}\text{Sr}/^{86}\text{Sr}$, reflecting a shallow marine setting with close proximity to the Curnamona Province, thus rendering a greater susceptibility to weathering of highly evolved cratonic material. Evolved $^{87}\text{Sr}/^{86}\text{Sr}$ values and high degree of terrigenous input adhere with paleogeography that the Gammon Ranges hosted a more marginal marine setting than Willouran Ranges' equivalents. (Preiss, 2000).

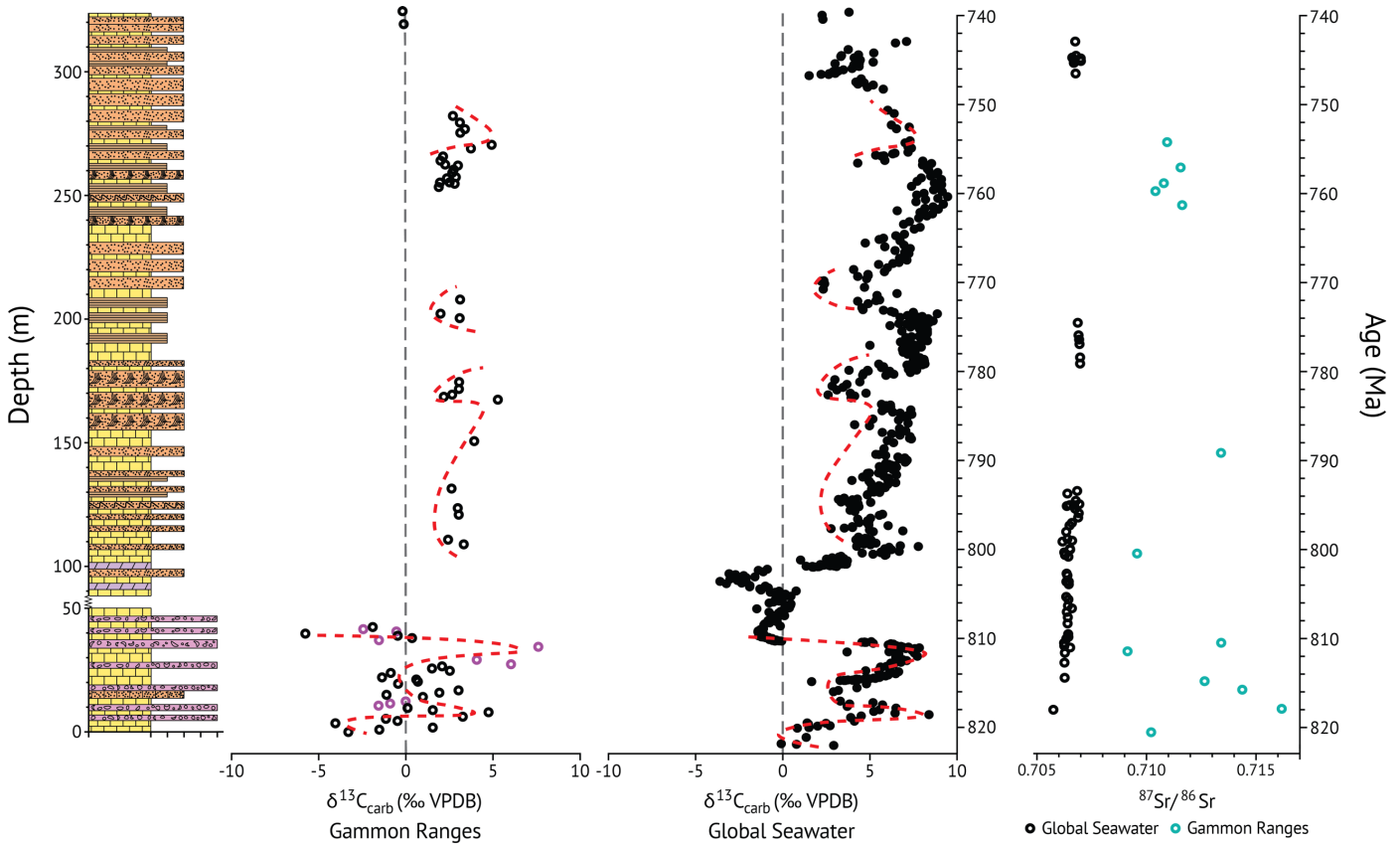


Figure 3: Chemostratigraphic correlation of the Skillogalee Formation, exposure in the Gammon Ranges S.A. All $\delta^{13}\text{C}$ and $^{87}\text{Sr}/^{86}\text{Sr}$ analysis performed through the Gammon Ranges section was done on dolomitic carbonates. The dashed red line highlights coherent trends between $\delta^{13}\text{C}$ in the Gammon Ranges dolomitic carbonates and the global seawater $\delta^{13}\text{C}$ documented through the Late Tonian (Halverson, 2006; Halverson, Hoffman, Schrag, Maloof, & Rice, 2005). Global seawater $^{87}\text{Sr}/^{86}\text{Sr}$ data compiled from (Cox et al., 2016; Fairchild, Sprio, Herrington, & Song, 2000; Halverson, Dudás, Maloof, & Bowring, 2007; Rooney et al., 2014).

4.1.3 CHEMOSTRATIGRAPHY OF THE WILLOURAN RANGES – COPLEY

Increased frequency of thinly laminated siltstone and cessation of desiccation structures throughout the Myrtle Springs Formation is consistent with a deepening marine environment interpretation. Despite this transgression, however, a convincing trend between measured $\delta^{13}\text{C}$ and global seawater is not obvious, though a $-8\text{\textperthousand}$ shift is observed, attaining $\delta^{13}\text{C}$ values as low as $-3.6\text{\textperthousand}$. A lack of correlation with $\delta^{18}\text{O}$ (see appendix) argues against this excursion being a

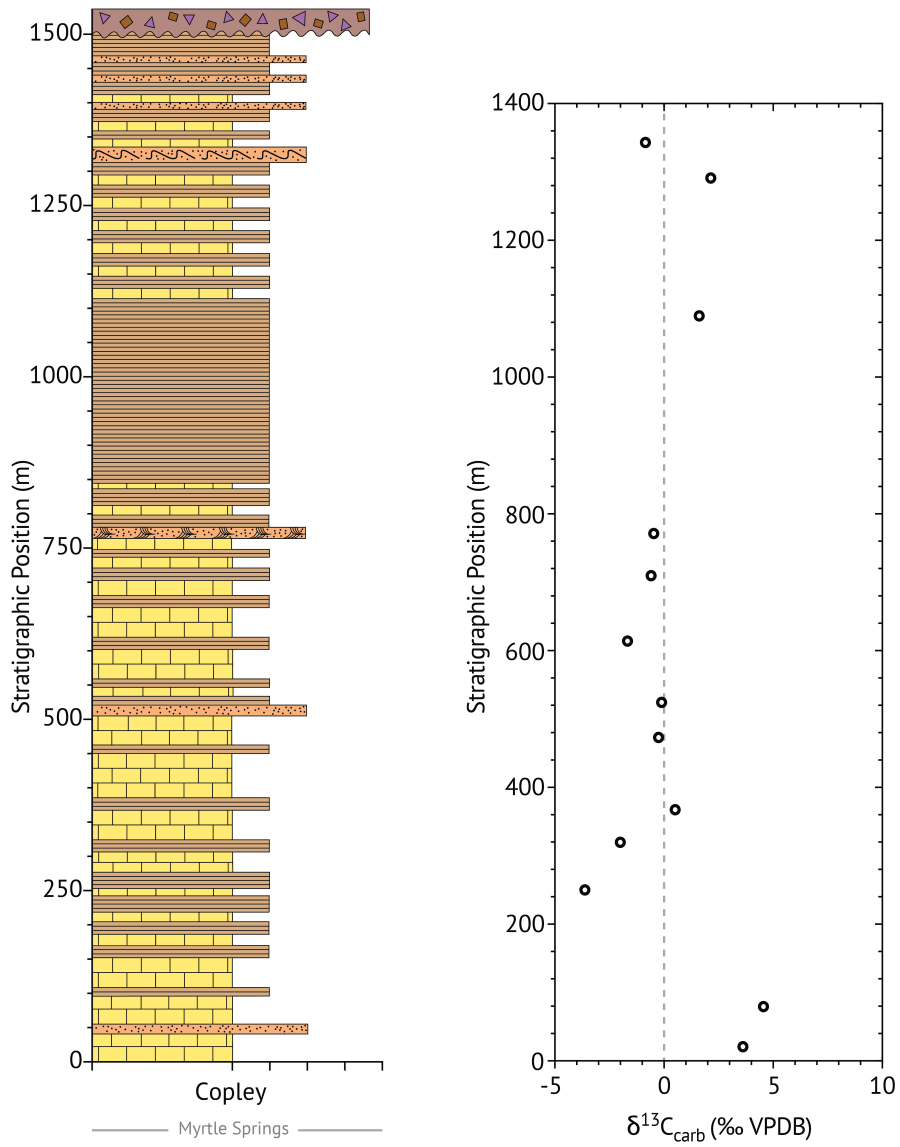


Figure 4: $\delta^{13}\text{C}$ as a function of stratigraphic position for the Myrtle Springs Formation; exposure at Copley, S.A. All samples are dolomitic carbonates. See below for full description of stratigraphic profile

function of alteration. The Baucaut Volcanics constrain deposition of the Myrtle Springs sediments to no younger than ca. 777 Ma (Forbes, 1977), however the Myrtle Springs Formation lies stratigraphically above the Skillogalee Formation, here shown to contain the Bitter Springs Anomaly. The negative excursion throughout Myrtle Springs strata is therefore rendered as either

an undocumented anomaly, or a local basin effect involving oxidation of organic matter (Hill & Walter, 2000).

4.2 Sedimentology

4.2.1 MAGNESITE FACIES

Throughout the Skillogalee Formation sedimentary magnesite occurs almost entirely as clastic supported beds of well-rounded intraclasts (Fig. 5). Individual beds display a wide range of thicknesses, ranging from less than 0.1 to 3.5 m. Although outcrops typically extend for tens to hundreds of metres, thicker units (around Copley and Arkaroola) can extend for several km, suggesting that the intraclastic magnesites were deposited in extensive sheets (Forbes, 1960). The intraclasts range between 0.1 to 3 cm and are spherical to peloidal, with larger clasts commonly banana shaped. Beds with granule to small pebble size intraclasts show current wave-form structures, including tabular cross bedding and low angle ripple cross-laminations. Beds at Termination Hill, on occasion, display reverse grading, possibly representing single high energy events.

A depositional environment consistent with regionally extensive intraclastic magnesite beds is one with low depositional gradients in which transgressive sheet floods may have eroded micritic magnesite muds from broad lagoon environments. Nodular magnesite intraclasts were transported basinward, creating the laterally extensive magnesite conglomerates with minor sand and silt matrix, characteristic of the Skillogalee Formation (Eugster & Hardie, 1978; Hardie, 1977; Uppill, 1990). Horizons of micritic magnesite muds are also observed on occasion throughout the Skillogalee Formation, sometimes interbedded with thinly laminated dolomites. Deposition of the magnesite mudstones would have occurred in very low energy depositional environments, distal

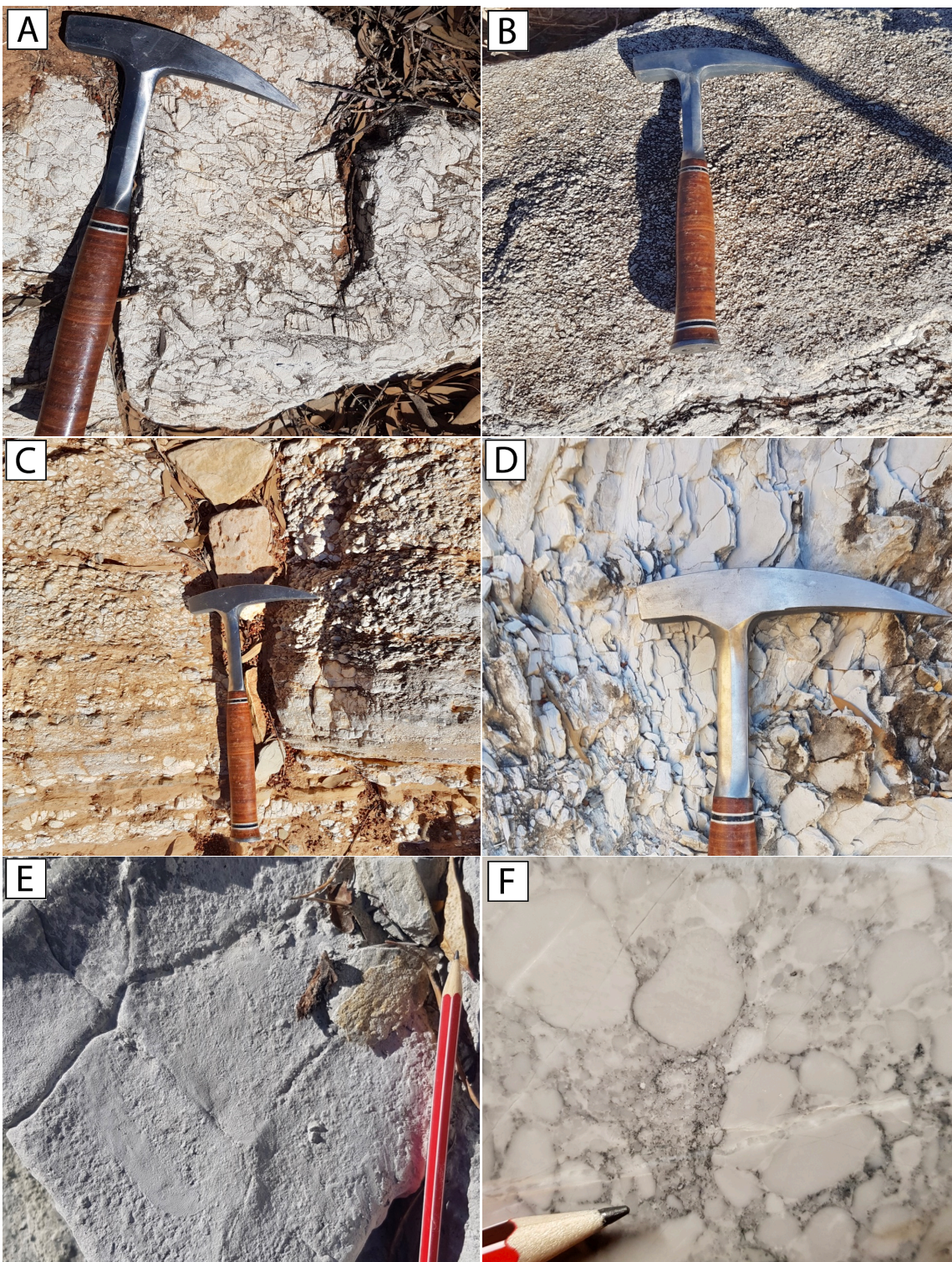


Figure 5: A) Skillogalee intraclastic magnesite at Termination Hill. B) Normally grading Skillogalee magnesite at Termination Hill. C) Reverse grading through lower Skillogalee magnesite at Termination Hill. D) Thinly laminated magnesite muds at the in lower Skillogalee at Termination Hill. E) Mud-crack structures through lower Skillogalee in the Gammon Ranges. F) Polished surface of intraclastic magnesite from the Skillogalee Formation at Termination Hill, with clastic framework grains making a notable contribution to the matrix. For scale, geological hammer head spans a length of 18 cm, whilst the pencil displays a width of 0.7 cm.

to detrital influence. This holds for more current interpretations that the magnesite muds may have precipitated out of lagoon waters in low-rainfall settings. Here, magnesite deposited from suspension, creating homogeneous mud laminae, in a manner analogous to the modern-day Coorong lakes in South Australia (Borch & Lock, 1979).

4.2.2 DOLOMITIC FACIES

Finely laminated micritic dolomites make up most of the Skillogalee Formation, comprising some 50-80% of sediments (Uppill, 1990), and contain an assortment of sedimentary structures including crenulated to stratiform organic laminae, low angle waveforms and stromatolitic carbonates. The dolomite is largely microsparitic, though micritic phases are also present. Some finer dolomitic muds show irregular wavy laminations, possibly reflecting an algal influence. Previous studies report disrupted sediment in the centre of occasional small tepee structures which are spatially associated with desiccated beds (Uppill, 1990), suggestive of formation under the influence of groundwater flux through hardened mudstone crusts (Borch & Lock, 1979). Mud-crack structures are also pervasive throughout lower Skillogalee Formation, particularly towards the east, also suggestive of intermittent exposure, consistent with an evaporative setting. Columnar stromatolite *Baicalia burra* (Fig. 6) (Preiss, 2000) is commonly encountered, particularly throughout the upper member of the Skillogalee Formation. Stromatolites are finely laminated, columnar and domical, and sometimes overturned. Stromatolite biostrome are abundant throughout the Skillogalee Formation (Preiss, 1973; Uppill, 1990) suggesting an extensive uniform substrate and depositional environment. Flaser bedding is observed throughout the Skillogalee Formation in the Gammon Ranges, marking fluctuating

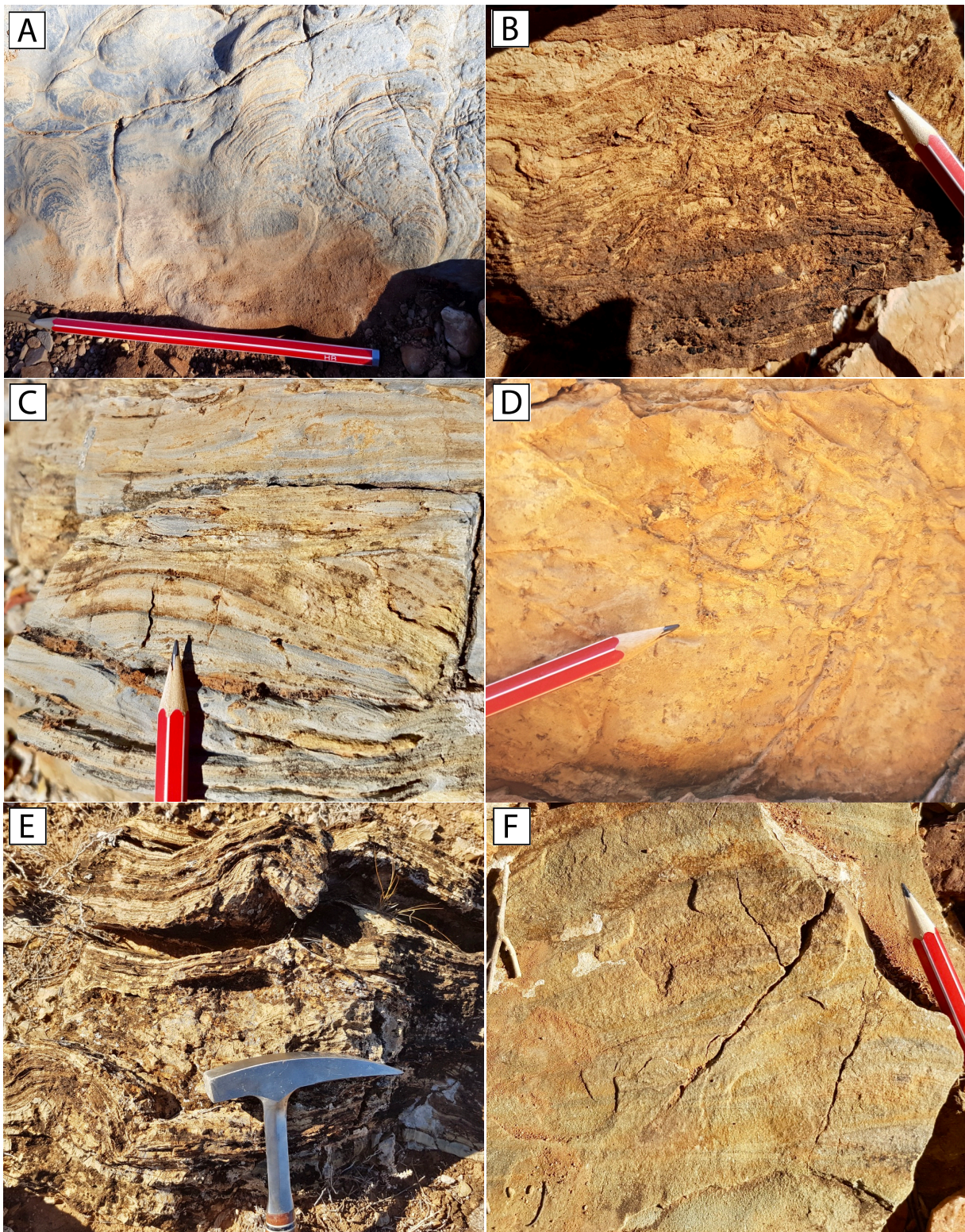


Figure 6: A) Stromatolitic biostrome colony hosting *Baicalia burra* throughout the Skillogalee at Termination Hill. B) Convoluted intraclastic dolomite up section in the Skillogalee, interbedded with sands and silts, and containing minor tepee structures. C) Flaser bedding throughout the dolomite interbeds of the Skillogalee in the Gammon Ranges. D) Mud-crack structures throughout the lower Skillogalee in the Gammon Ranges. E) Tepee and crenulated wave-form structures throughout the Myrtle Springs Formation at Copley. F) Hummocky and swaley cross stratification throughout the Myrtle Springs Formation at Copley. For scale, geological hammer head spans a length of 18 cm, whilst the pencil displays a width of 0.7 cm.

hydraulic conditions, associated with a tidal mud/sand-flat environment. Hummocky cross-stratification, containing both hummocks and swales, is observed throughout the lower Myrtle Springs Formation indicating a shallow marine environment within storm wave base. Although dolomite facies of the Skillogalee Formation contain evidence of exposure, these structures are only minor, and with a lack of documented fenestral features (Uppill, 1990), a dominantly submarine sedimentary environment may be inferred.

4.2.3 FACIES DISTRIBUTION

The facies detailed above display no obvious cyclicity, though Markov Chain Analysis outlined by (Miall, 1973), shows that there is a slight preference to cycle between intraclastic magnesite – dolomitic sandstone – dolomite mudstone and magnesite mudstone throughout the Skillogalee Formation (Uppill, 1990) suggestive of a progressive change from clastic to chemical deposition, such as in the uppermost part of a shallowing environment.

Units throughout the Skillogalee Formation in the Gammon Ranges display higher terrigenous input than coeval strata in the Willouran Ranges, with frequent fine to coarse sands and interbedded siltstone suggesting a more shoreline setting, and periodic carbonate mudflat exposure reflected by mud crack structures in the lower units. An increasing frequency of dolomitic sandstone – siltstone interbeds through the Skillogalee may reflect sheet flooding events and/or a transgressive sea-level rise. The Skillogalee at Termination Hill trends more dolomitic up section, with an increased abundance of microbial and stromatolitic biostromes. At Copley, the Myrtle Springs Formation displays less frequent facies changes than Termination Hill Skillogalee, with beds thickening by roughly 50% (Uppill, 1990). Given the lateral continuity of facies observed throughout Burra Group sediments, the thickening of beds is suggested to match increasing rates of subsidence, maintaining shallow paleoslopes (Belperio, 1990; Murrell, 1977).

The increased abundance of siltstone facies, as well as the lack of cross stratification structures up section is consistent with a relative transgressive sea-level rise interpretation for the Myrtle Springs Formation.

Gammon Ranges and Termination Hill equivalents (*Fig. 7*) show distinct differences in the relative contributions of terrigenous input and desiccation structures. More energetic, siliciclastic sedimentation is present throughout the Gammon Ranges facies relative to Termination Hill, agreeing with previous interpretations that Willouran Ranges sediments host more seaward environments, relative to coeval Gammon Ranges sediments that are more proximal to the basin

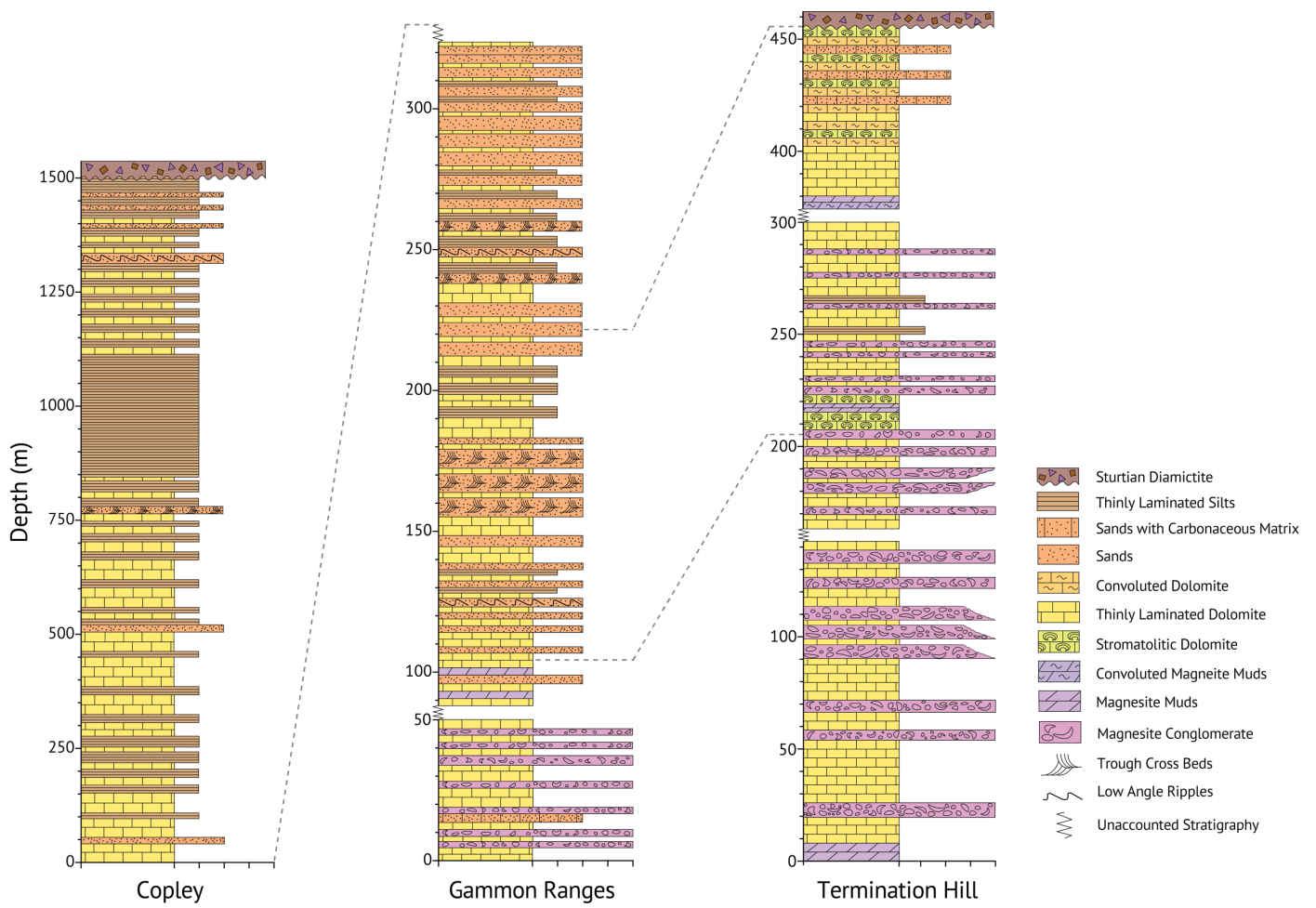


Figure 7: Stratigraphic profiles of the Skillogalee Formation sediments at Termination Hill (Willouran Ranges) and the Gammon Ranges, and the Myrtle Springs Formation at Copley, S.A. Dashed grey line between Termination Hill and the Gammon Ranges mark time equivalent strata based on correlation of $\delta^{13}\text{C}$ and the global seawater curve.

margin. Desiccation structures, however, are still present in Willouran Ranges sediments, indicating that shallow water conditions ultimately prevailed throughout the basin. From sedimentological evidence the depositional basin is suggestive of a shallow water system throughout, with a series of shallow perennial and small ephemeral lagoons containing exposed mudflats, and a very low paleoslope, that trends shallower towards the Gammon Ranges and Arkaroola. Lithostratigraphic correlation broadly supports chemostratigraphic correlation, showing the bulk of magnesite-dolomite interbeds are concentrated throughout lower units, with a shift to more terrigenous and sandy carbonate strata broadly consistent between sections. Biostratigraphic and facies association correlations would further constrain coeval Termination Hill and Gammon ranges strata, however are beyond the scope of this study.

4.2.4 PALEO-REDOX PROXIES

Though it is clear that the Neoproterozoic displays marked enrichments in atmospheric oxygen (Och & Shields-Zhou, 2012), estimates towards the relative timing, magnitude and stepwise or continuous nature remain obscure. Ce/Ce*, Zn/Fe ratios and some petrographic features of the Skillogalee and Myrtle Spings Formations provide insights into the relative timing of Neoproterozoic oxygenation, constraining it, at the very least, to post-Sturtian.

4.2.5 PALEO-REDOX OF THE SKILLOGALEE FORMATION

To the west, the Willouran ranges Ce/Ce* oscillate between positive (>1) and negative (<1) values, displaying a fairly even distribution across both, evincing anoxic-dysoxic conditions associated with active oxidative cycling of Ce throughout the water column. $\delta^{13}\text{C}_{\text{carb}}$ shows a negative covariation with Ce/Ce*, suggesting that free oxygen content moves in response to changes in organic carbon burial (f_{org}) (Fig. 8). Zn/Fe ratios broadly mirror Ce/Ce* throughout

Skillogalee Formation at Termination Hill, further instating confidence of biogenically driven oxygen production.

Further east, the Gammon Ranges display Ce/Ce* that show no obvious relationship with f_{org} , and commonly yield values that plot as indistinguishable (i.e. $0.95 < Ce/Ce^* < 1.05$) when cross plotted with praseodymium anomalies (*Fig. 10*). The interpretation that the Gammon Ranges marine setting is dysoxic or approaching a redox boundary is unlikely given corresponding enriched $\delta^{13}C_{carb}$ values, suggestive of higher f_{org} contributions that would likely drive Ce/Ce* to positive states. Though enrichment of $\delta^{13}C_{carb}$ may be an evaporative effect, it does not account for the correlation with the global seawater record. The subdued Ce/Ce* throughout the Gammon Ranges are therefore suggested to be a paleogeographic effect associated with closer proximity to terrigenous sources, contaminating and enriching shallow marine waters and driving REY distributions more “continental like”. This is consistent with both sedimentological features (discussed above) and REE relationships (discussed below). Gammon Ranges marine carbonates, commonly display subdued Zn/Fe values evincing anoxic conditions. At the base of the section, however, Zn/Fe shows negative covariation with $\delta^{13}C$, suggestive that free oxygen content moves in response to changes in f_{org} . The presence of pyrite is documented throughout the Skillogalee Formation (Belperio, 1990). The precipitation of authigenic pyrite requires sufficient sulfate for bacterial sulfate reduction along with broadly anoxic conditions within the water column of a sediment pile (Severmann, Lyons, Anbar, McManus, & Gordon, 2008). The presence of pyrite, Ce/Ce* and Zn/Fe data point towards anoxic to dysoxic conditions throughout Skillogalee carbonate marine waters.

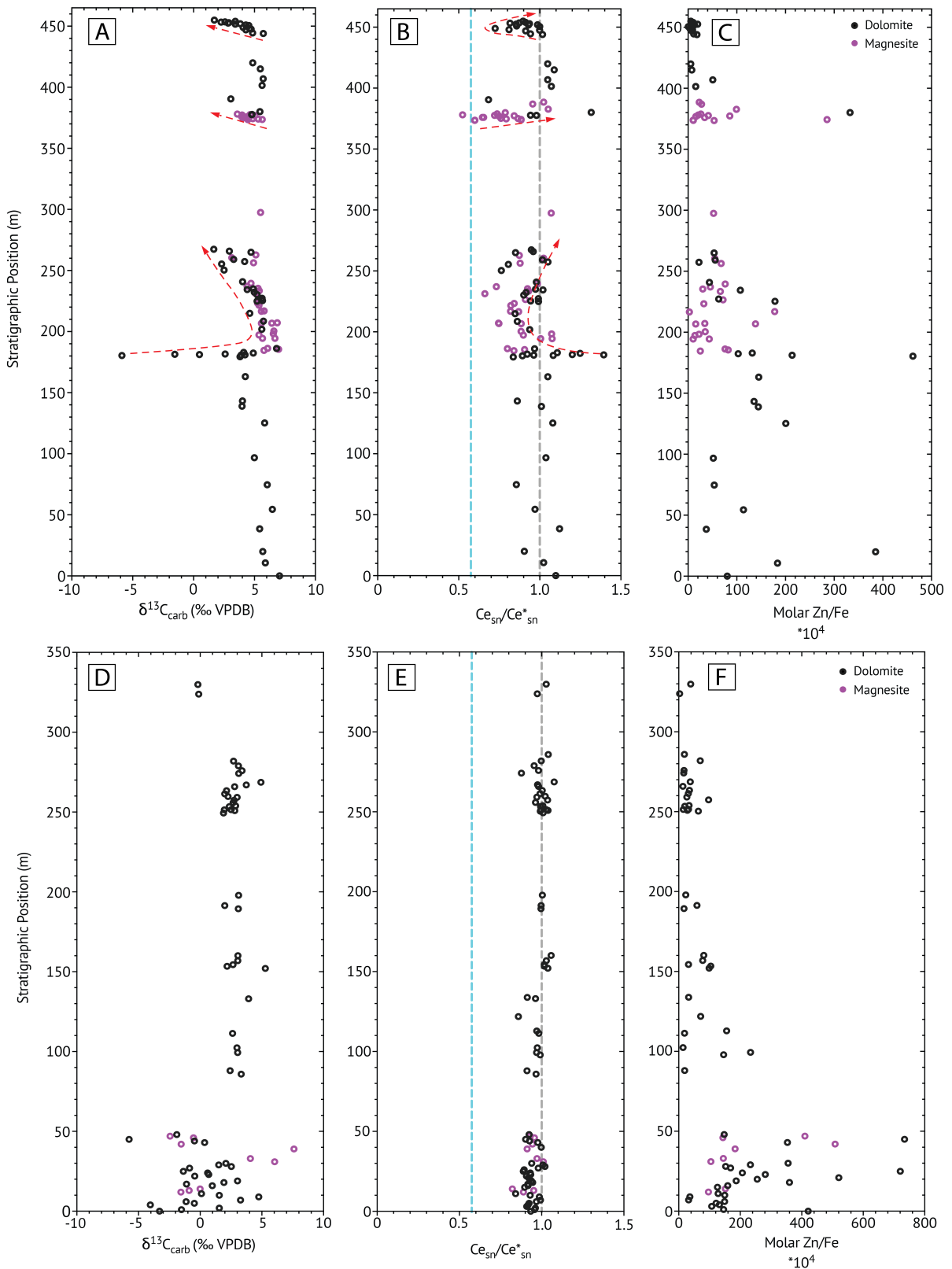


Figure 8: $\delta^{13}\text{C}$, Ce/Ce* and Zn/Fe molar ratios for Willouran Ranges' Termination Hill Skillogalee carbonates (A, B & C), and Gammon Ranges Skillogalee carbonates (D, E & F). The dashed blue line in Ce/Ce* plots represents a bootstrapped average for modern day surface waters, equating to 0.575 (Nozaki & Zhang, 1995). Dashed red arrows in plots A and B mark the dominant trends up section.

PALEOREDOX OF THE MYRTLE SPRINGS FORMATION – COPLEY

The Myrtle Springs Formation displays predominantly negative Ce/Ce*, with values trending close to modern day surface waters (*Fig. 9*). The cross relationship between Ce/Ce* and Pr/Pr* reinforces this oxic interpretation showing a strong correlation that trends into the field considered to represent an unequivocal negative Ce/Ce* (*Fig. 10*). Interpretations of marine oxygenation are, however, subdued with Zn/Fe ratios displaying consistently mild values, suggestive of more dysoxic conditions. A lack of correlation between Ce/Ce* and $\delta^{13}\text{C}$ as well as Zn/Fe and $\delta^{13}\text{C}$, suggests that free oxygen content is not directly coupled to f_{org} throughout this interval.

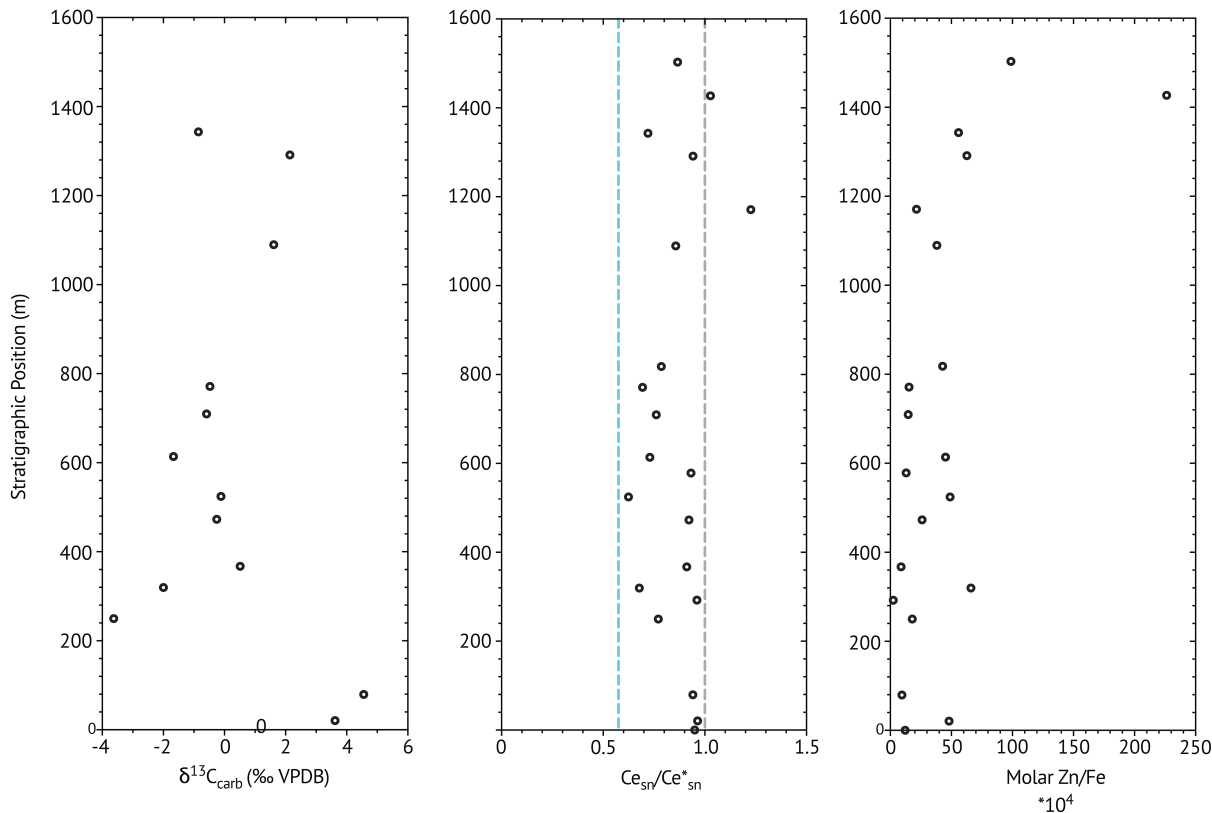


Figure 9: $\delta^{13}\text{C}$, Ce/Ce* and Zn/Fe molar ratios for Willouran Ranges Myrtle Springs Formation, exposure at Copley. The dashed blue line in Ce/Ce* plots represents a bootstrapped average for modern day surface waters, equating to 0.575 (Nozaki & Zhang, 1995).

4.2.6 A LATE TONIAN PALEO-REDOX MODEL

Ce/Ce^* data provides a rigorous constraint between oxic and anoxic endmember environments. Cross plotting Ce/Ce^* with Pr/Pr^* confirms that Ce/Ce^* data identifies redox potential, and is not simply a function of large positive La/La^* . A kernel density estimation model of Ce/Ce^* and Pr/Pr^* data for Skillogalee and Myrtle Springs carbonates constrains paleoredox potential to mildly dysoxic conditions (*Fig. 10*). This interpretation is influenced by sampling density, length of each section sampled, and the distribution and number of sample section localities, however, may still serve as a general indicator of marine redox conditions prevailing during the Late Tonian. Since global $\delta^{13}\text{C}$ is represented throughout these Burra Group sediments, their concomitant redox potentials may therefore be extended to reflect the same regional scale marine paleo-redox state (i.e. mildly dysoxic).

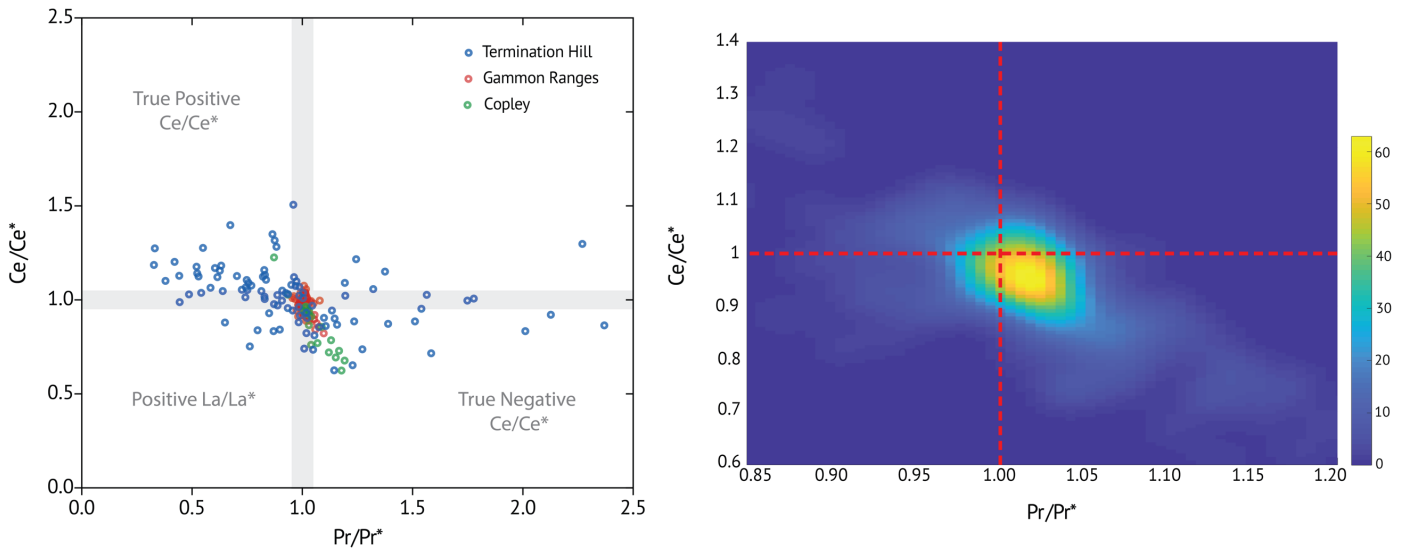


Figure 10: left; cross plot of Ce/Ce^* and Pr/Pr^* data for individual samples. Right; KDE index for Ce/Ce^* Pr/Pr^* cross plot data, with density units expressed as %.

4.3 REY interpretation for the Burra Group's marine setting

4.3.1 MARINE SETTING OF THE SKILLOGALEE FORMATION

Y/Ho ratios, or Y anomalies (Y^*), through the Skillogalee Formation at Termination Hill show a marked increase at precisely the interval where $\delta^{13}\text{C}$ shifts to coherent trends with respect to the global seawater $\delta^{13}\text{C}$ record, suggesting a change in environment to more open waters. Throughout this central interval Y^* oscillate between two general distributions, one approximately centred at 18 and the other at 52, with some samples attaining enrichments of up to 191. This reflects a very shallow marine environment that is in a dynamic state shifting between open and restricted marine environments, a consequence of minor relative sea-level change. A marked increase in Eu/Eu* coincides with a change to more open marine conditions, concordant with Y^* (Fig. 11) and $\delta^{13}\text{C}$ indicators. Seawater variation in Eu/Eu* may account for values up to 1.5 (Tostevin et al., 2016). Termination Hill marine carbonates, however, record significant Eu/Eu* reaching magnitudes of up to 3.6, strongly evincing that a hydrothermal source for marine waters was present during deposition (Meyer, Quicksall, Landis, Link, & Bostick, 2012).

Shale normalised Yb/Nd ratios quantify HREE enrichment relative to LREE. Seawater is characterised by HREE enrichment relative to LREE yielding large Yb/Nd ratios (Elderfield & Pagett, 1986). A positive correlation between Y^* and Yb/Nd ratios is expected for typical marginal marine and seawater environments. Throughout Termination Hill marine carbonates, however, Yb/Nd ratios not only decrease, but commonly yield values <1 , indicating HREE depletion relative to LREEs. Two scenarios are suggested to account for such shifts. Firstly, although riverine REE distributions vary with aeolian and sediment input, they typically display flat “continental type” shale normalised REY patterns, sometimes showing HREE depletion (Elderfield et al., 1990). A flux in riverine contribution to the water column may have caused typical seawater HREE

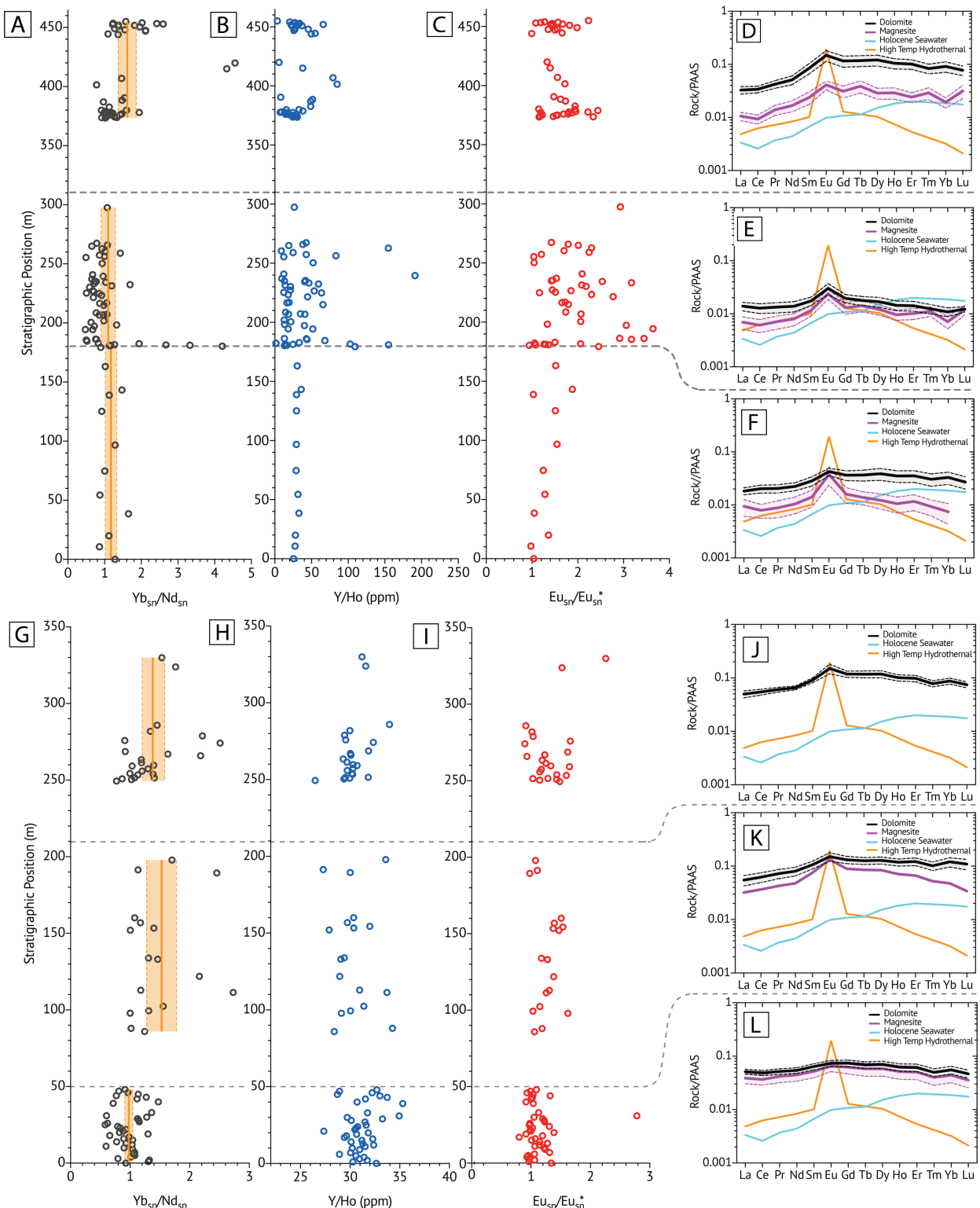


Figure 11: Plots A to F are hosted by Termination Hill Skillogalee carbonates in the Willouran Ranges S.A. Plots G to L are hosted by Gammon Ranges Skillogalee carbonates. Note that the intervals selected for REE plots are not stratigraphically equivalent between Termination Hill and Gammon Ranges sediments, but rather were selected based on marked changes in chemostratigraphy and REE interpretations that suggested discrete changes in marine environments. In REE distribution plots (D, E, F, & J, K, L) solid fill line for dolomite (black) and magnesites (purple) marks the bootstrapped average, with dotted lines above and below marking the 95% confidence interval. Also in these plots, Holocene seawater bootstrapped average multiplied by 10^4 (blue) (Webb & Kamber, 2000) is used so as to avoid anthropogenic influence, and high temperature hydrothermal seawater curve (orange) is the literature value (James et al., 1995) multiplied by 10^3 . The solid orange line in $\text{Yb}_{\text{Sr}}/\text{Nd}_{\text{Sn}}$ plots represent the bootstrapped average of the interval specified by the dashed grey lines, with the shaded orange area adjacent denoting the 95% confidence interval.

enrichment patterns to shift towards HREE depleted states. Secondly, the open marine reservoir may have had a large input from a hydrothermal source. Such likely explains the lack of correlation between Y^* and Yb/Nd ratios, accounts for the immediate appearance of significant Eu/Eu^* and would promote HREE depleted states. Termination Hill Skillogalee carbonates shift towards typical seawater REY distributions up section, recording a step increase in average Yb/Nd ratios, consistent with a transgressive sea-level rise throughout Burra Group sedimentation.

Gammon Ranges Skillogalee carbonates display flatter “continental type” patterns relative to coeval Willouran Ranges sediments, evincing a more marginal marine environment (Elderfield et al., 1990) with far more subdued (though still significant) Eu/Eu^* , indicative of regional mixing of hydrothermally affected waters. Y^* range between 26.4 and 35.3 suggesting a significant aeolian influence to the waterbody, exacerbated by a marginal setting (Dilek & Furnes, 2013; Elderfield et al., 1990). Less significant Eu/Eu^* through lower strata may suggest poorer mixing with hydrothermally affected waters, consistent with minor Y^* , flat REE patterns and highly evolved $^{87}Sr/^{86}Sr$ isotopic signatures that all imply a restricted to marginal marine setting. Mid-section Gammon Ranges Skillogalee and Willouran Ranges equivalents mark an increase in Yb/Nd ratios, suggesting a basin wide transgressive sea-level rise. In summary, previous interpretations that the Skillogalee Formation marine sediments were hosted in a shallow water system, with a very low paleoslope, shallowing towards the Gammon Ranges (Belperio, 1990; Murrell, 1977; Uppill, 1990), holds with REY interpretations, though with the additional insight that a major source of Eu was also present, likely from a hydrothermal flux into the basin. This may provide an alternate explanation for the source of Mg responsible for the pervasive deposition of sedimentary magnesites to the long-held analogy with the Coorong lakes in South Australia, in which ground water flux is used to account for increasing Mg/Ca ratios (Borch & Lock, 1979). A

hydrothermal source of Mg is an attractive suggestion given the correlation between magnesite and high temperature hydrothermal REY patterns (*Fig. 11*), particularly within the lower Skillogalee Formation sediments at Termination Hill.

4.3.2 MARINE SETTING OF THE MYRTLE SPRINGS FORMATION - COPLEY

Whilst a decreased abundance of desiccation structures, and an increased abundance of deeper marine sediments infer a deepening sequence for the Myrtle Springs Formation, REY distribution patterns show modest Y* that otherwise suggest a shallowing sequence (*Fig. 12*). A positive correlation between Y* and Eu/Eu*, both trending to smaller values in the lower Myrtle Springs Formation, is explained by a phase of sea-level regression and/or a flux of riverine or aeolian input that would “flatten” REY distributions, suppressing anomalous behaviours. Bootstrapped averages of Yb/Nd ratios display a stepped decrease throughout up section sediments, consistently yielding values <1, signifying HREE depletion relative to LREEs, and adopting a more hydrothermal REY distribution. This hydrothermal flux may reflect a phase of Torrensian rifting, concordant with previous interpretations that sedimentation of Burra Group sediments were simultaneous with early phases of Torrensian rifting (Preiss, 2000). The deepening of the marine environment up section is supported both by thickening and increased frequency of thinly laminated silt horizons, as well as a marked increase in Y*.

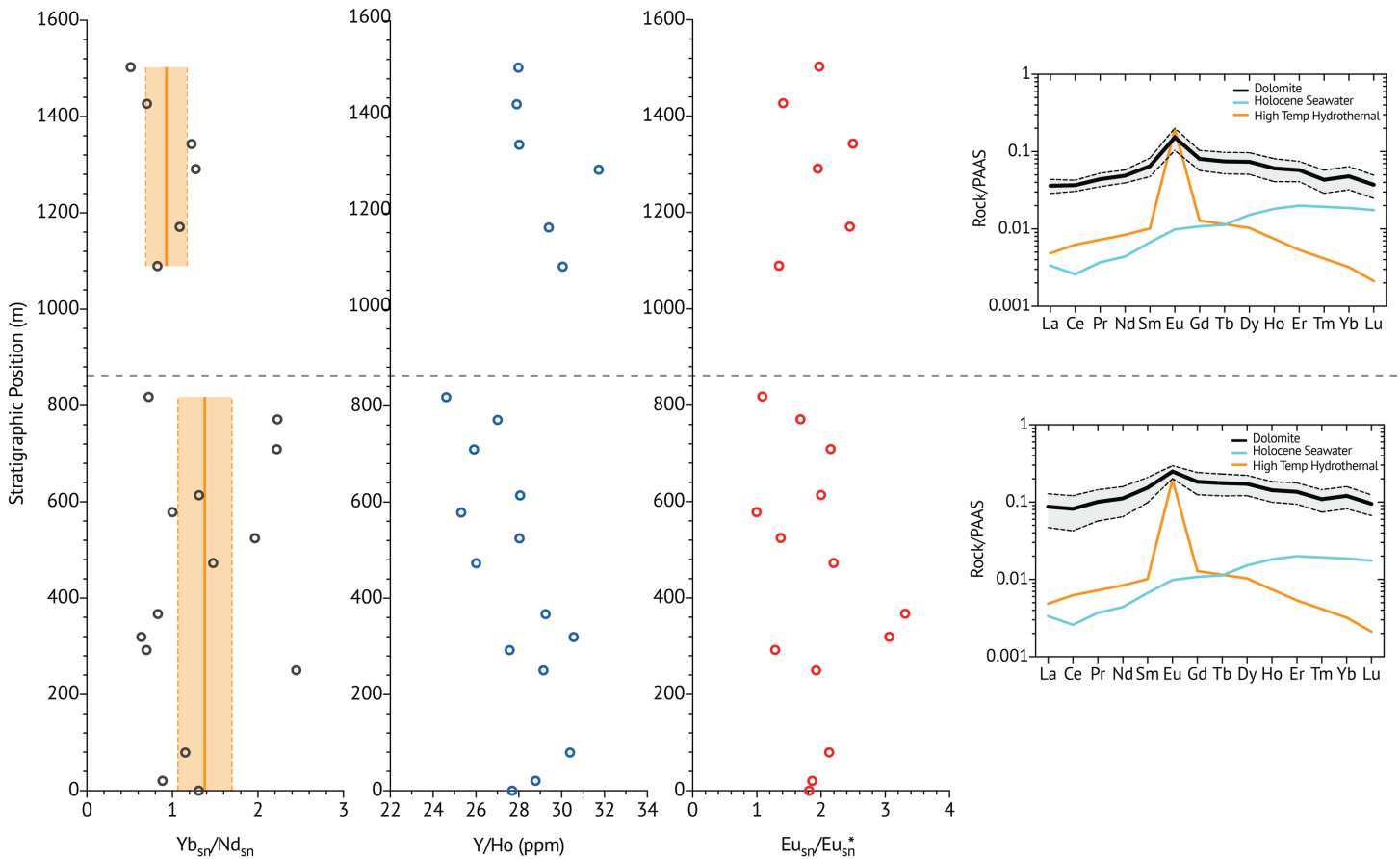


Figure 12: All plots denoting Myrtle Springs Formation sediments, outcropped at Copley S.A. In plots D & E the solid fill line for dolomite (black) marks the bootstrapped average, with dotted lines above and below marking the 95% confidence interval. Holocene seawater bootstrapped average multiplied by 10^4 (blue) is used so as to avoid anthropogenic influence (Webb & Kamber, 2000). High temperature hydrothermal seawater curve multiplied by 10^3 (orange) (James, Elderfield, & Palmer, 1995). The solid orange line in $\text{Yb}_{\text{Sn}}/\text{Nd}_{\text{Sn}}$ plot marks the bootstrapped average of the interval specified by the dashed grey line, with orange area adjacent denoting the 95% confidence interval.

4.3.3 IMPLICATIONS OF A HYDROTHERMAL FLUX THROUGH BURRA GROUP MARINE WATERS

The Adelaide Rift Complex (ARC) is composed of extensive, deeply subsided sedimentary successions, recording a series of regionally extensive mafic volcanism (Jenkins, 1990), accounted for in the global record of relative LIP abundances (*Fig 13*), showing a peak between ca. 850 Ma and ca. 750 Ma; herein overlapping with Burra Group sedimentation. This peak reflects the large Gairdner-Willouran LIP, responsible for the mafic magmatism throughout the Willouran Province.

The Willouran Province contains mafic dykes, sills and pervasive continental flood basalts that spread across the Gawler Craton, the Musgrave block in south central Australia, the ARC and the Amadeus Basin (Wang, Li, Li, Liu, & Yang, 2010), emplaced between ca. 830 Ma \pm 50 Ma (Compston, Crawford, & Bofinger, 1966) and ca. 802 Ma \pm 10 Ma (Fanning et al., 1986), though these ages remain poorly constrained. Volcanism kept pace with subsidence, recognised by lava plateaux complexes, and was sustained until the cessation of eruption with subsequent major graben subsidence (Hilyard, 1990). Rift valleys formed, where contemporaneous sedimentation of the Curdimurka Subgroup and Burra Group sequences subsequently occurred (Preiss, 2000). Incessant thermal heating accounting for the longevity of marine Eu/Eu* likely reflects long-standing mafic magmatism, associated with early ARC rift phases. Hydrothermal alteration is documented throughout the Willouran mafic volcanics (Crawford & Hilyard, 1990), further accrediting the Eu/Eu* source to a hydrothermal flux. Though it is difficult to predict exactly which rift phase the documented Eu/Eu*'s pertain towards, it still remains that a magmatic flux was

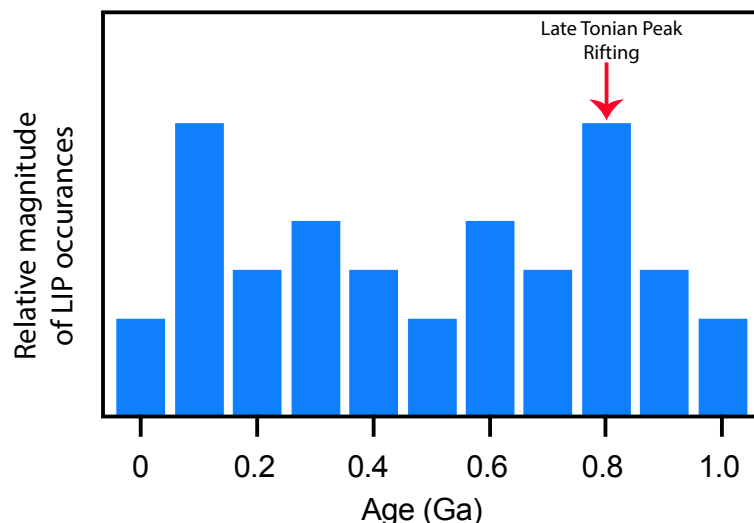


Figure 13: Relative abundance of Large Igneous Province (LIP) abundances through time. LIP record compiled from (Ernst & Buchan, 2001). Red arrow marks a peak in the Late Tonian, associated with the emplacement of the Gairdner-Willouran LIP.

present through Burra Group sedimentation, induced, no doubt, by the larger scale breakup of Rodinia. The confirmation of hydrothermal sources throughout Burra Group sedimentation provides three major insights; firstly, though eruption of vast continental flood basalts (predominantly) ended with the cessation of the Wooltana basalts, magmatic activity remained active through Burra Group sedimentation. Secondly, hydrothermal influence is recognised throughout more open marine environments, suggestive of regional scale magmatic flux. Thirdly, hydrothermal fluid sources passing through underlying thick basalt sequences provide both a means of mobility and a rich source of Mg that could account for the widespread precipitation of sedimentary magnesite.

4.3.4 OVERWHELMING INFLUENCE OF RIFTING ON MARINE WATERS

The second rift phase of the ARC (S-S Willouran 2), emplaced the Gairdner Willouran large igneous province (LIP) at ca. 825 Ma (Ernst, Wingate, Buchan, & Li, 2008), hosting the thick Wooltana basalts. Some basaltic flows are reported through the Rhynie sandstone, suggesting that mafic volcanism was still prevalent during the Late Tonian (Preiss, 1987). Mafic volcanism brings with it a suite distinctive geochemical features that differ from average continental crust, including a drive towards primitive Nd isotopic compositions (Cox et al., 2016). Since the residence time of Nd is much less than the average mixing time of the ocean, interpretation of Nd isotopes typically only extends to a local context. The steady increase in ε Nd through the Tonian, however, is replicated globally, associated with the weathering of vast continental flood basalts (Cox et al., 2016; Halverson et al., 2010). Skillogalee Formation marine carbonates show extraordinary correlation with global average ε Nd signatures (*Fig. 14*), suggesting that global seawater was also perturbed by the same primitive sources as that of marine shales. The explanation accounting for

trends in Skillogalee ε Nd signatures is the same as the explanation behind the secular trend observed in fine grained shales; the weathering of globally abundant continental flood basalts. The ca. 830 Ma Willouran and Guibei LIP's in Australia and South China were major sources of mafic volcanism associated with the breakup of Rodinia, covering a combined area of $\sim 106 \text{ km}^2$

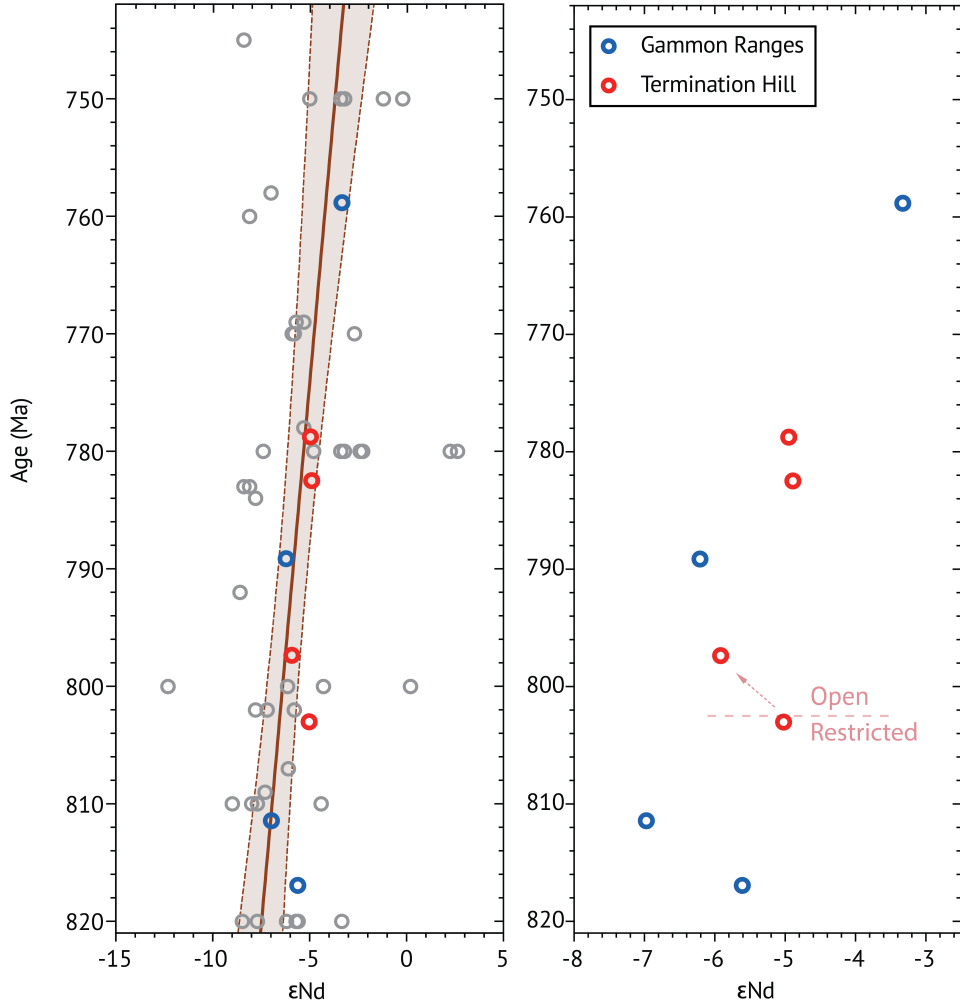


Figure 14: Left; brown solid line marks the average linear regression of ε Nd in ambient seawater, generated from mudstone data (grey) through the Late Tonian (Barovich & Foden, 2000; Chen & Jahn, 1998; Cox et al., 2016; Li & McCulloch, 1996; Wade, Hand, & Barovich, 2005; Wang, Li, Li, Li, & Zhang, 2011; Zhao, McCulloch, & Bennett, 1992). The adjacent brown shaded area and dashed brown line mark the 95% confidence interval of the linear regression. In both plots red denotes Termination Hill and blue denotes Gammon Ranges data. Right; A shift towards mean seawater ε Nd throughout Termination Hill Skillogalee carbonates with a change in marine setting to more open conditions is marked by red indicators.

(Cox et al., 2016; Ernst et al., 2008). Erosion of these continental flood basalts supply marine sediments with a prominent source of isotopically primitive Nd, thus shifting average ε Nd values in the sediments towards the detrital basalt primitive endmember. Leaching of these isotopically primitive sediments into the water column drives seawater ε Nd towards this same primitive endmember (*Fig. 14*). Basalts display rapid weatherability, with erosion rates some 5 to 10 times greater than felsic continental crust (White & Brantley, 1995). Prominent emplacement of continental flood basalts caused a concomitant draw down of CO₂, through intensified silicate weathering, yielding major implications on the Earth system (Cox et al., 2016).

4.3.5 GLOBAL AND LOCAL VARIATIONS IN ORGANIC CARBON BURIAL

Isotopic fractionation of ¹³C varied widely throughout the Neoproterozoic with average rates of f_{org} significantly higher relative to carbonate carbon burial (f_{carb}) (Derry, Kaufman, & Jacobsen, 1992; Kaufman & Knoll, 1995). Prolonged enrichment of f_{org} is accounted for by the breakup of Rodinia extending continental margins that promoted accumulation of chemoautotrophic products (Hayes et al., 1999), whilst the weathering of pervasive continental flood basalts also fuelled primary productivity through enhanced nutrient supply (Cox et al., 2016; Hoffman et al., 2017). If a constant isotopic composition of C entering the oceans is assumed, secular variations in $\delta^{13}\text{C}$ may be interpreted as a direct result of variations in the relative rates of organic carbon burial (Broecker, 1970). Like the global record, Skillogalee and Myrtle Springs carbonates display significant contributions from f_{org} (*Fig. 15*), holding important ramifications for the drawdown of CO₂ and broader scale descent into Cryogenian glaciations (Hoffman et al., 1998).

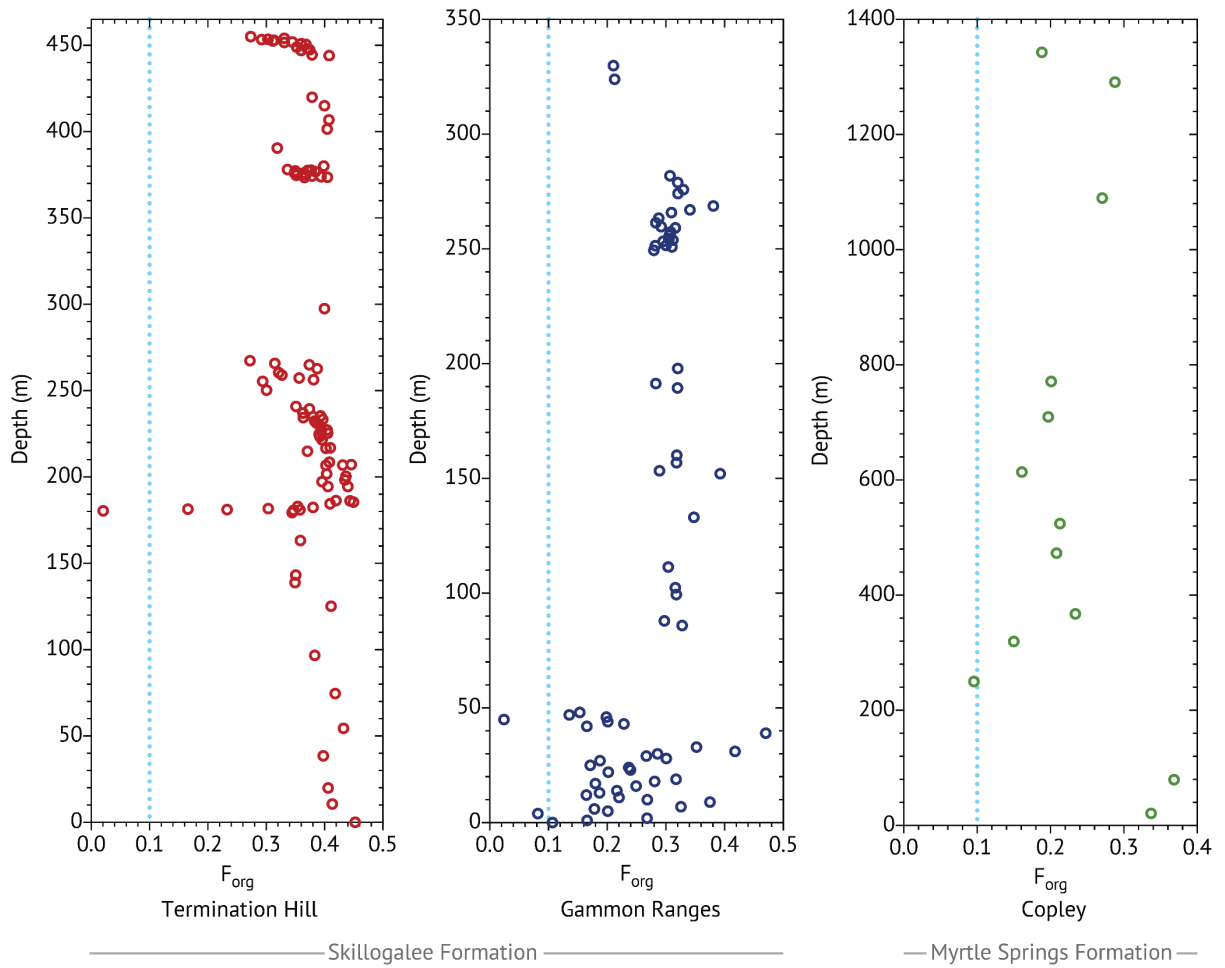


Figure 15: Modelled organic carbon burial (f_{org}), derived from (Hayes, Strauss, & Kaufman, 1999). Dashed blue line represents modern oceanic f_{org} (Schlünz & Schneider, 2000).

5 CONCLUSION

The Skillogalee and Myrtle Springs Formation's seawater chemistry reinforce sedimentological and paleoenvironmental interpretations, suggesting a shallow water system throughout, with frequent flooding of a series of shallow perennial and small ephemeral lagoons containing exposed mudflats, occurring throughout early phases of sedimentation. An overarching transgressive sea-level rise was felt throughout the basin, though shallow water conditions

remained, suggesting a low paleoslope environment that was sustained through rapid sedimentation.

The redox state throughout the Skillogalee and Myrtle Springs Formation's marine waters was largely dysoxic, though phases of anoxia are also felt, particularly throughout the lower Skillogalee.

Elevated Eu/Eu* infer a significant hydrothermal flux to the rift basin with a shift to more open marine waters. Such is indicative of a regional scale magmatic flux that endured long after the cessation of mafic eruption. A flux of hydrothermal fluids through underlying basalts provide both a means of mobility and a rich source of Mg, perhaps accounting for the enigmatic widespread deposition of sedimentary magnesites throughout the Skillogalee Formation.

A mafic weathering flux, concordant with global interpretations, is reflected throughout Burra Group marine chemistry, also coinciding with high levels of organic carbon burial. The break-up of Rodinia and detailed drawdown of CO₂ instated global ice-house conditions that continued to ensnare the Earth for some 58 million years. The South Australian paleoenvironment during the late Tonian contributed to this phenomenon.

ACKNOWLEDGMENTS

I would like to thank Grant Cox for supervising this project and for reviewing this thesis. Thanks to Sarah Gilbert and Adelaide Microscopy for assistance with, and the use of, the solution ICP-MS. I would like to acknowledge David Bruce's contributions regarding his technical assistance with the laboratory work in this project.

6 APPENDIX

Implications on the use of Ce/Ce* and Zn/Fe redox proxies

The absolute contribution of free oxygen on Ce/Ce* is difficult to predict due to numerous complicating processes including the scavenging of Ce⁴⁺ from siderophiles (Kraemer, Kopf, & Bau, 2015), microbial activity catalysing the oxidation of Ce³⁺ (Moffett, 1990), effects of changes in pH (Brookins, 1989), water depth (Piepgras & Jacobsen, 1992) and the age of the waterbody, all contributing to variations in shale normalised Ce/Ce* (German & Elderfield, 1990).

Caution must be taken when using Zn/Fe ratios, with Fe containing greater partition coefficients during diagenesis (Brand & Veizer, 1980) and labile iron sourced from eroding continents cycling back to a soluble phase in reducing margin sediments during diagenesis (Raiswell et al., 2006); both contributing to a decrease in the Zn/Fe ratio observed in carbonates (X. Liu et al., 2014).

Calculation of f_{org}

f_{org} was calculated through a simple carbon isotope mass balance approach, using the formula;

$$f_{org} = [(\delta^{13}\text{C}_{org} + \Delta_{org-carb}) + ^{13}\text{C}_{in}] / \Delta_{org-carb}$$
 .(Kump et al., 2011)

Parameters included a variable volcanic input of carbon isotopic composition, ranging between -5‰ to -8‰ (Javoy et al., 1986), whilst a fractionation factor between organic and inorganic carbon was assumed to be ~ 28‰ to 32‰ (Hayes et al., 1999). A Monte Carlo simulation approach was used to account for variability in both $\delta^{13}\text{C}_{in}$ and $\Delta_{org-carb}$.

Solution ICP absolute concentration outputs

Table 5: Relating to all sample element concentration tables (below); All values are expressed in ppm concentration. Mg/Ca and Zn/Fe ratios are molar ratios. Yb/Ho ratios are raw concentration ratios. Both Yb and Nd species in Yb/Nd ratios are normalised to PAAS. Note: “BDL” indicates the element concentration fell below the detection limit.

Sample ID	WR101	WR102	WR103	WR104	WR105	WR106	WR107
[Li]	1.924	1.061	1.199	2.113	33.995	0.969	0.587
[Mg]	46583.409	48830.840	40765.001	20844.460	11435.154	44200.413	37681.662
[Al]	213.704	123.867	158.343	633.616	31584.353	74.913	116.590
[Si]	242.862	165.796	140.589	487.119	14285.092	93.252	119.066
[P]	2.212	1.544	3.209	31.705	55.807	2.474	15.526
[K]	87.077	64.299	51.221	67.747	17439.086	42.400	16.608
[Ca]	76483.402	80118.677	66496.850	61159.118	BDL	72109.664	69693.939
[Sc]	2.984	1.525	2.470	2.493	6.261	1.664	1.052
[V]	0.960	0.217	1.395	3.157	86.637	0.697	1.503
[Mn]	707.536	264.256	526.753	403.609	2082.542	409.956	438.471
[Fe]	5480.434	2629.994	4056.718	3359.289	170641.544	2859.756	5799.537
[Co]	3.799	2.169	2.385	0.669	80.185	0.926	2.229
[Ni]	204.769	60.714	56.636	5.540	5859.625	22.644	5.776
[Zn]	7.253	14.882	4.027	6.208	45.074	20.360	5.656
[Rb]	0.639	0.547	0.189	0.634	55.166	0.305	0.132
[Sr]	121.010	119.164	83.522	226.092	55.727	132.081	123.373
[Y]	3.617	1.624	1.187	2.536	5.328	2.014	1.853
[Zr]	0.054	0.026	0.038	0.346	0.496	0.030	0.023
[Nb]	0.042	0.035	BDL	BDL	BDL	BDL	BDL
[Mo]	BDL	BDL	BDL	BDL	BDL	BDL	BDL
[La]	2.072	1.390	0.857	0.751	7.246	2.495	1.877
[Ce]	4.724	3.163	1.872	1.405	14.892	3.700	3.807
[Pr]	0.630	0.409	0.244	0.233	1.751	0.631	0.491
[Nd]	2.589	1.651	0.964	1.096	6.471	2.445	1.888
[Sm]	0.697	0.364	0.254	0.384	1.264	0.536	0.461
[Eu]	0.277	0.142	0.113	0.181	0.354	0.352	0.321
[Gd]	0.727	0.347	0.243	0.504	1.303	0.536	0.443
[Tb]	0.123	0.051	0.040	0.083	0.187	0.074	0.065
[Dy]	0.675	0.303	0.224	0.466	0.954	0.384	0.377
[Ho]	0.131	0.056	0.039	0.087	0.193	0.066	0.063
[Er]	0.363	0.151	0.106	0.247	0.481	0.182	0.167
[Tm]	0.047	0.022	0.013	0.036	0.072	0.022	0.023
[Yb]	0.296	0.128	0.097	0.235	0.395	0.136	0.137
[Lu]	0.042	0.018	0.013	0.044	0.054	0.019	0.019
[Pb]	0.475	0.237	0.493	0.341	45.531	0.935	0.151
Ce/Ce*	0.951	0.965	0.941	0.771	0.961	0.678	0.912
Pr/Pr*	1.023	1.017	1.031	1.069	1.014	1.192	1.041
Eu/Eu*	1.817	1.863	2.127	1.923	1.285	3.066	3.312
Mg/Ca	1.004	1.005	1.011	0.562	BDL	1.011	0.891
Zn/Fe	0.001	0.005	0.001	0.002	0.000	0.007	0.001
Y/Ho	27.693	28.784	30.396	29.159	27.576	30.563	29.252
Yb/Nd	1.308	0.887	1.152	2.450	0.698	0.638	0.831

Sample ID	WR108	WR109	WR110	WR111	WR112	WR113	WR114
[Li]	3.466	2.389	60.967	1.854	8.732	3.823	40.588
[Mg]	39295.607	23486.460	29022.423	33701.224	19164.741	29837.885	19025.465
[Al]	1117.080	1126.856	26264.617	911.124	6118.022	2306.638	26765.021
[Si]	1180.097	775.432	21427.390	839.375	2257.228	1981.851	19501.356
[P]	7.723	6.810	45.534	4.280	9.364	2.455	119.679
[K]	173.250	244.836	5316.353	92.225	1065.982	192.847	6150.838
[Ca]	60251.673	34652.614	#VALUE!	54588.708	28464.454	47854.060	#VALUE!
[Sc]	3.861	3.743	9.733	4.002	5.241	7.497	8.875
[V]	0.923	1.661	8.357	0.148	5.750	0.740	13.523
[Mn]	255.098	64.091	76.696	416.857	409.592	269.118	284.741
[Fe]	2282.672	954.301	18940.207	1073.789	7965.194	3246.545	29659.933
[Co]	0.812	0.239	1.942	6.215	3.760	0.675	7.992
[Ni]	8.810	12.728	43.048	10.077	130.647	37.656	45.266
[Zn]	6.532	5.465	30.169	5.339	13.086	5.234	150.772
[Rb]	2.038	1.511	24.637	0.432	6.877	0.740	30.490
[Sr]	132.997	76.563	11.251	96.849	54.708	67.806	23.406
[Y]	3.487	3.180	8.746	3.580	2.819	4.063	5.425
[Zr]	0.279	0.209	2.721	0.111	0.208	0.228	1.736
[Nb]	BDL						
[Mo]	BDL						
[La]	1.650	0.952	9.344	1.692	1.239	1.176	7.712
[Ce]	3.746	1.439	19.507	3.105	2.052	2.037	13.615
[Pr]	0.529	0.295	2.478	0.565	0.310	0.387	2.055
[Nd]	2.272	1.406	9.923	2.445	1.399	1.793	7.842
[Sm]	0.626	0.451	2.266	0.748	0.420	0.617	1.600
[Eu]	0.305	0.147	0.469	0.327	0.223	0.242	0.356
[Gd]	0.669	0.556	2.125	0.779	0.556	0.731	1.465
[Tb]	0.112	0.098	0.328	0.121	0.092	0.125	0.219
[Dy]	0.685	0.590	1.800	0.698	0.561	0.754	1.172
[Ho]	0.134	0.113	0.345	0.128	0.109	0.150	0.220
[Er]	0.366	0.302	0.978	0.354	0.295	0.416	0.607
[Tm]	0.046	0.043	0.138	0.047	0.042	0.057	0.081
[Yb]	0.294	0.242	0.869	0.280	0.272	0.350	0.496
[Lu]	0.042	0.037	0.118	0.042	0.043	0.051	0.065
[Pb]	0.469	0.267	0.276	0.402	1.236	0.131	0.495
Ce/Ce*	0.922	0.624	0.932	0.730	0.761	0.694	0.786
Pr/Pr*	1.031	1.178	1.013	1.167	1.040	1.152	1.130
Eu/Eu*	2.198	1.371	0.997	2.000	2.151	1.681	1.086
Mg/Ca	1.075	1.117	BDL	1.018	1.110	1.028	BDL
Zn/Fe	0.002	0.005	0.001	0.005	0.001	0.002	0.004
Y/Ho	26.014	28.035	25.314	28.066	25.913	27.014	24.612
Yb/Nd	1.477	1.967	1.000	1.311	2.221	2.229	0.723

Sample ID	WR115	WR116	WR117	WR118	WR119	WR120	THM 401
[Li]	1.531	1.834	0.896	0.975	1.705	3.241	2.834
[Mg]	42387.729	44540.839	42719.615	40063.884	1121.091	BDL	42981.574
[Al]	174.351	22.520	147.104	226.355	3650.041	4361.110	31.405
[Si]	189.553	48.995	198.673	225.557	1261.082	2168.554	71.187
[P]	44.313	24.234	30.240	10.311	28.287	23.831	12.373
[K]	128.566	21.201	29.442	133.065	337.372	737.342	6.240
[Ca]	68651.723	72404.353	73580.186	77236.011	24665.063	26014.019	64530.052
[Sc]	1.149	0.439	0.442	3.122	0.229	0.497	0.318
[V]	2.753	2.709	0.188	1.108	3.004	8.276	1.324
[Mn]	261.931	321.390	905.694	185.013	42.009	33.151	46.316
[Fe]	1042.782	2316.286	682.161	1104.248	176.643	562.526	430.913
[Co]	0.701	0.457	3.337	1.511	0.442	0.572	0.258
[Ni]	2.940	12.919	7.903	253.293	527.628	268.311	56.391
[Zn]	4.700	5.510	4.994	7.158	4.745	6.606	4.079
[Rb]	0.337	0.037	0.185	1.765	1.829	4.730	0.068
[Sr]	59.042	121.243	164.137	166.170	97.615	47.834	311.601
[Y]	2.096	1.237	3.068	2.392	1.383	0.688	0.807
[Zr]	0.091	0.024	0.033	0.046	0.287	0.095	0.013
[Nb]	BDL	BDL	BDL	BDL	BDL	BDL	0.168
[Mo]	BDL	BDL	BDL	BDL	BDL	BDL	0.170
[La]	1.985	1.001	1.464	1.287	0.889	1.443	0.644
[Ce]	3.877	2.703	3.309	2.225	2.368	2.510	1.630
[Pr]	0.545	0.257	0.445	0.391	0.315	0.308	0.180
[Nd]	2.087	1.034	1.907	1.771	1.553	1.147	0.681
[Sm]	0.453	0.236	0.503	0.491	0.395	0.207	0.143
[Eu]	0.131	0.131	0.217	0.273	0.122	0.080	0.033
[Gd]	0.456	0.263	0.536	0.531	0.414	0.172	0.151
[Tb]	0.068	0.041	0.083	0.084	0.054	0.024	0.024
[Dy]	0.369	0.236	0.494	0.463	0.281	0.133	0.158
[Ho]	0.070	0.042	0.097	0.085	0.050	0.025	0.032
[Er]	0.191	0.126	0.256	0.222	0.134	0.072	0.087
[Tm]	0.024	0.014	0.034	0.031	0.018	0.008	0.013
[Yb]	0.151	0.098	0.213	0.190	0.096	0.051	0.076
[Lu]	0.021	0.012	0.030	0.026	0.013	0.008	0.010
[Pb]	10.447	0.461	0.025	0.235	0.617	0.252	0.405
Ce/Ce*	0.857	1.226	0.942	0.721	1.028	0.866	1.099
Pr/Pr*	1.088	0.872	1.007	1.121	0.935	1.030	0.974
Eu/Eu*	1.347	2.450	1.951	2.496	1.411	1.972	1.035
Mg/Ca	1.018	1.014	0.957	0.855	0.075	0.000	1.098
Zn/Fe	0.004	0.002	0.006	0.006	0.023	0.010	0.008
Y/Ho	30.055	29.408	31.738	28.028	27.902	27.985	25.463
Yb/Nd	0.826	1.086	1.275	1.225	0.703	0.513	1.284

Sample ID	THM 402	THM 403	THM 404	THM 405	THM 406	THM 407	THM 408
[Li]	3.080	2.256	3.431	3.685	5.440	1.992	4.662
[Mg]	45678.661	48105.957	40922.423	49501.658	47107.750	50280.913	50545.128
[Al]	44.286	64.890	440.832	28.263	150.401	75.542	48.254
[Si]	77.851	149.992	532.766	93.775	280.242	147.921	124.829
[P]	13.570	10.176	13.492	10.860	19.176	20.075	28.340
[K]	7.614	11.942	108.096	9.979	8.301	13.377	10.040
[Ca]	69408.782	73061.137	62770.885	77837.932	71296.781	78041.047	78258.493
[Sc]	0.139	0.460	1.276	0.091	0.209	0.185	0.146
[V]	3.100	1.060	1.383	0.751	1.282	2.752	0.936
[Mn]	25.866	72.613	175.108	37.026	61.027	72.001	22.313
[Fe]	188.338	333.975	1395.104	219.802	565.661	578.100	108.842
[Co]	0.025	0.164	0.879	0.153	0.092	0.038	0.120
[Ni]	2.701	2.242	154.501	7.331	3.320	1.212	1.870
[Zn]	4.148	15.128	5.490	3.001	3.542	3.498	2.735
[Rb]	0.087	0.139	0.565	0.086	0.085	0.107	0.061
[Sr]	191.516	363.371	179.848	264.743	199.363	138.085	224.702
[Y]	0.593	1.430	2.178	0.669	0.859	1.059	0.677
[Zr]	0.011	BDL	0.153	BDL	0.048	0.062	BDL
[Nb]	0.107	0.079	0.068	0.047	0.047	BDL	BDL
[Mo]	0.089	BDL	BDL	BDL	BDL	BDL	BDL
[La]	0.768	1.120	0.952	0.871	0.800	0.824	0.863
[Ce]	1.674	2.445	2.578	1.816	1.555	1.904	1.952
[Pr]	0.184	0.345	0.293	0.213	0.218	0.216	0.200
[Nd]	0.671	1.304	1.161	0.737	0.857	0.786	0.731
[Sm]	0.125	0.293	0.331	0.143	0.181	0.161	0.135
[Eu]	0.025	0.084	0.076	0.037	0.044	0.055	0.043
[Gd]	0.117	0.285	0.346	0.127	0.149	0.169	0.129
[Tb]	0.019	0.045	0.061	0.019	0.024	0.027	0.019
[Dy]	0.104	0.278	0.350	0.120	0.148	0.159	0.111
[Ho]	0.021	0.051	0.066	0.021	0.029	0.036	0.023
[Er]	0.055	0.139	0.180	0.063	0.088	0.102	0.064
[Tm]	0.007	0.020	0.026	0.008	0.013	0.015	0.010
[Yb]	0.051	0.127	0.168	0.056	0.075	0.089	0.059
[Lu]	0.007	0.017	0.023	0.007	0.010	0.011	0.008
[Pb]	0.219	0.482	0.894	0.603	0.224	0.062	0.089
Ce/Ce*	1.024	0.904	1.122	0.970	0.855	1.038	1.081
Pr/Pr*	0.987	1.098	0.963	1.045	1.076	1.003	0.951
Eu/Eu*	0.976	1.359	1.052	1.283	1.246	1.547	1.511
Mg/Ca	1.085	1.086	1.075	1.049	1.089	1.062	1.065
Zn/Fe	0.018	0.039	0.004	0.011	0.005	0.005	0.020
Y/Ho	27.678	28.054	32.939	31.629	29.132	29.283	29.558
Yb/Nd	0.862	1.117	1.654	0.874	1.005	1.291	0.921

Sample ID	THM 409	THM 410	THM 411	THM 201	THM 202	THM 203	THM 204
[Li]	3.821	2.327	4.066	5.558	0.735	6.525	0.547
[Mg]	47761.558	45969.408	47263.471	58271.429	59113.572	55334.794	28151.962
[Al]	39.271	37.032	47.142	BDL	BDL	BDL	BDL
[Si]	76.796	86.865	108.926	71.074	BDL	73.106	BDL
[P]	19.301	13.869	13.403	44.772	BDL	BDL	BDL
[K]	10.314	10.644	3.602	4.279	BDL	7.005	
[Ca]	76659.804	71702.021	72524.726	96026.346	104026.849	93535.750	56065.451
[Sc]	0.407	0.127	0.040	0.051	#VALUE!	0.169	#VALUE!
[V]	2.757	2.135	2.455	1.591	0.604	1.140	1.917
[Mn]	24.435	31.090	27.587	36.340	165.965	22.384	66.379
[Fe]	206.298	249.246	137.033	223.472	84.987	118.573	3753.604
[Co]	0.122	0.059	0.093	2.820	1.847	0.562	129.606
[Ni]	1.176	1.468	7.725	1.413	4.545	BDL	51.238
[Zn]	3.543	4.018	2.387	BDL	4.709	BDL	BDL
[Rb]	0.103	0.102	0.023	BDL	BDL	BDL	BDL
[Sr]	304.933	202.321	235.802	292.807	123.327	389.456	136.829
[Y]	1.160	0.841	0.375	1.585	0.644	0.368	2.074
[Zr]	0.023	BDL	0.016	BDL	BDL	BDL	BDL
[Nb]	BDL						
[Mo]	BDL						
[La]	1.010	0.685	0.336	0.642	0.323	0.782	0.287
[Ce]	2.286	1.254	0.718	1.028	0.631	1.866	0.605
[Pr]	0.268	0.164	0.074	0.124	0.082	0.200	0.073
[Nd]	1.008	0.563	0.295	0.442	0.372	0.707	0.325
[Sm]	0.218	0.131	0.057	0.098	0.101	0.149	0.075
[Eu]	0.047	0.050	0.020	0.050	0.024	0.032	0.025
[Gd]	0.209	0.118	0.066	0.091	0.139	0.127	0.100
[Tb]	0.036	0.019	0.009	0.018	0.026	0.019	0.016
[Dy]	0.214	0.121	0.052	0.064	0.186	0.128	0.068
[Ho]	0.039	0.023	0.012	0.014	0.049	0.023	0.013
[Er]	0.122	0.072	0.032	0.040	0.145	0.074	0.038
[Tm]	0.018	0.011	0.005	0.006	0.022	0.012	0.008
[Yb]	0.099	0.073	0.026	0.035	0.137	0.070	0.033
[Lu]	0.013	0.010	0.004	BDL	0.020	0.009	BDL
[Pb]	0.558	0.193	0.106	BDL	0.402	BDL	1.038
Ce/Ce*	1.010	0.861	1.049	0.836	0.893	1.083	0.963
Pr/Pr*	1.004	1.106	0.909	1.050	0.959	0.992	0.932
Eu/Eu*	1.031	1.883	1.519	2.456	0.941	1.080	1.362
Mg/Ca	1.027	1.057	1.074	1.000	0.937	0.975	0.828
Zn/Fe	0.014	0.014	0.015	BDL	0.046	BDL	BDL
Y/Ho	29.459	35.949	30.474	109.365	13.240	16.311	155.126
Yb/Nd	1.127	1.473	1.017	0.896	4.209	1.135	1.163

Sample ID	THM 205	THM 206	THM 207	THM 208	THM 412	THM 209	THM 210
[Li]	0.649	1.230	7.087	4.231	1.156	2.742	5.853
[Mg]	50941.892	48723.578	59674.030	53185.935	54388.376	101231.088	104042.693
[Al]	BDL	BDL	BDL	BDL	11.921	BDL	BDL
[Si]	BDL	BDL	163.341	BDL	46.304	BDL	133.705
[P]	BDL	BDL	BDL	BDL	15.745	BDL	BDL
[K]	BDL	BDL	21.303	BDL	1.654	BDL	7.540
[Ca]	87761.374	82269.746	97423.282	85933.495	82364.700	4126.558	25659.480
[Sc]	BDL	BDL	0.098	BDL	0.057	BDL	0.041
[V]	1.255	0.536	3.850	0.661	4.733	1.277	1.953
[Mn]	152.661	105.171	100.796	44.002	97.678	48.315	67.752
[Fe]	210.289	52.144	228.603	231.991	207.452	623.393	770.995
[Co]	3.277	1.140	0.797	0.644	0.492	1.609	2.897
[Ni]	5.727	1.713	0.899	0.449	2.738	1.615	2.640
[Zn]	5.233	BDL	BDL	2.540	3.259	1.835	6.888
[Rb]	BDL	BDL	BDL	0.206	0.021	BDL	BDL
[Sr]	109.081	217.993	465.808	248.431	125.093	26.751	291.372
[Y]	0.993	0.833	2.568	0.139	0.639	0.372	0.466
[Zr]	BDL	BDL	0.055	BDL	0.027	BDL	BDL
[Nb]	BDL						
[Mo]	BDL						
[La]	0.488	0.291	0.516	1.110	0.675	0.197	0.481
[Ce]	1.690	0.876	0.984	3.142	1.449	0.323	0.858
[Pr]	0.159	0.097	0.116	0.302	0.134	0.039	0.099
[Nd]	0.756	0.435	0.494	1.291	0.573	0.179	0.428
[Sm]	0.195	0.120	0.103	0.284	0.102	BDL	0.071
[Eu]	0.065	0.038	0.050	0.072	0.033	0.016	0.055
[Gd]	0.282	0.168	0.126	0.351	0.103	0.042	0.092
[Tb]	0.051	0.026	0.020	0.060	0.015	0.007	0.011
[Dy]	0.347	0.184	0.110	0.399	0.080	0.030	0.068
[Ho]	0.071	0.034	0.025	0.088	0.019	0.005	0.011
[Er]	0.228	0.108	0.080	0.242	0.051	0.019	0.035
[Tm]	0.035	0.015	0.011	0.038	0.006	0.002	0.005
[Yb]	0.220	0.102	0.055	0.219	0.041	0.008	0.019
[Lu]	0.028	0.011	0.010	0.032	0.005	BDL	BDL
[Pb]	1.063	0.139	BDL	0.164	0.165	BDL	BDL
Ce/Ce*	1.394	1.200	0.923	1.248	1.108	0.841	0.906
Pr/Pr*	0.800	0.891	0.949	0.851	0.836	0.932	0.925
Eu/Eu*	1.294	1.263	2.062	1.058	1.499	BDL	3.174
Mg/Ca	0.957	0.976	1.010	1.020	1.089	40.445	6.685
Zn/Fe	0.021	BDL	BDL	0.010	0.013	0.003	0.008
Y/Ho	13.962	24.619	102.767	1.575	33.170	68.213	43.857
Yb/Nd	3.326	2.671	1.271	1.940	0.827	0.518	0.502

Sample ID	THM 211	THM 212	THM 213	THM 214	THM 215	THM 216	THM 217
[Li]	4.942	5.019	4.135	6.348	1.366	2.338	3.060
[Mg]	65435.738	97440.995	142181.107	104620.761	60567.496	95131.498	99668.317
[Al]	BDL						
[Si]	BDL						
[P]	18.249	BDL	BDL	BDL	BDL	BDL	BDL
[K]	BDL						
[Ca]	105067.745	44642.911	4331.350	5160.308	44957.504	11913.551	10729.036
[Sc]	BDL						
[V]	0.797	1.488	0.861	0.219	0.971	0.123	0.463
[Mn]	37.081	85.250	148.631	60.797	69.271	48.829	48.752
[Fe]	118.039	716.069	2477.043	785.390	2734.462	987.214	530.784
[Co]	0.391	14.055	2.726	4.909	0.912	1.165	22.132
[Ni]	1.149	29.117	26.125	2.341	0.564	25.954	7.936
[Zn]	BDL	6.693	2.913	3.759	4.413	2.258	2.333
[Rb]	BDL						
[Sr]	217.838	145.657	18.314	13.824	97.359	43.682	22.824
[Y]	0.598	0.265	0.147	0.260	0.377	0.167	0.117
[Zr]	BDL						
[Nb]	BDL						
[Mo]	BDL						
[La]	0.715	0.684	0.292	0.186	0.267	0.269	0.178
[Ce]	1.307	1.122	0.644	0.357	0.500	0.638	0.321
[Pr]	0.135	0.152	0.065	0.036	0.061	0.069	0.039
[Nd]	0.549	0.649	0.269	0.171	0.227	0.276	0.170
[Sm]	0.081	0.129	0.058	BDL	0.047	0.062	0.040
[Eu]	0.066	0.084	0.048	0.037	0.034	0.018	0.018
[Gd]	0.098	0.140	0.065	0.038	0.057	0.062	0.040
[Tb]	0.013	0.019	0.008	0.007	0.008	0.013	0.006
[Dy]	0.069	0.098	0.043	0.026	0.037	0.071	0.031
[Ho]	0.014	0.020	0.008	0.005	0.009	0.013	0.005
[Er]	0.040	0.065	0.023	0.017	0.027	0.038	0.017
[Tm]	0.006	0.008	0.003	0.003	0.004	0.007	0.002
[Yb]	0.037	0.043	0.016	0.007	0.014	0.032	0.009
[Lu]	0.006	0.007	BDL	BDL	BDL	BDL	BDL
[Pb]	BDL	BDL	3.020	BDL	0.749	BDL	BDL
Ce/Ce*	0.968	0.801	1.076	1.006	0.899	1.073	0.885
Pr/Pr*	0.905	1.011	0.885	0.822	1.035	0.940	0.952
Eu/Eu*	3.446	2.918	3.643	BDL	3.059	1.337	2.066
Mg/Ca	1.027	3.599	54.120	33.426	2.221	13.165	15.316
Zn/Fe	BDL	0.008	0.001	0.004	0.001	0.002	0.004
Y/Ho	43.087	13.008	18.194	51.836	40.374	13.236	21.858
Yb/Nd	0.776	0.757	0.677	0.478	0.718	1.327	0.633

Sample ID	THM 218	THM 219	THM 220	THM 221	THM 222	THM 223	THM 224
[Li]	1.117	0.840	5.434	5.875	6.349	0.761	10.693
[Mg]	47705.89	48015.18	126694.2	109260.7	62538.22	311585.1	BDL
[Al]	BDL	BDL	BDL	BDL	BDL	BDL	88.802
[Si]	BDL	BDL	BDL	BDL	BDL	93.499	BDL
[P]	BDL	BDL	BDL	BDL	BDL	96.257	BDL
[K]	BDL	BDL	BDL	BDL	BDL	2.501	BDL
[Ca]	80231.71	20739.43	2450.414	2279.091	103136.1	508484.2	125378.2
[Sc]	BDL	BDL	BDL	BDL	BDL	0.037	BDL
[V]	5.893	2.220	0.876	0.529	1.098	1.817	2.302
[Mn]	41.356	53.777	40.421	34.166	17.103	146.948	69.056
[Fe]	2247.11	2611.74	536.88	372.56	112.74	60653.05	21837.29
[Co]	17.976	79.827	38.797	6.986	0.569	35.206	3.044
[Ni]	8.028	34.390	46.306	3.124	BDL	16.121	3.557
[Zn]	BDL	4.451	8.652	1.485	BDL	BDL	6.416
[Rb]	BDL	BDL	BDL	BDL	BDL	BDL	0.206
[Sr]	212.565	205.334	7.964	13.534	218.804	270.253	106.601
[Y]	0.055	0.138	0.142	0.242	0.150	0.564	0.324
[Zr]	BDL						
[Nb]	BDL						
[Mo]	BDL						
[La]	0.238	0.111	0.192	0.140	0.339	0.269	0.626
[Ce]	0.381	0.198	0.287	0.214	0.580	0.454	1.211
[Pr]	0.037	0.024	0.040	0.031	0.071	0.056	0.164
[Nd]	0.132	0.084	0.161	0.114	0.251	0.209	0.625
[Sm]	BDL	BDL	0.035	BDL	0.046	0.048	0.124
[Eu]	0.011	0.016	0.019	0.026	0.021	0.020	0.048
[Gd]	0.033	0.020	0.051	0.032	0.067	0.054	0.147
[Tb]	0.005	0.003	0.009	0.007	0.008	0.015	0.025
[Dy]	0.023	BDL	0.026	0.032	0.046	0.035	0.111
[Ho]	0.004	0.003	0.008	0.007	0.010	0.009	0.020
[Er]	0.015	0.006	0.019	0.019	0.025	0.022	0.060
[Tm]	0.002	BDL	0.005	0.005	0.004	0.006	0.012
[Yb]	0.011	0.006	0.014	0.011	0.017	0.018	0.048
[Lu]	BDL	BDL	BDL	BDL	BDL	BDL	0.008
[Pb]	1.750	0.487	BDL	BDL	BDL	1.620	BDL
Ce/Ce*	0.938	0.885	0.748	0.745	0.861	0.848	0.869
Pr/Pr*	0.927	1.051	1.070	1.132	1.053	1.040	1.069
Eu/Eu*	BDL	BDL	2.073	BDL	1.738	1.793	1.655
Mg/Ca	0.980	3.817	85.243	79.040	1.000	1.010	13.283
Zn/Fe	BDL	0.002	0.014	0.003	BDL	BDL	0.000
Y/Ho	12.819	41.024	18.755	35.005	14.700	65.599	16.535
Yb/Nd	0.977	0.856	0.969	1.067	0.773	0.976	0.869

Sample ID	THM 225	THM 226	THM 227	THM 228	THM 229	THM 230	THM 231
[Li]	3.069	8.999	3.801	5.432	5.384	3.311	9.345
[Mg]	102446.557	96048.060	94548.592	53598.939	52330.794	84071.184	57312.757
[Al]	BDL						
[Si]	BDL	BDL	BDL				
[P]	BDL	BDL	BDL	17.049	BDL	BDL	BDL
[K]	BDL	BDL	BDL	BDL			
[Ca]	3420.971	5243.422	17569.711	84864.630	78943.500	10015.842	88508.396
[Sc]	BDL						
[V]	1.126	0.608	1.275	3.025	1.875	1.054	2.686
[Mn]	45.557	40.809	50.520	16.218	14.428	25.713	16.046
[Fe]	349.421	372.856	789.828	78.974	98.386	353.449	110.663
[Co]	2.281	3.928	29.114	0.400	1.080	4.490	1.290
[Ni]	1.368	2.661	13.063	3.890	BDL	38.242	0.809
[Zn]	7.015	BDL	2.829	BDL	2.027	2.713	0.779
[Rb]	BDL	0.103	BDL	BDL	BDL	BDL	BDL
[Sr]	8.556	96.278	96.244	265.079	294.151	63.093	277.068
[Y]	0.213	0.443	0.289	0.675	0.253	0.384	0.318
[Zr]	BDL						
[Nb]	BDL						
[Mo]	BDL						
[La]	0.213	0.177	0.331	0.390	0.768	0.206	0.583
[Ce]	0.354	0.319	0.615	0.791	1.542	0.375	1.170
[Pr]	0.046	0.045	0.085	0.086	0.184	0.044	0.126
[Nd]	0.240	0.184	0.359	0.310	0.714	0.199	0.458
[Sm]	0.057	0.036	0.080	0.059	0.148	0.046	0.094
[Eu]	0.023	0.024	0.044	0.016	0.047	0.018	0.029
[Gd]	0.069	0.045	0.098	0.066	0.143	0.046	0.094
[Tb]	0.012	0.010	0.015	0.010	0.020	0.010	0.012
[Dy]	0.052	0.036	0.080	0.050	0.114	0.049	0.062
[Ho]	0.011	0.010	0.016	0.011	0.021	0.007	0.015
[Er]	0.035	0.022	0.048	0.028	0.067	0.029	0.038
[Tm]	0.007	0.005	0.006	0.005	0.009	0.004	0.005
[Yb]	0.022	0.011	0.029	0.023	0.032	0.012	0.027
[Lu]	0.006	BDL	0.006	0.005	0.008	BDL	0.005
[Pb]	BDL						
Ce/Ce*	0.820	0.822	0.842	0.992	0.943	0.911	0.991
Pr/Pr*	0.902	1.055	1.029	0.988	0.997	0.906	0.981
Eu/Eu*	1.721	2.773	2.303	1.162	1.512	1.852	1.444
Mg/Ca	49.373	30.201	8.872	1.041	1.093	13.839	1.068
Zn/Fe	0.018	BDL	0.003	BDL	0.018	0.007	0.006
Y/Ho	19.487	44.708	18.305	63.720	12.145	53.650	21.203
Yb/Nd	1.055	0.694	0.917	0.853	0.508	0.703	0.678

Sample ID	THM 232	THM 233	THM 234	THM 235	THM 236	THM 237	THM 238
[Li]	2.475	3.351	1.945	11.431	4.823	10.340	6.454
[Mg]	43756.29	108424.1	48277.04	97392.43	44864.39	43231.44	91750.25
[Al]	BDL						
[Si]	71.193	BDL	BDL	BDL	BDL	BDL	BDL
[P]	BDL!	BDL	BDL	BDL	BDL	BDL	BDL
[K]	3.739	BDL	BDL	BDL	BDL	BDL	BDL
[Ca]	73694.6	5181.443	79325.457	5834.750	72349.036	67265.502	3291.060
[Sc]	0.059	BDL	BDL	BDL	BDL	BDL	BDL
[V]	2.346	1.878	5.658	0.736	2.170	1.950	0.933
[Mn]	20.972	27.615	10.866	31.769	18.289	14.640	31.991
[Fe]	93.965	355.660	62.401	329.466	90.323	94.268	559.995
[Co]	0.669	3.403	6.552	6.654	0.848	0.475	3.227
[Ni]	0.753	1.848	7.218	20.873	1.707	BDL	2.015
[Zn]	BDL	BDL	BDL	2.441	1.122	BDL	1.825
[Rb]	BDL	BDL	BDL	0.165	BDL	BDL	BDL
[Sr]	293.875	23.149	238.240	77.814	199.748	266.285	23.990
[Y]	0.193	0.096	0.277	0.425	0.505	0.282	0.349
[Zr]	BDL						
[Nb]	BDL						
[Mo]	BDL						
[La]	0.397	0.139	0.172	0.234	0.528	0.598	0.303
[Ce]	0.738	0.205	0.270	0.476	1.055	1.247	0.567
[Pr]	0.089	0.037	0.027	0.059	0.107	0.145	0.066
[Nd]	0.372	0.174	0.081	0.244	0.403	0.515	0.255
[Sm]	0.074	0.038	BDL	0.054	0.083	0.097	0.052
[Eu]	0.035	0.017	0.008	0.041	0.045	0.031	0.016
[Gd]	0.077	0.038	0.027	0.067	0.081	0.105	0.053
[Tb]	0.010	0.006	0.003	0.009	0.013	0.019	0.009
[Dy]	0.053	0.034	0.019	0.048	0.067	0.087	0.052
[Ho]	0.009	0.007	0.005	0.009	0.012	0.021	0.008
[Er]	0.024	0.017	0.012	0.026	0.043	0.044	0.024
[Tm]	0.004	0.003	0.002	0.004	0.008	0.006	0.004
[Yb]	0.019	0.018	0.012	0.015	0.036	0.035	0.016
[Lu]	BDL	BDL	BDL	BDL	0.005	0.005	BDL
[Pb]	BDL	BDL	BDL	BDL	BDL	0.167	BDL
Ce/Ce*	0.901	0.661	0.915	0.932	1.020	0.974	0.924
Pr/Pr*	0.969	1.101	1.030	0.982	0.933	1.028	0.979
Eu/Eu*	2.183	2.090	BDL	3.172	2.538	1.422	1.451
Mg/Ca	0.979	34.500	1.003	27.520	1.022	1.060	45.964
Zn/Fe	BDL	BDL	BDL	0.007	0.011	BDL	0.003
Y/Ho	21.456	13.970	59.626	46.430	40.752	13.181	41.815
Yb/Nd	0.596	1.195	1.693	0.717	1.033	0.773	0.725

Sample ID	THM 239	THM 240	THM 241	THM 242	THM 243	THM 244	THM 245
[Li]	8.433	2.419	5.920	4.802	9.173	4.165	5.412
[Mg]	107109.0	84319.95	57917.58	33346.04	49146.56	102299.16	63639.37
[Al]	BDL						
[Si]	BDL	BDL	52.526	BDL	BDL	BDL	BDL
[P]	BDL	BDL	BDL	BDL	25.853	BDL	BDL
[K]	BDL	BDL	5.466	BDL	BDL	BDL	BDL
[Ca]	5988.365	1103.924	87416.709	52660.390	78509.315	1665.665	85364.295
[Sc]	BDL	BDL	0.141	BDL	BDL	BDL	BDL
[V]	2.196	0.217	2.440	1.115	2.215	0.999	4.160
[Mn]	41.390	26.600	24.951	9.917	13.683	23.297	18.997
[Fe]	621.303	309.067	325.796	59.186	46.936	224.389	446.744
[Co]	6.187	1.935	1.679	0.060	0.468	5.056	1.097
[Ni]	2.958	11.350	1.192	BDL	BDL	45.249	1.203
[Zn]	3.138	2.513	1.605	BDL	BDL	1.686	1.142
[Rb]	BDL						
[Sr]	46.116	3.841	476.613	201.560	150.120	5.242	212.597
[Y]	0.102	0.715	0.260	0.432	0.175	0.419	0.565
[Zr]	BDL						
[Nb]	BDL						
[Mo]	BDL						
[La]	0.502	0.111	0.849	0.364	0.724	0.107	0.487
[Ce]	0.727	0.212	1.825	0.587	1.167	0.185	1.059
[Pr]	0.104	0.022	0.216	0.086	0.153	0.022	0.110
[Nd]	0.442	0.095	0.774	0.308	0.597	0.111	0.429
[Sm]	0.085	BDL	0.153	0.068	0.114	BDL	0.090
[Eu]	0.028	0.013	0.067	0.015	0.024	0.012	0.024
[Gd]	0.084	0.023	0.147	0.065	0.098	0.038	0.093
[Tb]	0.013	0.003	0.021	0.008	0.015	0.010	0.013
[Dy]	0.052	0.027	0.119	0.057	0.076	0.031	0.072
[Ho]	0.011	0.004	0.021	0.008	0.014	0.005	0.013
[Er]	0.038	0.014	0.066	0.025	0.040	0.028	0.042
[Tm]	0.005	0.002	0.009	0.004	0.006	0.007	0.005
[Yb]	0.025	0.008	0.045	0.025	0.026	0.010	0.032
[Lu]	BDL	BDL	0.008	BDL	0.005	BDL	0.006
[Pb]	BDL	BDL	0.040	BDL	0.123	BDL	0.348
Ce/Ce*	0.732	0.986	0.979	0.763	0.807	0.879	1.050
Pr/Pr*	1.040	0.882	1.034	1.149	1.042	0.868	0.931
Eu/Eu*	1.535	BDL	2.094	1.047	1.041	BDL	1.205
Mg/Ca	29.489	125.931	1.092	1.044	1.032	101.258	1.229
Zn/Fe	0.005	0.008	0.004	BDL	BDL	0.007	0.002
Y/Ho	9.571	191.160	12.247	52.205	12.246	83.332	42.855
Yb/Nd	0.654	0.960	0.671	0.937	0.493	0.998	0.858

Sample ID	THM 246	THM 247	THM 248	THM 249	THM 250	THM 251	THM 413
[Li]	3.459	3.022	3.875	5.520	3.334	3.771	1.985
[Mg]	51445.21	51916.26	85850.34	50779.54	46041.58	45752.75	60079.23
[Al]	BDL	BDL	BDL	56.643	#VALUE!	BDL	65.854
[Si]	BDL	BDL	BDL	BDL	45.131	BDL	72.362
[P]	BDL	BDL	BDL	24.510	16.989	20.701	13.126
[K]	BDL	BDL	BDL	BDL	4.642		14.767
[Ca]	85419.23	7674.22	2606.93	79351.43	75858.65	74775.99	6988.85
[Sc]	BDL	BDL	BDL	BDL	0.043	BDL	0.069
[V]	5.053	0.891	0.597	0.697	0.615	3.653	1.435
[Mn]	24.182	18.132	40.558	34.462	34.682	22.095	66.878
[Fe]	334.841	191.654	592.817	204.519	158.790	96.504	1384.290
[Co]	2.153	0.847	2.698	0.714	0.570	0.225	0.233
[Ni]	8.808	BDL	2.641	1.139	BDL	0.768	5.048
[Zn]	2.018	1.120	BDL	1.267	BDL	BDL	7.826
[Rb]	BDL	BDL	0.085	0.277	0.114	0.252	0.083
[Sr]	361.636	76.673	13.852	386.448	246.493	205.136	81.957
[Y]	0.439	0.139	0.862	0.533	0.603	0.928	0.365
[Zr]	BDL	BDL	BDL	BDL	BDL	BDL	0.023
[Nb]	BDL						
[Mo]	BDL						
[La]	0.557	0.353	0.163	0.904	0.473	0.839	0.268
[Ce]	1.070	0.795	0.306	1.648	0.906	1.684	0.670
[Pr]	0.105	0.090	0.040	0.220	0.100	0.199	0.077
[Nd]	0.403	0.368	0.140	0.831	0.376	0.733	0.295
[Sm]	0.082	0.093	0.036	0.155	0.082	0.146	0.071
[Eu]	0.042	0.030	0.017	0.067	0.035	0.044	0.042
[Gd]	0.095	0.074	0.032	0.156	0.101	0.143	0.064
[Tb]	0.016	0.017	0.006	0.025	0.015	0.021	0.011
[Dy]	0.087	0.082	0.033	0.148	0.072	0.118	0.063
[Ho]	0.018	0.016	0.006	0.028	0.016	0.022	0.014
[Er]	0.055	0.051	0.016	0.078	0.042	0.065	0.036
[Tm]	0.008	0.008	0.004	0.012	0.005	0.009	0.004
[Yb]	0.050	0.033	0.011	0.047	0.035	0.050	0.028
[Lu]	0.008	0.006	BDL	0.007	0.005	0.007	0.004
[Pb]	0.276	BDL	BDL	0.403	0.147	0.125	0.083
Ce/Ce*	1.017	1.024	0.874	0.850	0.960	0.948	1.070
Pr/Pr*	0.910	0.948	1.095	1.067	0.970	1.018	0.986
Eu/Eu*	2.249	1.701	2.301	2.013	1.791	1.426	2.929
Mg/Ca	0.993	11.154	54.295	1.055	1.001	1.009	14.173
Zn/Fe	0.006	0.005	BDL	0.005	BDL	BDL	0.005
Y/Ho	24.830	8.960	154.718	19.000	38.348	42.742	26.671
Yb/Nd	1.429	1.016	0.926	0.651	1.075	0.783	1.075

Sample ID	THM 101	THM 102	THM 103	THM 104	THM 105	THM 106	THM 107
[Li]	6.087	7.227	7.102	1.277	1.126	2.182	3.032
[Mg]	77948.58	84004.05	72393.924	35783.998	48036.659	47394.124	78789.238
[Al]	BDL						
[Si]	BDL	BDL	47.617	BDL	BDL	BDL	BDL
[P]	BDL						
[K]	BDL	BDL	16.623	BDL	BDL	BDL	BDL
[Ca]	20725.80	7431.18	25088.74	13872.45	23553.63	8102.34	15240.54
[Sc]	BDL	BDL	0.279	BDL	BDL	BDL	BDL
[V]	1.516	0.853	1.792	1.230	1.234	1.494	2.439
[Mn]	53.298	64.786	63.885	28.689	34.653	36.646	61.854
[Fe]	1038.136	1276.316	1347.643	547.938	582.020	667.892	1360.870
[Co]	2.299	6.049	3.080	1.290	1.419	0.592	3.773
[Ni]	1.221	3.895	1.473	3.662	BDL	BDL	2.563
[Zn]	6.579	1.590	1.452	17.622	BDL	BDL	BDL
[Rb]	0.207	BDL	BDL	BDL	BDL	0.092	BDL
[Sr]	100.486	95.186	254.410	76.469	127.917	66.597	106.624
[Y]	1.177	0.325	0.738	0.442	0.659	0.375	0.908
[Zr]	BDL						
[Nb]	BDL						
[Mo]	BDL						
[La]	0.742	0.230	0.422	0.242	0.409	0.272	0.664
[Ce]	1.057	0.297	0.816	0.520	0.780	0.571	1.176
[Pr]	0.222	0.056	0.106	0.075	0.125	0.084	0.190
[Nd]	0.999	0.272	0.425	0.330	0.553	0.377	0.899
[Sm]	0.228	0.049	0.103	0.084	0.121	0.088	0.206
[Eu]	0.059	0.031	0.036	0.022	0.040	0.031	0.056
[Gd]	0.248	0.081	0.125	0.088	0.125	0.095	0.224
[Tb]	0.044	0.017	0.033	0.016	0.024	0.014	0.037
[Dy]	0.220	0.067	0.133	0.082	0.132	0.081	0.204
[Ho]	0.039	0.013	0.026	0.015	0.024	0.017	0.036
[Er]	0.122	0.044	0.071	0.050	0.069	0.042	0.106
[Tm]	0.018	0.010	0.017	0.007	0.008	0.009	0.013
[Yb]	0.089	0.022	0.050	0.037	0.061	0.034	0.085
[Lu]	0.013	BDL	0.010	BDL	0.009	BDL	0.008
[Pb]	BDL						
Ce/Ce*	0.599	0.600	0.885	0.885	0.793	0.866	0.761
Pr/Pr*	1.229	1.127	1.027	1.033	1.081	1.035	1.052
Eu/Eu*	1.156	2.339	1.462	1.177	1.530	1.559	1.226
Mg/Ca	6.201	18.637	4.757	4.253	3.362	9.644	8.523
Zn/Fe	0.005	0.001	0.001	0.029	BDL	BDL	BDL
Y/Ho	30.556	24.503	28.519	30.471	27.506	22.041	25.096
Yb/Nd	1.022	0.921	1.335	1.279	1.266	1.020	1.084

Sample ID	THM 108	THM 109	THM 110	THM 111	THM 112	THM 112b	THM 113
[Li]	2.401	1.810	3.277	2.061	2.588	4.287	6.138
[Mg]	49275.19	63281.43	59398.32	36803.05	51712.19	51349.30	56374.62
[Al]	BDL	BDL	BDL	BDL	BDL	BDL	BDL
[Si]	BDL	BDL	BDL	BDL	BDL	109.051	193.126
[P]	BDL	64.131	BDL	89.616	BDL	BDL	BDL
[K]	BDL	BDL	BDL	BDL	BDL	12.250	22.344
[Ca]	6501.24	34487.80	11299.74	30888.24	17592.65	79034.41	81282.47
[Sc]	BDL	BDL	BDL	BDL	BDL	0.278	0.307
[V]	1.380	3.788	2.159	2.900	2.864	6.072	4.084
[Mn]	31.535	45.086	47.372	36.593	45.322	40.692	44.670
[Fe]	684.513	652.233	1109.072	498.287	803.505	407.957	492.565
[Co]	1.119	1.844	0.944	0.892	0.764	4.876	0.746
[Ni]	0.908	2.353	1.016	1.060	0.928	2.070	BDL
[Zn]	BDL	2.669	1.898	4.939	4.160	BDL	BDL
[Rb]	0.111	BDL	0.161	0.120	BDL	BDL	0.227
[Sr]	53.082	183.163	66.254	159.886	125.776	576.324	498.781
[Y]	0.449	0.762	0.734	1.205	0.467	0.744	0.295
[Zr]	BDL	BDL	BDL	BDL	BDL	BDL	0.020
[Nb]	BDL	BDL	BDL	BDL	BDL	BDL	0.099
[Mo]	BDL	BDL	BDL	BDL	BDL	BDL	0.053
[La]	0.317	0.485	0.448	0.641	0.371	0.798	0.744
[Ce]	0.515	0.784	0.817	1.500	0.640	1.723	1.586
[Pr]	0.106	0.156	0.140	0.261	0.112	0.205	0.201
[Nd]	0.434	0.672	0.565	1.167	0.402	0.790	0.776
[Sm]	0.120	0.161	0.152	0.347	0.097	0.157	0.183
[Eu]	0.044	0.067	0.065	0.091	0.050	0.063	0.065
[Gd]	0.121	0.188	0.173	0.368	0.112	0.167	0.156
[Tb]	0.033	0.039	0.041	0.076	0.030	0.027	0.033
[Dy]	0.095	0.163	0.162	0.287	0.096	0.146	0.137
[Ho]	0.031	0.042	0.042	0.070	0.035	0.030	0.040
[Er]	0.063	0.081	0.086	0.136	0.065	0.084	0.092
[Tm]	0.019	0.023	0.027	0.032	0.021	0.010	0.021
[Yb]	0.054	0.071	0.073	0.113	0.043	0.073	0.067
[Lu]	0.017	0.022	0.025	0.033	0.021	0.010	0.023
[Pb]	0.267	0.290		0.182		0.067	0.093
Ce/Ce*	0.646	0.654	0.749	0.842	0.721	0.980	0.943
Pr/Pr*	1.276	1.225	1.173	1.122	1.258	0.998	1.031
Eu/Eu*	1.692	1.787	1.868	1.193	2.222	1.807	1.809
Mg/Ca	12.496	3.025	8.667	1.964	4.846	1.071	1.143
Zn/Fe	BDL	0.003	0.002	0.009	0.004	BDL	BDL
Y/Ho	14.682	18.142	17.483	17.299	13.429	24.434	7.299
Yb/Nd	1.424	1.205	1.467	1.112	1.218	1.051	0.986

Sample ID	THM 114	THM 115	THM 116	THM 414	THM 117	THM 118	THM 119
[Li]	1.373	4.137	2.391	1.231	2.014	4.130	3.936
[Mg]	49114.25	89314.02	50537.83	53924.34	71277.33	71677.64	82407.50
[Al]	BDL	BDL	BDL	27.260	BDL	78.653	BDL
[Si]	BDL	BDL	BDL	67.081	BDL	BDL	BDL
[P]	BDL	BDL	BDL	21.891	BDL	BDL	BDL
[K]	BDL	BDL	BDL	5.127	BDL	BDL	BDL
[Ca]	8243.240	3305.496	10219.793	79374.305	20839.121	10881.340	61736.805
[Sc]	BDL	BDL	BDL	0.129	BDL	BDL	BDL
[V]	0.508	1.249	1.030	3.268	1.578	1.472	2.633
[Mn]	26.906	81.970	43.786	26.561	49.075	64.641	82.412
[Fe]	570.890	1583.529	941.744	114.856	640.103	1540.351	1853.841
[Co]	0.799	3.123	2.494	0.033	0.347	4.907	2.280
[Ni]	1.083	2.052	1.685	0.235	BDL	2.359	4.232
[Zn]	1.352	4.939	BDL	4.753	7.430	4.991	5.079
[Rb]	BDL	0.212	0.109	0.056	BDL	0.127	0.113
[Sr]	49.618	91.791	75.932	162.775	79.509	42.517	103.635
[Y]	0.240	0.421	0.262	1.518	0.452	0.775	1.524
[Zr]	BDL	BDL	BDL	0.091	BDL	BDL	BDL
[Nb]	BDL						
[Mo]	BDL						
[La]	0.247	0.187	0.306	1.054	0.237	0.385	0.461
[Ce]	0.314	0.289	0.580	3.045	0.565	0.836	1.073
[Pr]	0.077	0.043	0.094	0.268	0.064	0.105	0.126
[Nd]	0.251	0.196	0.381	0.994	0.255	0.430	0.507
[Sm]	0.070	0.046	0.105	0.200	0.042	0.098	0.116
[Eu]	0.029	0.026	0.041	0.050	0.018	0.037	0.047
[Gd]	0.067	0.053	0.093	0.206	0.046	0.102	0.154
[Tb]	0.022	0.011	0.016	0.034	0.008	0.018	0.026
[Dy]	0.070	0.058	0.084	0.220	0.047	0.091	0.119
[Ho]	0.026	0.011	0.017	0.046	0.009	0.016	0.030
[Er]	0.050	0.026	0.046	0.149	0.028	0.049	0.099
[Tm]	0.018	0.005	0.006	0.023	0.003	0.007	0.014
[Yb]	0.043	0.017	0.030	0.139	0.025	0.036	0.065
[Lu]	0.018	BDL	0.005	0.023	BDL	0.007	0.010
[Pb]	BDL	BDL	BDL	0.283	BDL	BDL	0.106
Ce/Ce*	0.524	0.737	0.787	1.317	1.052	0.956	1.024
Pr/Pr*	1.557	1.032	1.136	0.875	0.965	0.995	0.971
Eu/Eu*	1.957	2.439	1.937	1.147	1.941	1.730	1.625
Mg/Ca	9.823	44.548	8.153	1.120	5.639	10.860	2.201
Zn/Fe	0.002	0.003	BDL	0.033	0.010	0.003	0.002
Y/Ho	9.238	38.259	15.787	32.976	48.841	48.976	51.433
Yb/Nd	1.944	1.013	0.914	1.599	1.128	0.967	1.476

Sample ID	THM120	THM121	THM122	THM123	THM124	THM125	THM126
[Li]	1.853	1.574	5.300	3.377	4.454	1.956	5.285
[Mg]	47106.724	51349.564	51883.931	52822.960	47135.268	53129.518	55070.467
[Al]	BDL	BDL	128.089	BDL	558.111	BDL	302.918
[Si]	BDL	BDL	261.354	BDL	BDL	BDL	BDL
[P]	BDL						
[K]	BDL	BDL	24.019	BDL	BDL	BDL	BDL
[Ca]	70183.941	86750.644	82116.880	87324.280	76052.997	88990.631	94104.408
[Sc]	BDL	BDL	0.437	BDL	4.234	BDL	BDL
[V]	1.625	3.241	4.642	1.871	2.681	2.666	0.730
[Mn]	32.867	102.896	122.066	228.360	220.142	150.495	185.308
[Fe]	319.062	682.507	742.612	1541.573	2420.831	1120.369	3350.158
[Co]	0.261	0.564	6.483	6.491	57.238	1.312	5.057
[Ni]	0.844	0.709	3.326	5.224	25.337	1.225	3.644
[Zn]	BDL	1.319	4.480	1.358	1.564	2.328	4.320
[Rb]	BDL	BDL	0.126	BDL	0.408	BDL	0.283
[Sr]	295.450	225.961	332.431	229.073	199.490	203.514	254.729
[Y]	0.412	1.144	3.280	4.173	0.905	1.558	2.899
[Zr]	BDL	BDL	0.097	BDL	BDL	BDL	BDL
[Nb]	BDL	BDL	0.046	BDL	BDL	BDL	BDL
[Mo]	BDL						
[La]	0.784	0.360	0.762	0.902	0.875	0.834	1.147
[Ce]	1.241	0.928	1.767	2.337	2.357	1.882	2.437
[Pr]	0.222	0.110	0.197	0.270	0.305	0.217	0.308
[Nd]	0.856	0.450	0.785	1.076	1.304	0.811	1.262
[Sm]	0.231	0.093	0.192	0.313	0.385	0.189	0.279
[Eu]	0.077	0.033	0.064	0.101	0.129	0.040	0.102
[Gd]	0.254	0.085	0.192	0.363	0.536	0.191	0.294
[Tb]	0.044	0.016	0.032	0.067	0.103	0.028	0.047
[Dy]	0.266	0.074	0.193	0.474	0.707	0.161	0.259
[Ho]	0.052	0.013	0.041	0.110	0.158	0.031	0.053
[Er]	0.137	0.051	0.127	0.379	0.482	0.101	0.156
[Tm]	0.023	0.005	0.016	0.055	0.078	0.014	0.028
[Yb]	0.116	0.031	0.101	0.408	0.520	0.097	0.121
[Lu]	0.020	0.006	0.013	0.064	0.077	0.013	0.022
[Pb]	0.294	BDL	0.178	0.111	1.729	0.077	BDL
Ce/Ce*	0.684	1.072	1.049	1.089	1.049	1.017	0.943
Pr/Pr*	1.223	0.968	0.950	0.968	0.989	0.999	0.999
Eu/Eu*	1.479	1.720	1.557	1.398	1.330	0.993	1.658
Mg/Ca	1.107	0.976	1.042	0.997	1.022	0.984	0.965
Zn/Fe	BDL	0.002	0.005	0.001	0.001	0.002	0.001
Y/Ho	7.955	84.933	79.259	38.070	5.710	49.706	54.930
Yb/Nd	1.548	0.780	1.466	4.332	4.557	1.369	1.094

Sample ID	THM127	THM128	THM129	THM130	THM131	THM132	THM133
[Li]	5.648	4.815	7.588	5.331	3.820	3.832	4.433
[Mg]	43336.602	43678.886	48653.219	57864.552	411772.918	53292.114	46140.713
[Al]	1327.941	964.990	737.312	132.284	1031.613	201.941	851.008
[Si]	BDL	BDL	BDL	BDL	BDL	BDL	BDL
[P]	BDL	BDL	BDL	BDL	BDL	BDL	BDL
[K]	BDL	BDL	BDL	BDL	BDL	BDL	BDL
[Ca]	80171.882	73532.021	90237.732	99436.626	681931.471	101240.635	79638.055
[Sc]	2.435	1.631	1.158	BDL	1.152	BDL	BDL
[V]	1.600	1.020	1.033	1.755	1.942	1.737	4.113
[Mn]	255.215	256.327	210.032	314.165	331.173	335.078	391.957
[Fe]	4593.749	3819.363	3137.988	2849.469	50411.848	3169.888	5121.699
[Co]	38.320	40.440	22.149	16.985	37.119	38.652	102.107
[Ni]	16.904	24.302	10.572	7.092	125.103	23.549	47.850
[Zn]	4.650	2.447	3.300	1.264	2.913	2.209	4.235
[Rb]	0.792	0.249	0.242	BDL	0.467	BDL	0.338
[Sr]	157.153	133.539	125.659	120.183	134.729	144.373	123.331
[Y]	2.543	2.573	4.148	3.717	3.077	3.686	2.722
[Zr]	BDL	BDL	BDL	BDL	BDL	BDL	BDL
[Nb]	BDL	BDL	BDL	BDL	BDL	BDL	BDL
[Mo]	BDL	BDL	BDL	BDL	BDL	BDL	BDL
[La]	1.113	0.855	1.141	2.055	1.218	1.314	1.260
[Ce]	2.530	2.116	2.215	3.408	3.031	2.706	2.940
[Pr]	0.365	0.277	0.346	0.569	0.399	0.401	0.419
[Nd]	1.484	1.206	1.543	2.467	1.804	1.780	1.827
[Sm]	0.407	0.367	0.428	0.649	0.517	0.528	0.563
[Eu]	0.144	0.118	0.151	0.303	0.174	0.213	0.181
[Gd]	0.487	0.450	0.479	0.780	0.608	0.563	0.632
[Tb]	0.087	0.079	0.080	0.117	0.106	0.085	0.110
[Dy]	0.499	0.488	0.458	0.663	0.637	0.515	0.618
[Ho]	0.098	0.095	0.091	0.132	0.129	0.100	0.122
[Er]	0.294	0.258	0.244	0.361	0.354	0.274	0.331
[Tm]	0.042	0.034	0.035	0.046	0.050	0.035	0.047
[Yb]	0.274	0.224	0.209	0.275	0.310	0.214	0.291
[Lu]	0.040	0.030	0.030	0.039	0.048	0.033	0.046
[Pb]	0.195	0.142	BDL	BDL	0.376	BDL	0.223
Ce/Ce*	0.913	0.999	0.811	0.725	1.000	0.857	0.931
Pr/Pr*	1.070	0.987	1.064	1.115	0.969	1.040	1.027
Eu/Eu*	1.505	1.352	1.556	1.986	1.444	1.823	1.411
Mg/Ca	0.891	0.979	0.889	0.959	0.996	0.868	0.955
Zn/Fe	0.001	0.001	0.001	0.000	0.000	0.001	0.001
Y/Ho	25.871	27.085	45.592	28.122	23.822	36.923	22.309
Yb/Nd	2.113	2.120	1.551	1.272	1.962	1.377	1.821

Sample ID	THM 134	THM 135	THM 136	THM 137	THM 138	THM 139	THM 140
[Li]	1.620	2.942	2.483	2.852	2.433	2.214	4.049
[Mg]	47076.90	57963.45	45065.26	49908.917	55617.59	45794.28	37975.66
[Al]	372.382	399.771	319.771	177.885	267.061	288.345	1416.106
[Si]	BDL	BDL	BDL	BDL	BDL	BDL	BDL
[P]	BDL	BDL	BDL	BDL	BDL	BDL	BDL
[K]	BDL	BDL	BDL	BDL	BDL	BDL	BDL
[Ca]	81750.9	103974.9	76405.9	83551.8	97076.2	79432.9	65004.8
[Sc]	BDL	1.426	2.182	1.646	BDL	2.067	3.509
[V]	3.949	2.906	1.885	1.241	1.584	0.934	1.026
[Mn]	420.290	436.280	410.464	420.656	507.488	462.923	358.795
[Fe]	4346.170	3862.470	5147.493	3684.465	3806.354	4054.923	5010.507
[Co]	41.876	76.013	95.596	13.675	34.089	15.122	7.412
[Ni]	18.070	32.716	46.154	7.590	12.480	8.795	5.664
[Zn]	6.701	9.186	5.235	4.351	2.689	4.738	3.241
[Rb]	0.275	0.192	0.301	0.127	0.154	0.220	0.527
[Sr]	117.048	127.094	108.595	89.906	94.347	99.479	109.913
[Y]	6.011	5.610	6.437	6.238	4.984	3.480	0.409
[Zr]	BDL	BDL	BDL	BDL	BDL	BDL	BDL
[Nb]	BDL	BDL	BDL	BDL	BDL	BDL	BDL
[Mo]	BDL	BDL	BDL	BDL	BDL	BDL	BDL
[La]	1.359	2.210	1.455	1.626	2.472	1.536	1.540
[Ce]	3.308	4.521	3.421	3.305	5.157	3.407	3.286
[Pr]	0.438	0.670	0.485	0.533	0.746	0.480	0.460
[Nd]	1.803	3.122	2.280	2.399	3.425	2.196	1.971
[Sm]	0.507	0.943	0.733	0.858	1.062	0.730	0.610
[Eu]	0.185	0.322	0.183	0.248	0.377	0.216	0.298
[Gd]	0.524	1.149	0.853	1.100	1.187	0.853	0.634
[Tb]	0.086	0.180	0.151	0.197	0.188	0.151	0.113
[Dy]	0.456	0.984	0.968	1.188	1.000	0.876	0.594
[Ho]	0.091	0.180	0.191	0.224	0.184	0.170	0.122
[Er]	0.281	0.465	0.558	0.587	0.479	0.449	0.338
[Tm]	0.039	0.063	0.077	0.080	0.062	0.063	0.049
[Yb]	0.217	0.333	0.518	0.509	0.369	0.389	0.272
[Lu]	0.036	0.052	0.074	0.074	0.051	0.056	0.039
[Pb]	1.093	0.153	1.033	0.349	BDL	BDL	0.447
Ce/Ce*	0.986	0.854	0.936	0.816	0.873	0.912	0.897
Pr/Pr*	1.019	1.013	0.987	1.076	1.009	0.998	1.028
Eu/Eu*	1.671	1.445	1.082	1.190	1.566	1.274	2.236
Mg/Ca	0.949	0.919	0.972	0.985	0.945	0.951	0.963
Zn/Fe	0.001	0.002	0.001	0.001	0.001	0.001	0.001
Y/Ho	65.895	31.236	33.676	27.869	27.109	20.425	3.348
Yb/Nd	1.378	1.220	2.599	2.424	1.231	2.022	1.578

Sample ID	Gr201	Gr202	Gr203	Gr204	Gr205	Gr206	Gr207
[Li]	1.430	1.086	1.255	1.037	2.052	1.275	1.254
[Mg]	52594.09	40277.63	49451.17	53208.31	71226.66	50676.85	53162.79
[Al]	76.275	93.638	86.091	72.928	124.600	129.435	141.131
[Si]	156.856	285.597	190.666	205.430	329.691	264.459	284.690
[P]	19.735	19.689	12.499	9.096	17.259	11.131	5.776
[K]	235.061	136.686	55.327	162.189	152.372	147.663	211.523
[Ca]	86328.02	74712.98	66468.78	64862.13	94520.97	67878.18	74020.70
[Sc]	0.281	0.277	0.263	0.265	0.279	0.315	0.378
[V]	2.577	0.918		0.645	1.235	0.867	0.744
[Mn]	87.727	30.054	25.990	28.581	46.230	32.970	35.818
[Fe]	204.342	206.898	280.664	313.685	319.302	231.349	188.860
[Co]	0.430	0.235	0.101	0.236	0.439	0.261	0.205
[Ni]	0.675	0.636	BDL	0.609	0.892	0.497	0.403
[Zn]	10.380	3.603	BDL	3.964	5.043	3.384	3.374
[Rb]	0.643	0.666	0.185	0.814	0.832	0.782	1.038
[Sr]	152.746	225.251	371.914	175.441	290.945	228.255	244.549
[Y]	0.695	2.071	1.981	1.069	1.132	1.819	1.838
[Zr]	BDL	0.044	BDL	0.049	0.155	0.045	BDL
[Nb]	BDL						
[Mo]	0.025	0.011	BDL	0.020	0.039	0.006	0.008
[La]	0.775	1.930	1.722	1.714	1.494	2.331	2.032
[Ce]	1.537	3.862	3.460	3.064	2.713	4.311	4.078
[Pr]	0.185	0.446	0.397	0.350	0.309	0.494	0.462
[Nd]	0.704	1.708	1.452	1.250	1.139	1.776	1.719
[Sm]	0.143	0.350	0.318	0.257	0.217	0.343	0.361
[Eu]	0.038	0.072	0.071	0.050	0.042	0.068	0.080
[Gd]	0.123	0.349	0.308	0.219	0.209	0.323	0.347
[Tb]	0.020	0.054	0.052	0.030	0.029	0.047	0.055
[Dy]	0.110	0.328	0.313	0.177	0.173	0.290	0.323
[Ho]	0.021	0.068	0.062	0.035	0.036	0.059	0.064
[Er]	0.064	0.201	0.173	0.108	0.110	0.172	0.191
[Tm]	0.010	0.029	0.027	0.014	0.015	0.023	0.025
[Yb]	0.057	0.195	0.168	0.087	0.101	0.168	0.159
[Lu]	0.009	0.031	0.025	0.015	0.014	0.024	0.023
[Pb]	0.676	0.382	1.459	1.046	0.426	0.743	0.886
Ce/Ce*	0.934	0.957	0.962	0.909	0.918	0.923	0.968
Pr/Pr*	1.011	0.987	1.007	1.017	1.000	1.015	0.992
Eu/Eu*	1.340	0.967	1.062	0.975	0.931	0.950	1.058
Mg/Ca	1.004	0.889	1.227	1.352	1.242	1.231	1.184
Zn/Fe	0.042	0.015	BDL	0.011	0.013	0.012	0.015
Y/Ho	32.639	30.289	31.727	30.954	31.417	30.582	28.930
Yb/Nd	0.929	1.306	1.323	0.796	1.017	1.079	1.058

Sample ID	Gr208	Gr209	Gr210	Gr211	Gr212	Gr213	Gr214
[Li]	10.583	2.248	2.277	3.865	3.368	4.236	2.513
[Mg]	33607.95	51976.54	59717.41	64427.72	63511.84	66771.30	51909.05
[Al]	571.740	272.603	129.862	176.952	153.630	216.741	163.852
[Si]	462.790	398.674	262.193	404.831	250.955	188.677	323.237
[P]	81.880	10.528	3.808	39.830	11.003	6.215	50.224
[K]	1071.038	325.312	109.246	211.155	97.269	153.141	237.286
[Ca]	35666.92	56707.02	72742.57	61679.19	50860.00	59284.62	44791.18
[Sc]	0.231	0.369	0.260	0.058	0.132	0.282	0.101
[V]	3.204	1.186	1.522	3.920	4.267		7.682
[Mn]	83.199	57.326	27.575	22.097	31.590	23.990	22.257
[Fe]	1254.826	1058.992	178.558	184.489	310.246	181.032	190.425
[Co]	1.461	2.395	0.161	0.152	0.081	0.314	0.112
[Ni]	18.638	15.587	0.378	0.563	0.319	BDL	0.655
[Zn]	4.674	4.462	3.232	2.901	3.580	BDL	3.507
[Rb]	3.991	1.857	0.759	1.306	0.586	0.677	1.317
[Sr]	200.939	225.895	394.345	292.382	276.377	409.196	235.451
[Y]	2.662	2.822	1.584	1.539	1.445	1.402	2.238
[Zr]	0.109	0.035	0.051	0.064	0.029	0.046	0.051
[Nb]	BDL						
[Mo]	0.436	1.059	0.001	0.002	0.006	BDL	0.005
[La]	2.390	2.540	2.018	2.534	1.561	1.543	2.249
[Ce]	5.410	5.476	3.894	4.247	2.802	3.157	4.127
[Pr]	0.657	0.642	0.459	0.530	0.336	0.377	0.592
[Nd]	2.596	2.407	1.644	1.908	1.225	1.394	2.276
[Sm]	0.540	0.522	0.310	0.372	0.258	0.267	0.460
[Eu]	0.147	0.135	0.081	0.081	0.063	0.073	0.112
[Gd]	0.502	0.497	0.314	0.339	0.254	0.267	0.450
[Tb]	0.077	0.078	0.045	0.047	0.039	0.041	0.068
[Dy]	0.449	0.454	0.253	0.242	0.223	0.226	0.370
[Ho]	0.089	0.091	0.052	0.049	0.045	0.045	0.074
[Er]	0.258	0.255	0.149	0.130	0.131	0.124	0.201
[Tm]	0.037	0.038	0.019	0.018	0.018	0.021	0.025
[Yb]	0.245	0.220	0.129	0.099	0.111	0.114	0.154
[Lu]	0.041	0.033	0.019	0.015	0.016	0.018	0.020
[Pb]	0.469	0.363	0.642	0.691	0.693	0.638	1.053
Ce/Ce*	0.993	0.986	0.931	0.842	0.890	0.952	0.822
Pr/Pr*	0.996	1.005	1.031	1.059	1.031	1.020	1.098
Eu/Eu*	1.314	1.238	1.217	1.064	1.141	1.276	1.147
Mg/Ca	1.554	1.511	1.353	1.722	2.059	1.857	1.911
Zn/Fe	0.003	0.004	0.015	0.013	0.010	BDL	0.015
Y/Ho	30.049	30.965	30.222	31.518	32.370	31.276	30.113
Yb/Nd	1.077	1.043	0.898	0.596	1.034	0.930	0.773

Sample ID	Gr215	Gr216	Gr217	Gr218	Gr219	Gr220	Gr221
[Li]	3.613	2.808	3.097	1.702	3.026	1.922	2.289
[Mg]	69881.57	58035.50	61243.14	57648.33	48635.56	56702.53	56785.17
[Al]	162.105	194.721	162.524	82.202	289.554	127.365	194.454
[Si]	245.683	369.827	341.397	239.546	452.816	308.801	521.923
[P]	37.860	15.686	6.196	4.954	30.706	BDL	106.498
[K]	224.816	214.948	148.835	113.249	389.456	132.874	217.342
[Ca]	33471.59	60285.02	73926.61	63293.26	53294.04	64239.85	53860.20
[Sc]	0.164	BDL	0.139	0.111	0.196	0.102	0.201
[V]	2.279	2.382		1.757	2.866	1.075	6.165
[Mn]	30.393	35.361	22.530	21.853	31.368	24.169	27.262
[Fe]	261.935	189.820	168.072	192.874	196.144	212.889	262.601
[Co]	0.081	1.105	0.346	0.105	0.178	0.172	0.281
[Ni]	0.467	0.658	BDL	0.532	0.457	0.465	0.632
[Zn]	3.950	3.606	BDL	8.353	4.502	6.622	16.140
[Rb]	1.256	1.295	0.965	0.878	1.985	0.983	1.157
[Sr]	244.632	496.711	604.729	306.562	357.941	318.050	269.776
[Y]	2.687	2.117	2.385	1.297	3.153	1.421	3.116
[Zr]	0.107	0.089	0.193	BDL	0.122	BDL	0.087
[Nb]	BDL	BDL	BDL	0.009	0.008	BDL	0.059
[Mo]	BDL	0.001	BDL	BDL	0.001	0.001	0.012
[La]	2.073	2.461	2.620	2.047	2.887	2.081	2.340
[Ce]	4.209	4.623	5.019	3.914	5.731	3.891	5.208
[Pr]	0.562	0.546	0.605	0.443	0.683	0.447	0.723
[Nd]	2.181	2.046	2.234	1.567	2.540	1.594	2.904
[Sm]	0.461	0.393	0.470	0.298	0.507	0.290	0.665
[Eu]	0.101	0.088	0.076	0.072	0.101	0.086	0.141
[Gd]	0.474	0.378	0.413	0.266	0.520	0.286	0.653
[Tb]	0.076	0.053	0.062	0.040	0.080	0.041	0.099
[Dy]	0.421	0.314	0.367	0.229	0.485	0.235	0.562
[Ho]	0.086	0.066	0.081	0.044	0.103	0.045	0.114
[Er]	0.243	0.193	0.218	0.119	0.296	0.127	0.304
[Tm]	0.034	0.024	0.030	0.016	0.044	0.019	0.040
[Yb]	0.199	0.160	0.192	0.090	0.289	0.115	0.224
[Lu]	0.030	0.024	0.028	0.012	0.045	0.015	0.033
[Pb]	0.746	2.309	1.038	0.743	1.706	1.540	1.264
Ce/Ce*	0.897	0.917	0.917	0.945	0.938	0.927	0.921
Pr/Pr*	1.054	1.008	1.026	1.016	1.017	1.021	1.056
Eu/Eu*	1.009	1.070	0.800	1.194	0.916	1.387	1.000
Mg/Ca	3.442	1.587	1.366	1.502	1.505	1.455	1.738
Zn/Fe	0.013	0.016	BDL	0.036	0.019	0.026	0.052
Y/Ho	31.192	32.291	29.432	29.633	30.666	31.830	27.353
Yb/Nd	1.045	0.894	0.984	0.660	1.302	0.821	0.883

Sample ID	Gr222	Gr223	Gr224	Gr225	Gr226	Gr227	Gr228
[Li]	3.736	3.363	2.781	4.076	3.127	3.640	1.143
[Mg]	55301.19	60798.35	62643.36	60280.98	53320.10	54563.06	47631.32
[Al]	440.490	121.054	66.787	108.811	70.612	84.420	92.432
[Si]	212.394	447.584	243.290	275.397	351.353	229.931	299.522
[P]	4.178	6.422	BDL	13.045	BDL	4.091	21.341
[K]	112.292	161.453	79.765	174.734	74.180	71.243	115.734
[Ca]	71632.82	66222.31	73830.36	67203.74	65106.47	70027.05	61617.23
[Sc]	0.281	0.141	0.146	0.120	0.132	0.140	0.226
[V]	BDL	6.259	1.011	2.485	BDL	0.635	0.852
[Mn]	22.366	26.092	23.860	7.737	18.503	15.517	39.193
[Fe]	139.677	155.673	177.109	120.008	158.254	137.468	190.173
[Co]	0.319	0.539	0.124	0.206	0.101	0.122	0.104
[Ni]	BDL	0.516	0.460	0.666	BDL	0.255	0.574
[Zn]	BDL	5.380	4.366	10.500	BDL	2.787	3.565
[Rb]	0.740	1.007	0.605	1.163	0.518	0.591	0.665
[Sr]	499.679	406.726	380.735	392.062	436.445	416.319	272.596
[Y]	2.170	2.116	1.538	0.818	1.570	1.148	1.843
[Zr]	0.066	0.106	#VALUE!	0.055	0.116	0.040	0.037
[Nb]	BDL	0.028	0.011	0.020	BDL	BDL	BDL
[Mo]	BDL	0.005	0.005	0.005	BDL	0.007	0.006
[La]	2.201	2.557	1.953	1.689	1.689	1.083	1.360
[Ce]	4.269	5.020	3.716	2.923	2.899	2.224	3.042
[Pr]	0.531	0.597	0.431	0.339	0.329	0.252	0.345
[Nd]	2.062	2.274	1.565	1.224	1.221	0.939	1.369
[Sm]	0.429	0.436	0.310	0.217	0.204	0.195	0.303
[Eu]	0.087	0.093	0.085	0.043	0.043	0.053	0.081
[Gd]	0.396	0.409	0.296	0.199	0.203	0.210	0.316
[Tb]	0.064	0.062	0.044	0.027	0.027	0.032	0.051
[Dy]	0.360	0.346	0.257	0.144	0.132	0.187	0.309
[Ho]	0.071	0.069	0.050	0.026	0.025	0.036	0.061
[Er]	0.193	0.193	0.139	0.074	0.074	0.108	0.170
[Tm]	0.027	0.026	0.019	0.010	0.010	0.013	0.023
[Yb]	0.168	0.165	0.108	0.062	0.066	0.095	0.137
[Lu]	0.025	0.024	0.015	0.009	0.010	0.012	0.021
[Pb]	0.774	1.653	0.782	0.816	2.852	0.723	1.472
Ce/Ce*	0.908	0.934	0.931	0.888	0.894	0.979	1.021
Pr/Pr*	1.017	1.005	1.016	1.018	0.994	0.990	0.962
Eu/Eu*	0.990	1.026	1.309	0.972	0.980	1.229	1.222
Mg/Ca	1.273	1.514	1.399	1.479	1.350	1.285	1.274
Zn/Fe		0.028	0.021	0.072	BDL	0.017	0.015
Y/Ho	30.483	30.605	30.765	31.626	61.665	31.502	30.114
Yb/Nd	0.931	0.831	0.792	0.581	0.620	1.153	1.143

Sample ID	Gr229	Gr230	Gr231	Gr232	Gr233	Gr234	Gr235
[Li]	1.881	1.657	1.099	2.036	3.855	2.635	2.039
[Mg]	49069.52	44360.04	73035.84	49345.81	83145.08	51124.13	47366.82
[Al]	115.046	339.322	83.515	433.727	193.686	290.878	234.080
[Si]	303.337	459.258	635.730	533.152	525.031	338.244	388.204
[P]	23.999	14.206	16.350	14.690	118.697	18.285	37.740
[K]	177.323	311.712	45.840	436.577	257.853	387.465	138.077
[Ca]	61534.00	56966.78	1145.50	43208.09	12083.60	63225.75	42305.03
[Sc]	0.169	0.407	BDL	0.323	0.061	0.776	0.173
[V]	0.692	0.660	0.646	0.869	1.456	BDL	6.890
[Mn]	36.255	53.794	42.964	53.562	51.575	117.553	37.564
[Fe]	206.980	191.087	621.089	423.097	914.202	1261.492	213.153
[Co]	0.099	0.702	0.061	0.688	0.291	0.383	1.419
[Ni]	0.337	0.709	0.114	0.513	0.886	BDL	1.255
[Zn]	5.820	8.132	7.545	7.178	19.388	BDL	12.802
[Rb]	0.826	1.464	0.345	2.107	1.790	2.290	0.831
[Sr]	313.215	257.536	10.837	207.077	65.039	409.672	229.711
[Y]	2.534	3.095	0.203	2.693	1.023	3.926	1.660
[Zr]	BDL	0.085	BDL	0.054	0.200	0.136	0.056
[Nb]	BDL	BDL	BDL	0.013	0.012	BDL	BDL
[Mo]	0.001	0.007	BDL	BDL	0.000	BDL	0.002
[La]	2.138	2.958	0.361	1.914	1.436	2.504	1.395
[Ce]	4.735	5.938	0.711	4.107	2.593	5.477	2.854
[Pr]	0.545	0.714	0.072	0.493	0.298	0.636	0.346
[Nd]	2.040	2.644	0.261	1.847	1.146	2.479	1.426
[Sm]	0.420	0.533	0.049	0.393	0.217	0.578	0.295
[Eu]	0.109	0.120	0.029	0.097	0.047	0.119	0.065
[Gd]	0.431	0.532	0.047	0.410	0.203	0.634	0.308
[Tb]	0.070	0.077	0.007	0.070	0.029	0.101	0.045
[Dy]	0.398	0.478	0.035	0.420	0.152	0.626	0.264
[Ho]	0.076	0.104	0.006	0.085	0.029	0.128	0.053
[Er]	0.231	0.303	0.018	0.245	0.096	0.368	0.157
[Tm]	0.033	0.047	0.002	0.034	0.012	0.052	0.022
[Yb]	0.201	0.296	0.014	0.220	0.072	0.319	0.139
[Lu]	0.029	0.045	0.001	0.031	0.011	0.047	0.020
[Pb]	1.240	1.611	0.257	0.777	0.160	1.271	0.912
Ce/Ce*	1.008	0.939	1.010	0.972	0.912	0.998	0.945
Pr/Pr*	0.997	1.024	0.956	1.017	0.982	0.981	0.974
Eu/Eu*	1.196	1.052	2.784	1.128	1.039	0.917	1.001
Mg/Ca	1.315	1.284	105.119	1.883	11.344	1.333	1.846
Zn/Fe	0.023	0.036	0.010	0.014	0.018	BDL	0.051
Y/Ho	33.267	29.711	34.945	31.763	35.311	30.701	31.542
Yb/Nd	1.123	1.279	0.603	1.360	0.716	1.473	1.117

Sample ID	Gr236	Gr237	Gr238	Gr239	Gr240	Gr241	Gr101
[Li]	2.908	2.274	2.479	2.194	2.223	3.396	5.496
[Mg]	54799.97	53853.50	48289.02	47262.70	66723.30	55696.19	44777.83
[Al]	209.308	79.672	108.033	164.236	131.497	334.657	1461.643
[Si]	335.316	221.527	350.600	277.366	236.499	378.695	1087.109
[P]	17.474	28.368	35.494	34.128	13.262	11.253	14.099
[K]	221.815	46.956	187.965	102.415	141.212	186.281	747.315
[Ca]	57891.76	67409.03	51162.72	35252.83	59085.37	60460.39	59248.09
[Sc]	0.245	0.084	0.087	0.168	0.279	0.240	0.438
[V]	1.225		0.708	1.251	1.147	0.971	
[Mn]	35.378	32.752	8.519	22.896	25.749	32.691	123.278
[Fe]	223.203	181.118	164.817	340.733	387.407	253.923	501.073
[Co]	0.147	0.908	0.478	0.381	0.317	0.327	1.145
[Ni]	0.614	BDL	0.936	1.352	0.840	0.631	BDL
[Zn]	9.432	BDL	14.710	5.731	18.679	4.488	BDL
[Rb]	1.374	0.535	1.383	0.678	0.926	1.251	3.394
[Sr]	290.230	318.006	197.071	179.024	232.882	301.092	442.314
[Y]	3.247	0.838	0.400	1.406	1.481	1.600	4.131
[Zr]	0.050	0.065	0.194	0.090	0.099	0.094	1.013
[Nb]	BDL	BDL	0.022	BDL	0.007	BDL	BDL
[Mo]	0.004		0.015	0.074	0.012	0.013	BDL
[La]	2.102	1.240	0.312	1.287	1.706	1.685	3.258
[Ce]	4.496	2.305	0.647	2.733	3.364	3.242	7.349
[Pr]	0.533	0.264	0.087	0.335	0.405	0.386	0.938
[Nd]	2.111	0.965	0.353	1.300	1.543	1.469	3.524
[Sm]	0.472	0.173	0.084	0.272	0.315	0.294	0.806
[Eu]	0.106	0.048	0.019	0.054	0.066	0.068	0.186
[Gd]	0.496	0.164	0.085	0.262	0.303	0.290	0.832
[Tb]	0.078	0.022	0.013	0.038	0.043	0.046	0.117
[Dy]	0.475	0.137	0.066	0.220	0.249	0.243	0.719
[Ho]	0.096	0.025	0.014	0.044	0.051	0.049	0.145
[Er]	0.267	0.072	0.037	0.125	0.138	0.144	0.425
[Tm]	0.036	0.010	0.005	0.017	0.019	0.020	0.063
[Yb]	0.235	0.065	0.035	0.110	0.110	0.118	0.384
[Lu]	0.032	0.009	0.005	0.016	0.017	0.019	0.064
[Pb]	1.149	1.438	BDL	0.428	0.774	0.723	0.595
Ce/Ce*	0.977	0.926	0.903	0.956	0.931	0.923	0.966
Pr/Pr*	0.983	1.006	1.035	1.011	1.009	1.007	1.048
Eu/Eu*	1.025	1.323	1.034	0.934	0.990	1.091	1.060
Mg/Ca	1.561	1.317	1.556	2.210	1.862	1.519	1.246
Zn/Fe	0.035	BDL	0.073	0.014	0.041	0.015	BDL
Y/Ho	33.747	33.011	28.723	32.222	28.937	32.710	28.409
Yb/Nd	1.270	0.768	1.136	0.964	0.812	0.917	1.224

Sample ID	Gr102	Gr103	Gr104	Gr105	Gr106	Gr107	Gr108
[Li]	3.777	3.870	1.517	6.844	1.986	3.895	22.672
[Mg]	65011.53	73307.14	49289.77	33774.78	28802.63	62471.25	34461.36
[Al]	810.076	210.954	236.641	854.249	871.051	401.668	1774.173
[Si]	1746.648	218.925	411.169	900.719	981.255	527.429	2537.572
[P]	10.249	48.103	209.599	38.621	73.326	60.129	85.681
[K]	488.739	142.968	128.289	560.030	534.373	210.905	2137.657
[Ca]	92457.30	16368.55	60820.67	43691.28	45393.51	67888.44	39190.64
[Sc]	0.745	0.051	0.117	0.358	0.218	0.316	0.367
[V]	1.298	0.838	0.651	1.701	1.171	2.837	3.456
[Mn]	164.937	96.101	108.973	171.948	183.813	90.650	218.148
[Fe]	3090.442	811.478	439.825	5228.317	4886.817	678.746	2698.931
[Co]	9.565	1.061	1.481	24.496	6.022	1.683	4.917
[Ni]	83.236	33.937	33.738	285.424	533.429	27.550	1334.210
[Zn]	6.470	13.845	12.218	8.298	9.894	12.502	21.282
[Rb]	2.728	1.642	2.660	6.102	1.203	1.500	13.095
[Sr]	470.393	81.633	335.864	284.551	294.358	363.618	187.248
[Y]	3.825	2.071	3.571	4.286	6.240	2.827	3.330
[Zr]	0.487	BDL	BDL	0.429	0.431	0.148	0.240
[Nb]	0.065	0.094	0.035	0.021	0.022	0.034	0.062
[Mo]	4.171	0.112	0.035	5.056	5.119	0.028	1.647
[La]	2.989	1.219	2.028	2.826	2.657	1.185	0.929
[Ce]	6.090	2.927	4.620	6.421	6.065	2.892	2.197
[Pr]	0.790	0.378	0.592	0.813	0.757	0.396	0.372
[Nd]	3.086	1.529	2.497	3.183	2.924	1.761	1.758
[Sm]	0.643	0.422	0.590	0.683	0.659	0.472	0.506
[Eu]	0.162	0.146	0.135	0.170	0.192	0.140	0.160
[Gd]	0.629	0.420	0.626	0.698	0.768	0.525	0.576
[Tb]	0.099	0.066	0.101	0.107	0.114	0.080	0.097
[Dy]	0.567	0.371	0.589	0.642	0.747	0.459	0.563
[Ho]	0.112	0.071	0.119	0.137	0.185	0.091	0.115
[Er]	0.322	0.193	0.344	0.425	0.613	0.249	0.331
[Tm]	0.044	0.026	0.050	0.062	0.098	0.031	0.048
[Yb]	0.274	0.134	0.286	0.434	0.699	0.182	0.333
[Lu]	0.047	0.017	0.044	0.072	0.123	0.026	0.055
[Pb]	2.426	1.763	1.279	9.430	5.578	2.261	3.674
Ce/Ce*	0.911	0.991	0.969	0.974	0.983	0.971	0.858
Pr/Pr*	1.035	1.016	0.991	1.022	1.022	0.997	1.077
Eu/Eu*	1.188	1.621	1.034	1.149	1.257	1.310	1.382
Mg/Ca	1.159	7.384	1.336	1.275	1.046	1.517	1.450
Zn/Fe	0.002	0.015	0.023	0.001	0.002	0.016	0.007
Y/Ho	34.264	29.128	30.047	31.376	33.712	30.962	28.966
Yb/Nd	1.016	1.001	1.311	1.557	2.731	1.178	2.164

Sample ID	Gr109	Gr110	Gr111	Gr112	Gr113	Gr114	Gr115
[Li]	5.474	43.432	8.009	7.638	16.369	10.639	1.693
[Mg]	59130.34	26322.06	56751.12	43609.12	57641.61	49169.42	55433.60
[Al]	557.052	2989.521	1347.404	1966.562	1965.092	2484.952	205.393
[Si]	828.394	3347.791	1772.930	1011.256	2824.393	2619.917	308.415
[P]	7.241	227.783	12.396	11.468	8.021	8.697	6.943
[K]	915.293	4267.898	1517.152	1139.021	2020.074	2014.482	BDL
[Ca]	84993.74	51484.55	77076.70	61125.86	79102.04	65557.53	65923.52
[Sc]	0.864	0.451	0.520	0.404	0.543	0.635	0.320
[V]		8.078	1.824	1.919	1.956	2.482	1.159
[Mn]	275.062	166.616	240.458	461.703	833.683	481.348	324.738
[Fe]	1281.021	9604.701	1020.274	1426.012	1287.392	1060.934	1177.237
[Co]	1.353	34.486	1.337	1.243	0.427	0.671	0.556
[Ni]	BDL	170.139	20.975	13.240	3.058	3.932	0.349
[Zn]	BDL	35.636	10.938	17.418	10.862	9.045	2.511
[Rb]	4.395	20.586	7.392	6.028	10.071	9.502	0.078
[Sr]	360.383	118.566	379.834	358.654	342.511	296.684	210.238
[Y]	4.747	3.601	3.770	3.841	4.835	3.564	1.189
[Zr]	0.081	0.231	0.553	0.219	0.262	0.333	0.105
[Nb]	BDL	0.073	0.040	0.038	0.056	0.043	BDL
[Mo]	BDL	5.809	0.118	0.011	0.042	0.225	0.002
[La]	2.524	2.453	2.919	2.267	3.169	2.542	0.242
[Ce]	5.755	5.347	7.438	5.699	8.046	6.772	0.684
[Pr]	0.747	0.739	0.930	0.732	1.020	0.851	0.103
[Nd]	3.148	3.039	3.656	2.920	4.050	3.346	0.489
[Sm]	0.799	0.722	0.778	0.660	0.929	0.697	0.166
[Eu]	0.225	0.185	0.245	0.193	0.277	0.223	0.037
[Gd]	0.844	0.748	0.776	0.647	0.928	0.685	0.183
[Tb]	0.147	0.111	0.119	0.100	0.140	0.105	0.032
[Dy]	0.847	0.610	0.664	0.600	0.801	0.584	0.191
[Ho]	0.163	0.122	0.135	0.126	0.163	0.117	0.040
[Er]	0.460	0.360	0.368	0.385	0.481	0.346	0.114
[Tm]	0.060	0.054	0.051	0.055	0.065	0.048	0.016
[Yb]	0.403	0.348	0.321	0.357	0.416	0.315	0.105
[Lu]	0.057	0.052	0.046	0.058	0.068	0.051	0.016
[Pb]	1.104	5.243	2.193	2.509	1.529	1.144	BDL
Ce/Ce*	0.963	0.913	1.038	1.017	1.029	1.058	0.996
Pr/Pr*	0.998	1.042	1.014	1.020	1.016	1.017	1.010
Eu/Eu*	1.277	1.176	1.469	1.374	1.392	1.509	0.979
Mg/Ca	1.147	0.843	1.214	1.176	1.201	1.237	1.386
Zn/Fe	BDL	0.003	0.010	0.010	0.008	0.008	0.002
Y/Ho	29.072	29.415	27.894	30.382	29.732	30.354	30.011
Yb/Nd	1.464	1.309	1.003	1.398	1.173	1.077	2.457

Sample ID	Gr116	Gr117	Gr118	Gr119	Gr120	Gr121	Gr122
[Li]	1.626	0.479	9.474	19.081	4.115	1.548	2.378
[Mg]	46365.98	41956.73	51101.91	44556.80	50337.21	60583.04	54762.63
[Al]	58.938	73.590	1867.235	1467.572	784.485	143.798	407.425
[Si]	116.005	78.663	936.274	1556.267	986.777	499.358	892.758
[P]	28.288	39.660	8.274	33.131	12.901	7.892	BDL
[K]	11.207	13.756	1744.213	2444.620	866.652	145.873	429.331
[Ca]	65071.34	64523.63	69229.28	57812.80	69643.74	86158.96	76245.45
[Sc]	0.175	0.096	0.423	0.408	0.393	1.244	0.726
[V]	0.685	0.483	BDL	2.134	2.194	1.290	1.366
[Mn]	211.739	797.702	218.576	168.135	148.883	168.788	168.138
[Fe]	879.444	1713.027	877.127	1306.252	1638.825	3064.923	1835.168
[Co]	1.754	0.468	0.337	0.700	0.291	11.239	20.376
[Ni]	1.348	0.577	BDL	1.599	3.456	277.993	20.313
[Zn]	6.072	4.040	BDL	9.801	5.427	4.914	6.183
[Rb]	0.147	0.122	9.736	15.130	5.600	1.644	3.476
[Sr]	204.658	161.730	420.747	320.426	383.159	301.080	332.570
[Y]	1.750	2.741	1.995	1.967	1.930	3.915	2.786
[Zr]	0.073	BDL	0.471	0.496	0.240	0.221	0.112
[Nb]	BDL	BDL	BDL	0.042	0.032	0.015	0.016
[Mo]	0.008	0.014		0.015	0.039	1.992	2.131
[La]	0.728	1.486	3.790	2.270	2.286	2.505	2.174
[Ce]	2.073	3.294	8.025	4.687	5.319	5.722	5.181
[Pr]	0.314	0.382	0.883	0.520	0.607	0.697	0.618
[Nd]	1.320	1.530	2.958	1.900	2.201	2.680	2.361
[Sm]	0.333	0.285	0.505	0.371	0.404	0.651	0.516
[Eu]	0.080	0.072	0.147	0.093	0.120	0.150	0.144
[Gd]	0.341	0.340	0.422	0.387	0.375	0.710	0.532
[Tb]	0.055	0.057	0.068	0.057	0.058	0.118	0.082
[Dy]	0.310	0.355	0.321	0.320	0.329	0.683	0.469
[Ho]	0.064	0.082	0.075	0.067	0.064	0.133	0.087
[Er]	0.166	0.265	0.200	0.190	0.189	0.373	0.246
[Tm]	0.022	0.036	0.033	0.025	0.027	0.052	0.035
[Yb]	0.131	0.228	0.199	0.170	0.167	0.329	0.223
[Lu]	0.017	0.038	0.037	0.029	0.027	0.050	0.038
[Pb]	0.124	1.194	0.183	0.433	0.619	0.731	1.000
Ce/Ce*	0.997	1.005	1.009	0.992	1.038	0.995	1.027
Pr/Pr*	1.079	0.968	1.030	0.990	1.008	1.012	1.005
Eu/Eu*	1.106	1.075	1.486	1.146	1.433	1.031	1.284
Mg/Ca	1.175	1.072	1.217	1.271	1.192	1.159	1.184
Zn/Fe	0.006	0.002	BDL	0.006	0.003	0.001	0.003
Y/Ho	27.294	33.592	26.487	29.387	29.973	29.520	31.838
Yb/Nd	1.133	1.703	0.771	1.025	0.866	1.405	1.077

Sample ID	Gr123	Gr124	Gr125	Gr126	Gr127	Gr128	Gr129
[Li]	2.859	4.457	1.672	5.695	3.044	12.157	3.847
[Mg]	58741.67	64624.89	59652.71	79449.63	62707.53	54965.83	55687.98
[Al]	509.023	380.256	99.857	325.066	201.251	786.877	220.257
[Si]	485.154	656.918	248.329	662.525	495.448	981.300	636.131
[P]	4.279	4.864	10.310	6.392	#VALUE!	11.687	5.941
[K]	277.295	598.025	148.653	611.484	314.023	1266.241	512.685
[Ca]	80405.57	81857.33	79637.82	77391.80	82973.16	69474.28	74585.44
[Sc]	0.819	1.148	0.921	0.588	0.887	0.543	0.816
[V]	1.046	0.881	1.419	BDL	1.182	1.952	
[Mn]	140.847	159.624	131.811	137.081	114.734	162.850	167.408
[Fe]	1656.746	1488.865	1228.823	1603.215	1630.291	1628.859	1754.597
[Co]	0.747	0.301	0.142	0.403	0.201	0.318	0.530
[Ni]	50.373	10.001	2.746	BDL	1.499	4.628	BDL
[Zn]	3.816	5.823	4.545	BDL	7.227	5.011	BDL
[Rb]	2.460	5.032	1.414	5.205	2.803	9.973	4.450
[Sr]	286.773	411.573	368.890	442.960	416.650	357.360	364.113
[Y]	2.331	3.623	2.678	2.599	3.148	2.077	2.839
[Zr]	0.118	0.072	BDL	0.094	0.078	0.169	0.165
[Nb]	BDL	0.010	BDL	BDL	0.010	0.023	BDL
[Mo]	0.008	0.003	0.004	BDL	0.001	0.005	BDL
[La]	1.731	1.979	1.941	2.183	1.717	1.900	1.802
[Ce]	4.133	4.906	4.572	4.712	4.287	4.056	4.380
[Pr]	0.528	0.633	0.551	0.580	0.527	0.485	0.539
[Nd]	2.014	2.525	2.139	2.209	2.125	1.807	2.024
[Sm]	0.439	0.583	0.505	0.466	0.535	0.362	0.488
[Eu]	0.148	0.190	0.164	0.113	0.144	0.130	0.145
[Gd]	0.426	0.655	0.491	0.453	0.610	0.374	0.524
[Tb]	0.070	0.102	0.078	0.077	0.100	0.058	0.083
[Dy]	0.387	0.619	0.456	0.432	0.571	0.333	0.492
[Ho]	0.077	0.120	0.084	0.087	0.104	0.068	0.094
[Er]	0.224	0.350	0.233	0.246	0.287	0.198	0.281
[Tm]	0.029	0.048	0.031	0.037	0.038	0.028	0.038
[Yb]	0.199	0.306	0.187	0.232	0.242	0.164	0.247
[Lu]	0.029	0.042	0.027	0.037	0.034	0.029	0.034
[Pb]	1.579	3.542	2.871	1.402	1.481	1.099	1.687
Ce/Ce*	0.994	1.007	1.017	0.963	1.036	0.971	1.022
Pr/Pr*	1.040	1.023	1.001	1.022	0.992	1.019	1.028
Eu/Eu*	1.596	1.436	1.537	1.149	1.174	1.647	1.335
Mg/Ca	1.204	1.302	1.235	1.693	1.246	1.304	1.231
Zn/Fe	0.002	0.003	0.003	BDL	0.010	0.003	BDL
Y/Ho	30.263	30.188	31.980	29.713	30.298	30.707	30.305
Yb/Nd	1.130	1.386	0.997	1.200	1.301	1.034	1.396

Sample ID	Gr130	Gr131	Gr132	Gr133	Gr134	Gr135	Gr136
[Li]	5.345	6.898	0.869	5.382	2.125	2.858	0.989
[Mg]	55191.61	50235.60	54464.94	64196.82	60321.49	58801.56	55028.97
[Al]	371.057	993.692	39.560	519.765	215.102	399.689	49.985
[Si]	520.980	999.352	241.164	912.536	389.057	485.660	206.097
[P]	4.884	3.684	6.934	BDL	4.604	BDL	5.830
[K]	536.419	1054.596	1.387	348.853	138.045	348.946	BDL
[Ca]	74344.09	66188.27	72895.32	76666.18	75811.13	73801.30	72108.35
[Sc]	0.747	0.737	1.298	1.000	0.470	0.674	0.337
[V]	1.018	1.160	1.854	BDL	2.518	4.009	3.633
[Mn]	218.193	263.052	168.403	136.944	76.019	137.082	82.163
[Fe]	1522.083	1388.078	1732.410	1529.644	893.343	1379.870	1085.256
[Co]	0.428	0.362	0.332	0.448	0.202	0.393	0.271
[Ni]	7.318	1.591	1.613	BDL	1.887	0.666	0.567
[Zn]	5.607	5.712	2.712	BDL	3.914	2.619	2.186
[Rb]	4.633	7.219	0.036	3.838	1.319	12.632	0.029
[Sr]	231.167	242.540	268.485	462.944	346.906	345.731	357.489
[Y]	3.380	2.626	4.541	3.530	1.555	5.285	1.388
[Zr]	0.042	0.065	BDL	0.119	0.041	0.114	BDL
[Nb]	BDL						
[Mo]	0.003	0.001	0.002	BDL	0.002	BDL	BDL
[La]	2.407	2.094	1.118	1.237	1.229	1.114	1.375
[Ce]	5.578	4.756	3.008	3.125	3.235	2.523	3.040
[Pr]	0.696	0.567	0.444	0.438	0.389	0.393	0.368
[Nd]	2.619	2.099	1.916	1.932	1.483	1.741	1.365
[Sm]	0.582	0.483	0.620	0.528	0.338	0.599	0.275
[Eu]	0.159	0.128	0.133	0.146	0.111	0.132	0.097
[Gd]	0.605	0.524	0.715	0.579	0.302	0.792	0.268
[Tb]	0.096	0.083	0.125	0.098	0.048	0.142	0.040
[Dy]	0.562	0.461	0.782	0.603	0.256	0.853	0.235
[Ho]	0.114	0.090	0.151	0.118	0.049	0.163	0.047
[Er]	0.314	0.250	0.427	0.323	0.140	0.464	0.124
[Tm]	0.042	0.035	0.059	0.046	0.018	0.060	0.018
[Yb]	0.273	0.218	0.366	0.276	0.119	0.383	0.109
[Lu]	0.043	0.036	0.050	0.042	0.017	0.056	0.016
[Pb]	2.776	0.823	1.761	2.033	4.470	2.223	1.992
Ce/Ce*	1.314	1.004	0.982	0.976	1.076	0.877	0.982
Pr/Pr*	1.035	1.019	1.051	1.014	1.008	1.066	1.028
Eu/Eu*	1.249	1.189	0.932	1.231	1.617	0.895	1.663
Mg/Ca	1.224	1.251	1.232	1.381	1.312	1.314	1.258
Zn/Fe	0.003	0.003	0.001	BDL	0.004	0.002	0.002
Y/Ho	29.685	29.315	30.088	30.038	31.870	32.338	29.561
Yb/Nd	1.191	1.188	2.184	1.635	0.919	2.512	0.912

Sample ID	Gr137	Gr138	Gr139	Gr140	Gr141
[Li]	1.387	2.252	2.053	5.041	2.804
[Mg]	58658.96	62703.18	54801.45	36943.81	61260.07
[Al]	108.008	195.078	111.405	1159.766	353.126
[Si]	455.634	450.342	298.517	2053.537	695.012
[P]	5.297	4.270	7.895	12.193	5.228
[K]	8.579	195.323	6.777	773.031	268.675
[Ca]	78135.179	85750.172	74763.642	66664.562	89517.622
[Sc]	1.576	0.942	0.219	1.358	1.964
[V]	BDL	0.974	0.729	2.048	1.357
[Mn]	140.101	206.424	179.067	823.721	1331.549
[Fe]	1531.635	1593.424	1108.021	13838.477	3823.444
[Co]	0.456	0.754	0.200	15.041	0.551
[Ni]	BDL	4.259	0.512	334.766	31.797
[Zn]	BDL	4.782	2.347	4.950	16.357
[Rb]	0.051	3.012	0.081	4.571	1.773
[Sr]	257.185	209.251	200.359	77.901	117.913
[Y]	4.441	3.536	1.669	4.374	4.976
[Zr]	0.044	0.088	0.401	0.198	0.267
[Nb]	BDL	BDL	BDL	0.069	BDL
[Mo]	BDL	0.001	0.002	4.145	0.004
[La]	1.267	3.053	0.552	1.482	1.248
[Ce]	3.146	6.523	1.545	3.565	3.605
[Pr]	0.453	0.739	0.211	0.478	0.520
[Nd]	1.961	2.763	0.905	2.150	2.396
[Sm]	0.575	0.542	0.226	0.668	0.851
[Eu]	0.140	0.127	0.046	0.242	0.457
[Gd]	0.692	0.624	0.250	0.822	1.047
[Tb]	0.118	0.095	0.042	0.136	0.173
[Dy]	0.741	0.547	0.243	0.753	0.949
[Ho]	0.151	0.118	0.049	0.139	0.159
[Er]	0.443	0.336	0.139	0.384	0.400
[Tm]	0.064	0.050	0.019	0.051	0.050
[Yb]	0.380	0.324	0.115	0.332	0.322
[Lu]	0.054	0.057	0.017	0.050	0.048
[Pb]	2.456	1.025	BDL	0.570	0.772
Ce/Ce*	0.954	0.998	1.041	0.974	1.028
Pr/Pr*	1.037	0.990	1.014	0.982	1.007
Eu/Eu*	1.037	1.016	0.913	1.522	2.259
Mg/Ca	1.238	1.206	1.208	0.914	1.128
Zn/Fe	BDL	0.007	0.002	0.000	0.004
Y/Ho	29.438	29.991	33.968	31.583	31.203
Yb/Nd	2.213	1.341	1.455	1.763	1.534

Sample ID	Replicate THM 120	Replicate THM 202	Replicate THM 234	JDo-1 (1)	JDo-1 (2)	JDo-1 (3)	Proc. Blank 1
[Li]	2.394	1.140	1.612	BDL	0.199	BDL	BDL
[Mg]	56610.980	64169.583	47335.205	45929.280	0.000	41798.607	BDL
[Al]	BDL	BDL	BDL	BDL	BDL	BDL	BDL
[Si]	BDL	BDL	BDL	BDL	BDL	BDL	BDL
[P]	BDL	BDL	BDL	59.337	67.398	40.734	BDL
[K]	BDL	BDL	BDL	BDL	BDL	BDL	BDL
[Ca]	75649.990	110013.008	73955.324	90875.840	101721.343	83887.362	BDL
[Sc]	BDL	BDL	BDL	BDL	BDL	BDL	BDL
[V]	2.103	1.113	5.564	1.398	1.663	1.356	BDL
[Mn]	38.188	170.502	10.164	22.376	24.924	20.857	BDL
[Fe]	414.230	115.964	71.707	58.253	67.079	55.002	BDL
[Co]	0.338	1.940	3.983	BDL	BDL	BDL	BDL
[Ni]	BDL	4.187	4.734	1.060	1.286	0.908	BDL
[Zn]	BDL	7.157	BDL	9.406	11.507	9.800	BDL
[Rb]	BDL	BDL	BDL	BDL	BDL	BDL	BDL
[Sr]	327.951	139.659	229.627	45.248	50.558	43.794	BDL
[Y]	1.644	1.641	0.158	4.621	5.326	4.741	BDL
[Zr]	BDL	BDL	BDL	BDL	BDL	BDL	BDL
[Nb]	BDL	BDL	BDL	BDL	BDL	BDL	BDL
[Mo]	BDL	BDL	BDL	BDL	BDL	BDL	BDL
[La]	0.812	0.360	0.211	3.519	3.970	3.691	BDL
[Ce]	1.303	0.634	0.385	0.906	1.067	0.993	BDL
[Pr]	0.223	0.079	0.032	0.468	0.532	0.478	BDL
[Nd]	0.991	0.411	0.104	1.847	2.251	1.922	BDL
[Sm]	0.248	0.098	BDL	0.302	0.336	0.283	BDL
[Eu]	0.074	0.032	0.012	0.073	0.079	0.068	BDL
[Gd]	0.296	0.138	0.032	0.388	0.456	0.375	BDL
[Tb]	0.043	0.028	0.005	0.052	0.059	0.053	BDL
[Dy]	0.272	0.204	0.026	0.318	0.368	0.339	BDL
[Ho]	0.057	0.048	0.006	0.073	0.081	0.071	BDL
[Er]	0.146	0.145	0.017	0.202	0.231	0.201	BDL
[Tm]	0.023	0.020	0.003	0.024	0.029	0.025	BDL
[Yb]	0.123	0.136	0.018	0.134	0.155	0.132	BDL
[Lu]	0.019	0.020	0.005	0.019	0.021	0.019	BDL
[Pb]	0.275	0.424	BDL	BDL	BDL	BDL	BDL

Sample ID	Proc Blank 2	Proc Blank 3	Acid Blank 1	Replicate Gr115	Replicate Gr218	JDo-1 (4)	JDo-1 (5)
[Li]	BDL	BDL	BDL	1.884	0.751	0.294	0.257
[Mg]	BDL	BDL	BDL	60234.390	26102.053	71637.146	74415.001
[Al]	BDL	BDL	BDL	243.418	42.485	16.559	17.754
[Si]	BDL	BDL	BDL	498.295	139.300	7.830	24.537
[P]	BDL	BDL	BDL	7.847	BDL	31.132	59.170
[K]	BDL	BDL	BDL	BDL	50.023	BDL	BDL
[Ca]	BDL	BDL	BDL	72763.952	32336.396	161358.726	137471.897
[Sc]	BDL	BDL	BDL	0.362	0.060	BDL	0.142
[V]	BDL	BDL	BDL	BDL	BDL	BDL	BDL
[Mn]	BDL	BDL	BDL	348.619	9.800	37.192	36.099
[Fe]	BDL	BDL	BDL	1314.289	87.462	74.944	93.641
[Co]	BDL	BDL	BDL	0.704	0.048	0.154	0.065
[Ni]	BDL	BDL	BDL	BDL	BDL	1.948	1.815
[Zn]	BDL	BDL	BDL	4.423	3.151	26.641	20.979
[Rb]	BDL	BDL	BDL	0.050	0.378	BDL	0.014
[Sr]	BDL	BDL	BDL	230.955	144.893	92.673	61.549
[Y]	BDL	BDL	BDL	1.217	0.608	9.745	7.267
[Zr]	BDL	BDL	BDL	0.066	BDL	BDL	0.065
[Nb]	BDL	BDL	BDL	BDL	BDL	BDL	BDL
[Mo]	BDL	BDL	BDL	0.050	0.378	BDL	0.014
[La]	BDL	BDL	BDL	BDL	BDL	BDL	BDL
[Ce]	BDL	BDL	BDL	0.262	0.974	7.647	5.284
[Pr]	BDL	BDL	BDL	0.693	1.835	1.818	1.473
[Nd]	BDL	BDL	BDL	0.114	0.211	0.893	0.711
[Sm]	BDL	BDL	BDL	0.501	0.780	3.724	2.782
[Eu]	BDL	BDL	BDL	0.141	0.138	0.591	0.439
[Gd]	BDL	BDL	BDL	0.032	0.031	0.127	0.107
[Tb]	BDL	BDL	BDL	0.188	0.145	0.744	0.541
[Dy]	BDL	BDL	BDL	0.030	0.018	0.100	0.081
[Ho]	BDL	BDL	BDL	0.184	0.109	0.601	0.515
[Er]	BDL	BDL	BDL	0.111	0.053	0.351	BDL
[Tm]	BDL	BDL	BDL	0.016	0.006	0.042	BDL
[Yb]	BDL	BDL	BDL	0.101	0.043	0.218	BDL
[Lu]	BDL	BDL	BDL	0.016	0.006	0.033	BDL
[Pb]	BDL	BDL	BDL	BDL	0.305	0.087	0.242

Sample ID	Proc. Blank 4	Proc. Blank 5	Acid Blank 2	REPLICATE WR104	REPLICATE CP133	JDo-1 (6)	JDo-1 (7)
[Li]	BDL	BDL	BDL	1.819	5.676	0.193	0.172
[Mg]	BDL	BDL	BDL	21660.103	52634.428	50151.494	46552.346
[Al]	BDL	BDL	BDL	487.356	732.201	18.394	13.726
[Si]	BDL	BDL	BDL	326.108	1426.984	21.617	13.295
[P]	BDL	BDL	BDL	26.897	3.092	46.106	41.500
[K]	BDL	BDL	BDL	56.831	450.049	3.189	1.262
[Ca]	BDL	BDL	BDL	66432.182	72163.906	89550.230	81379.856
[Sc]	BDL	BDL	BDL	2.683	0.954	0.096	0.096
[V]	BDL	BDL	BDL	2.754	2.471	1.804	1.616
[Mn]	BDL	BDL	BDL	448.899	117.000	24.002	21.710
[Fe]	BDL	BDL	BDL	BDL	BDL	67.765	60.508
[Co]	BDL	BDL	BDL	0.595	0.417	0.058	0.051
[Ni]	BDL	BDL	BDL	3.582	1.350	1.958	1.143
[Zn]	0.018	0.038	BDL	3.694	5.270	18.601	12.776
[Rb]	BDL	BDL	BDL	0.552	4.299	0.008	0.011
[Sr]	BDL	BDL	BDL	243.706	418.254	42.189	36.195
[Y]	BDL	BDL	BDL	2.862	3.266	5.350	4.227
[Zr]	BDL	BDL	BDL	0.119	0.079	0.048	0.033
[Nb]	BDL	BDL	BDL	0.047	BDL	BDL	BDL
[Mo]	BDL	BDL	BDL	BDL	BDL	BDL	BDL
[La]	BDL	BDL	BDL	0.826	1.160	4.052	3.090
[Ce]	BDL	BDL	BDL	1.538	2.939	1.157	0.875
[Pr]	BDL	BDL	BDL	0.255	0.404	0.551	0.416
[Nd]	BDL	BDL	BDL	1.219	1.800	2.134	1.621
[Sm]	BDL	BDL	BDL	0.408	0.513	0.344	0.257
[Eu]	BDL	BDL	BDL	0.185	0.131	0.083	0.066
[Gd]	BDL	BDL	BDL	0.547	0.562	0.414	0.347
[Tb]	BDL	BDL	BDL	0.088	0.092	0.061	0.048
[Dy]	BDL	BDL	BDL	0.490	0.548	0.367	0.291
[Ho]	BDL	BDL	BDL	0.091	0.110	0.083	0.065
[Er]	BDL	BDL	BDL	0.263	0.311	0.227	0.185
[Tm]	BDL	BDL	BDL	0.037	0.044	0.029	0.022
[Yb]	BDL	BDL	BDL	0.257	0.247	0.156	0.116
[Lu]	BDL	BDL	BDL	0.047	0.037	0.019	0.015
[Pb]	BDL	BDL	BDL	0.340	2.188	0.309	0.185

Sample ID	JDo-1 (8)	JDo-1 (9)	Proc. Blank 6	Proc. Blank 7	Acid Blank 3
[Li]	0.248	0.193	BDL	BDL	BDL
[Mg]	51736.629	51545.445	BDL	BDL	BDL
[Al]	6.614	19.280	BDL	BDL	BDL
[Si]	6.470	17.710	BDL	BDL	BDL
[P]	17.223	40.388	BDL	BDL	BDL
[K]	3.222	3.344	BDL	BDL	BDL
[Ca]	129960.403	95789.097	BDL	BDL	BDL
[Sc]	0.028	0.094	BDL	BDL	BDL
[V]	1.641	1.883	BDL	BDL	BDL
[Mn]	27.453	25.904	BDL	BDL	BDL
[Fe]	60.498	74.392	BDL	BDL	BDL
[Co]	0.127	0.063	BDL	BDL	BDL
[Ni]	2.682	2.530	BDL	BDL	BDL
[Zn]	16.621	19.611	BDL	BDL	BDL
[Rb]	0.004	0.015	BDL	BDL	BDL
[Sr]	70.798	43.619	BDL	BDL	BDL
[Y]	5.636	5.883	BDL	BDL	BDL
[Zr]	0.101	0.039	BDL	BDL	BDL
[Nb]	BDL	BDL	BDL	BDL	BDL
[Mo]	BDL	BDL	BDL	BDL	BDL
[La]	4.547	4.307	BDL	BDL	BDL
[Ce]	1.000	1.183	BDL	BDL	BDL
[Pr]	0.489	0.580	BDL	BDL	BDL
[Nd]	2.130	2.251	BDL	BDL	BDL
[Sm]	0.327	0.357	BDL	BDL	BDL
[Eu]	0.081	0.085	BDL	BDL	BDL
[Gd]	0.438	0.448	BDL	BDL	BDL
[Tb]	0.054	0.064	BDL	BDL	BDL
[Dy]	0.321	0.400	BDL	BDL	BDL
[Ho]	0.072	0.091	BDL	BDL	BDL
[Er]	0.195	0.244	BDL	BDL	BDL
[Tm]	0.023	0.032	BDL	BDL	BDL
[Yb]	0.129	0.172	BDL	BDL	BDL
[Lu]	0.019	0.023	BDL	BDL	BDL
[Pb]	0.113	0.171	BDL	BDL	BDL

Sr and Nd blank summary

Sample ID	Sr (pg)	Sample ID	Nd (pg)
Blank 1	313	Blank 1	9
Blank 2	345	Blank 2	80
Blank 3	170	Blank 3	18

Cross plots of REY and trace element abundances against contamination proxies

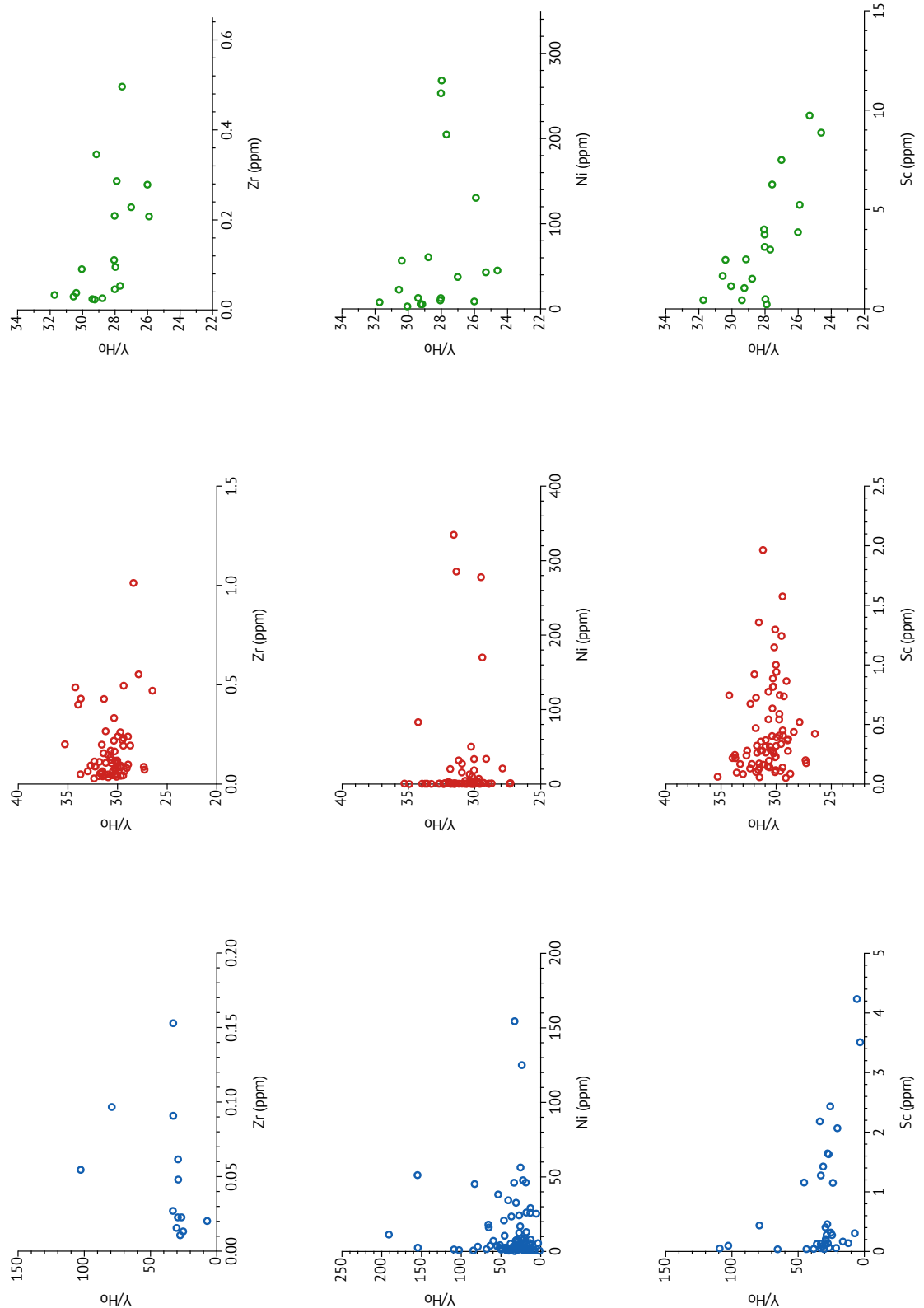


Figure 16: Termination Hill (blue), Gammon Ranges (red) and Copley (green). Gammon Ranges plots; 1 outlier in Zr and Sc and 2 outliers in Ni not included. Copley Plots; 2 outliers in Zr and Ni not included. Copley plots; $R^2 = 0.406$ between with Zr and Ni and $R^2 = 0.6027$ with Sc. All samples are marine carbonates from the Burra Group, South Australia.

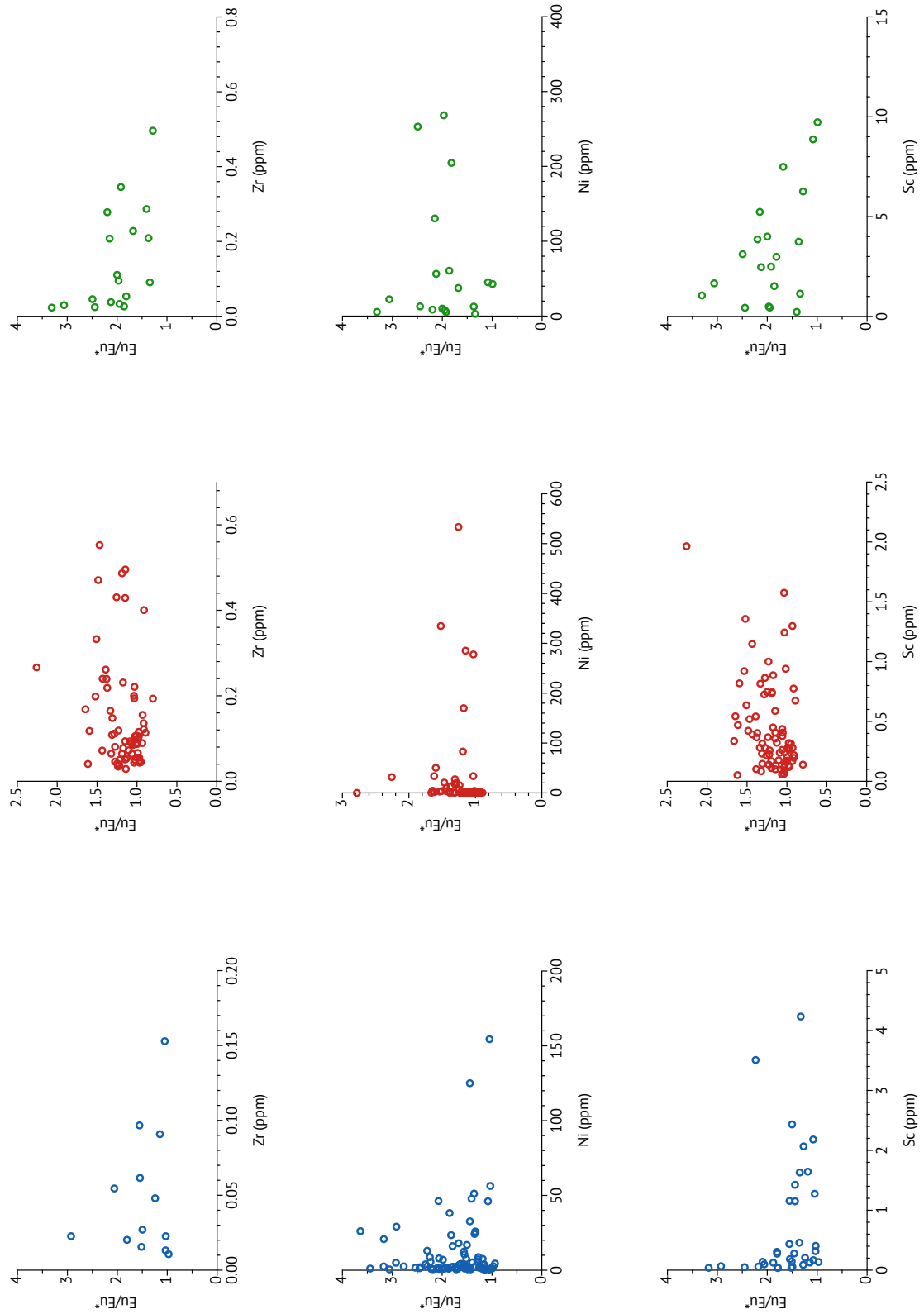


Figure 17: Termination Hill (blue), Gammon Ranges (red) and Copley (green). Gammon Ranges plots; 1 outlier in Zr and Ni. Copley Plots; 2 outliers in Zr and Ni not included. Copley plots; $R^2 = 0.3275$ between with Zr and $R^2 = 0.2747$ with Sc. All samples are marine carbonates from the Burra Group, South Australia.

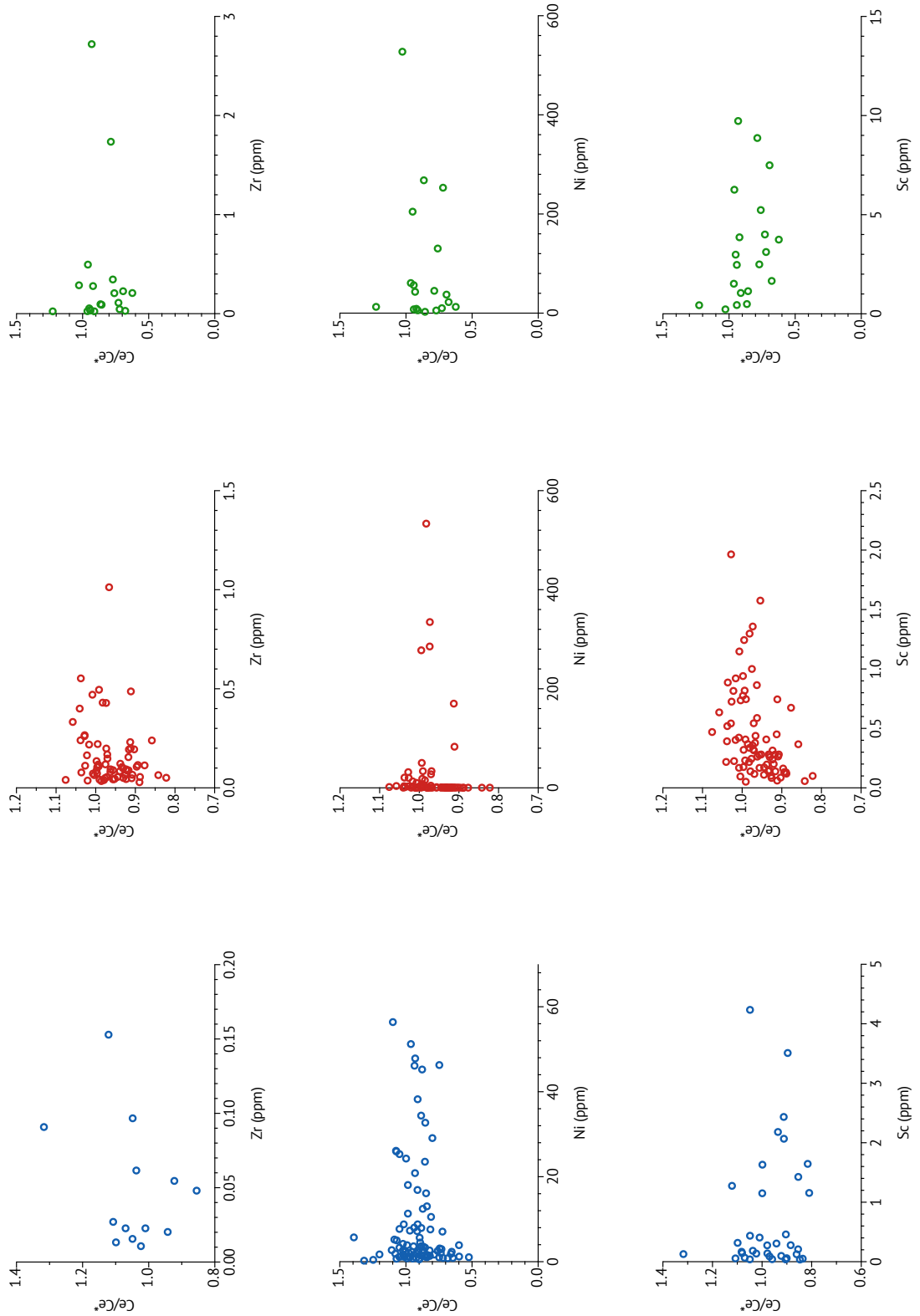


Figure 18: Termination Hill (blue), Gammon Ranges (red) and Copley (green). Gammon Ranges plots; 1 outlier in Ni not included. Copley Plots; 1 outlier in Ni not included. All samples are marine carbonates from the Burra Group, South Australia.

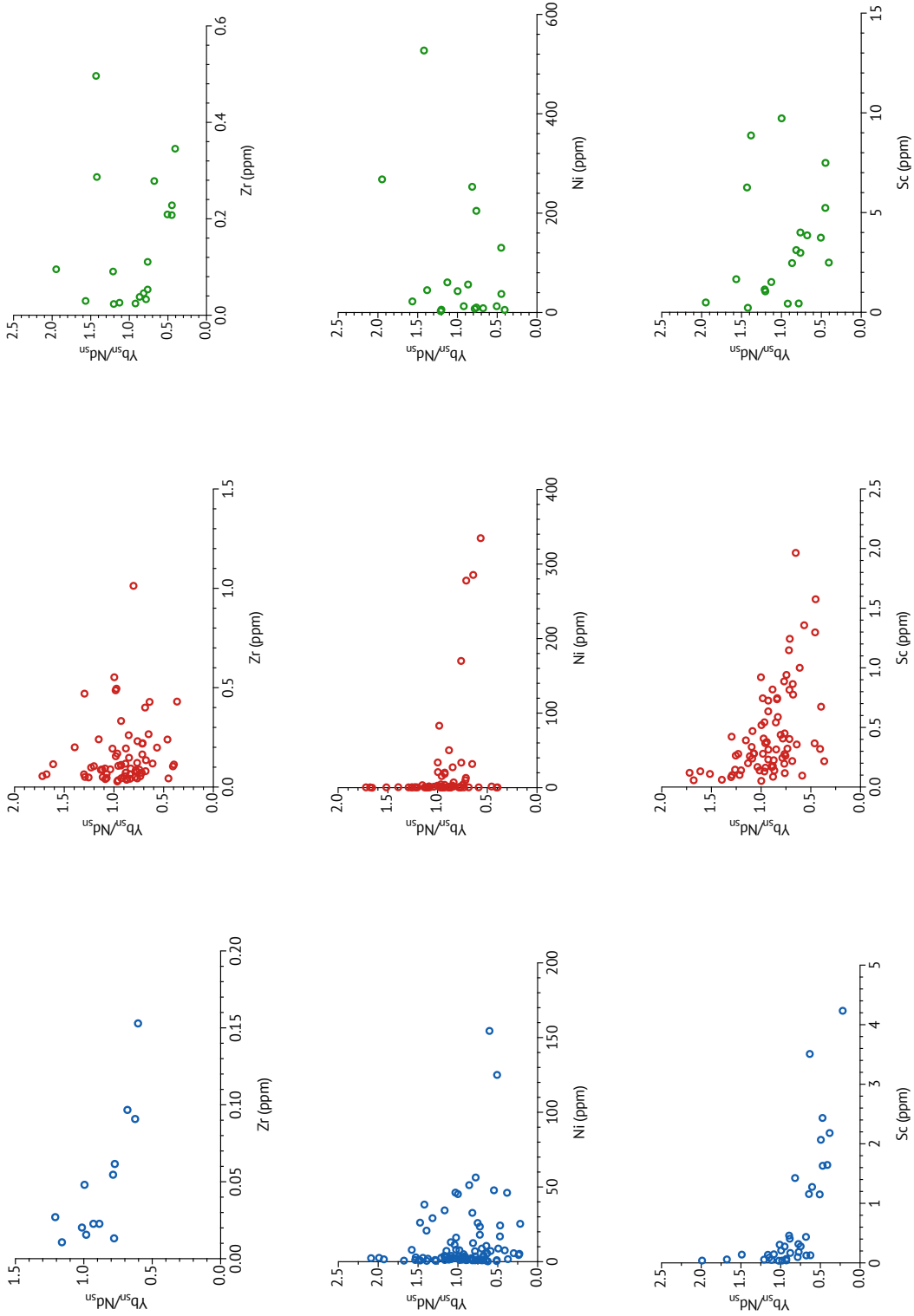


Figure 19: Termination Hill (blue), Gammon Ranges (red) and Copley (green). Termination Hill plots; $R^2 = 0.5728$ with Zr and $R^2 = 0.4192$ with Sc. Gammon Ranges plots; 2 outliers with Ni not included. Copley Plots; 2 outliers in Zr and 1 outlier in Ni not included. All samples are marine carbonates from the Burra Group, South Australia.

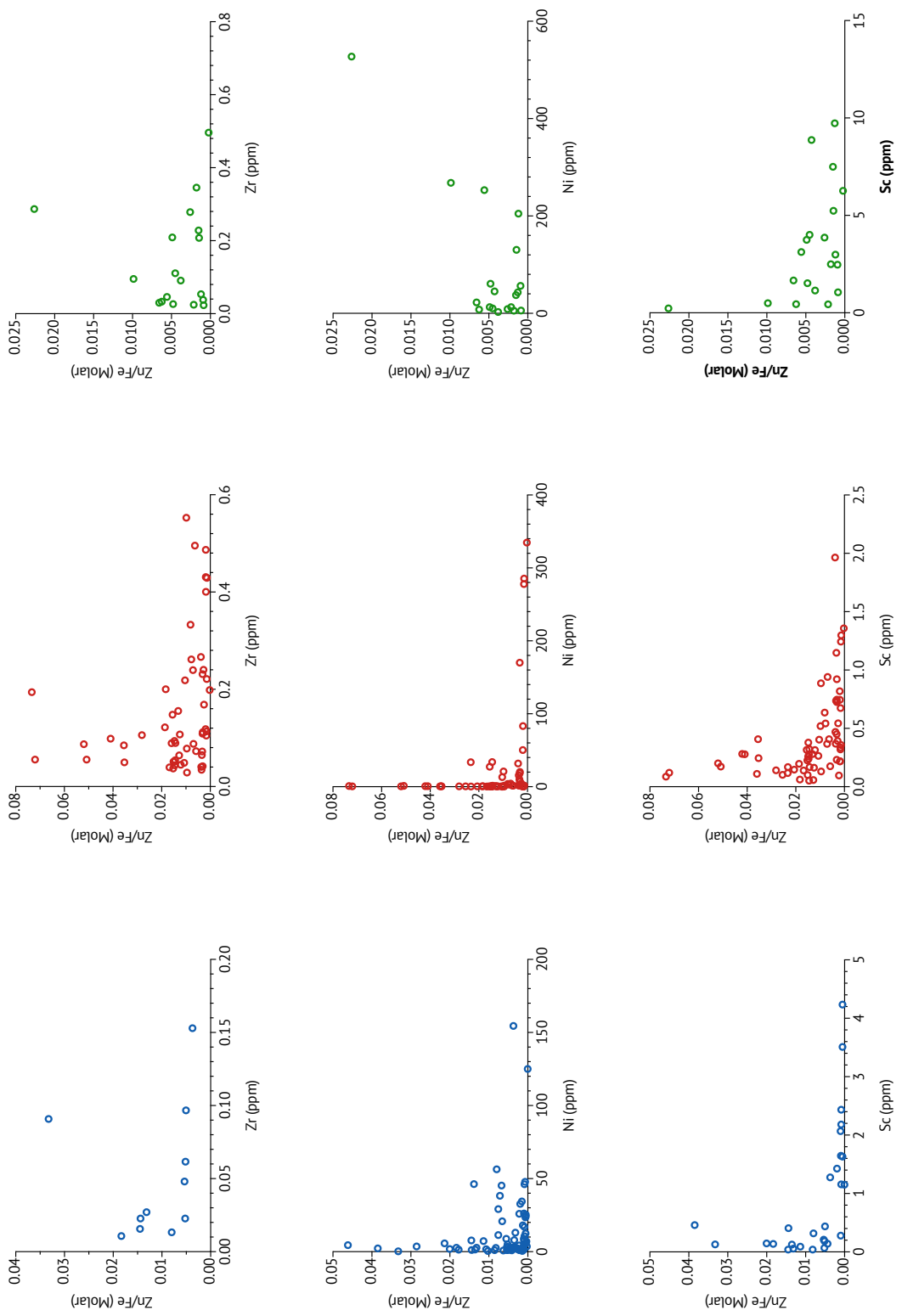


Figure 20: Termination Hill (blue), Gammon Ranges (red) and Copley (green). No outliers have been excluded from plots. All samples are marine carbonates from the Burra Group, South Australia.

Cross plots of REY and trace element abundances against alteration proxies

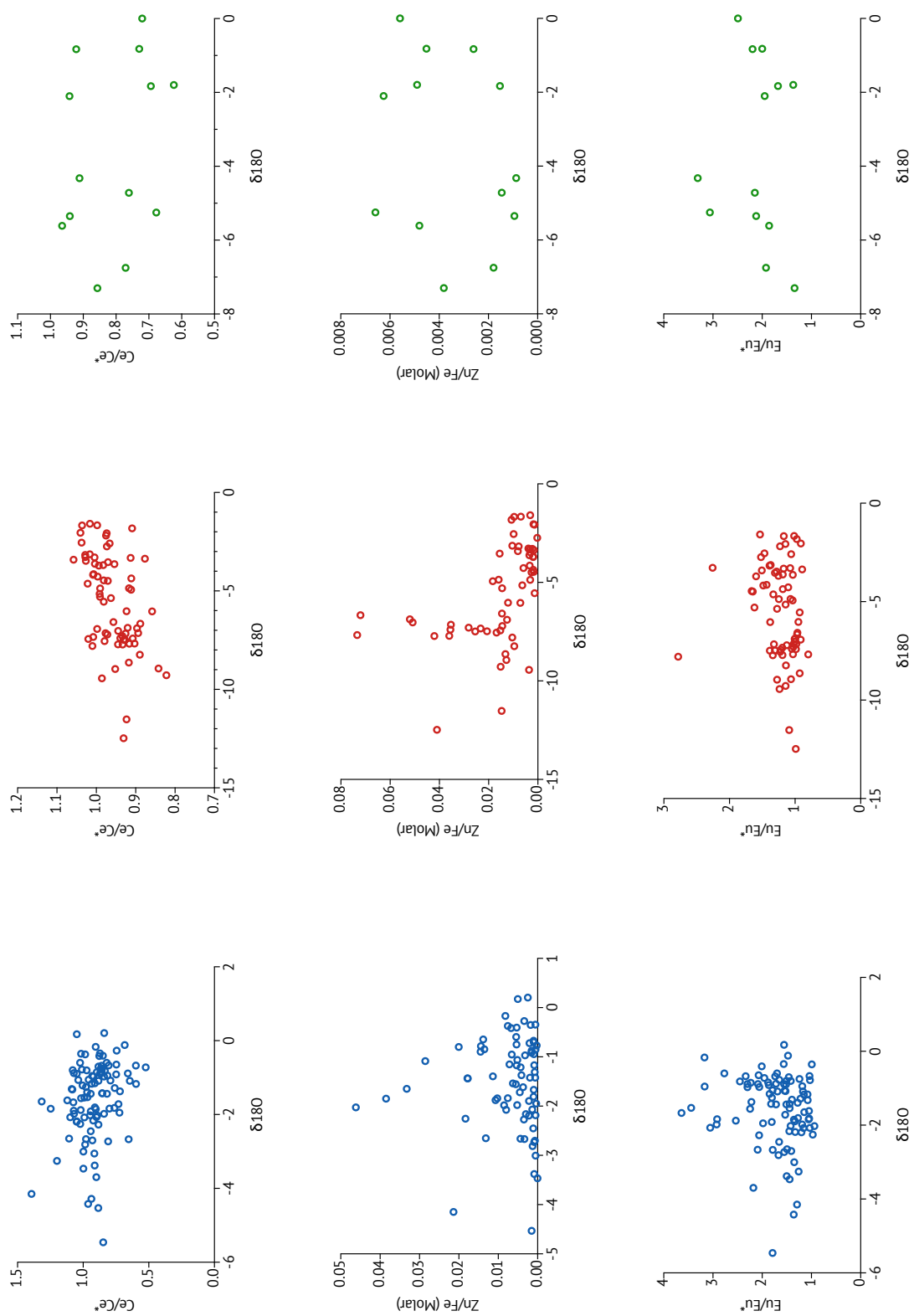


Figure 21: Termination Hill (blue), Gammon Ranges (red) and Copley (green). All samples are marine carbonates from the Burra Group, South Australia.

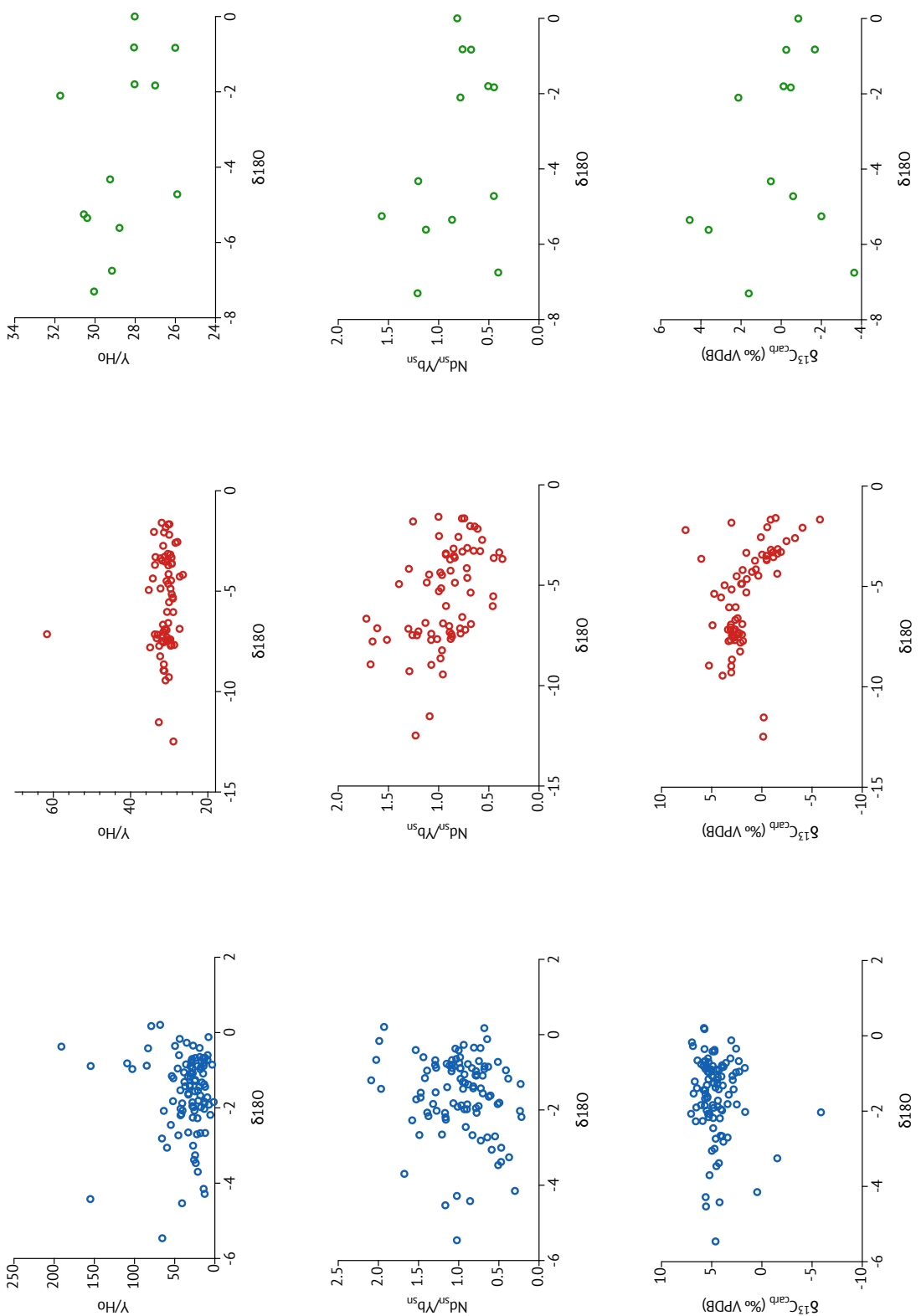


Figure 22: Termination Hill (blue), Gammon Ranges (red) and Copley (green). All samples are marine carbonates from the Burra Group, South Australia.

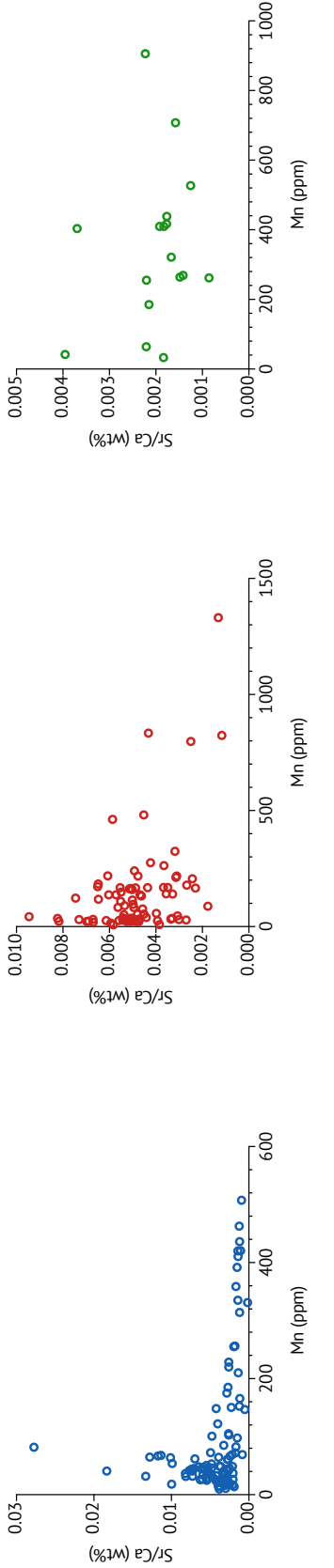
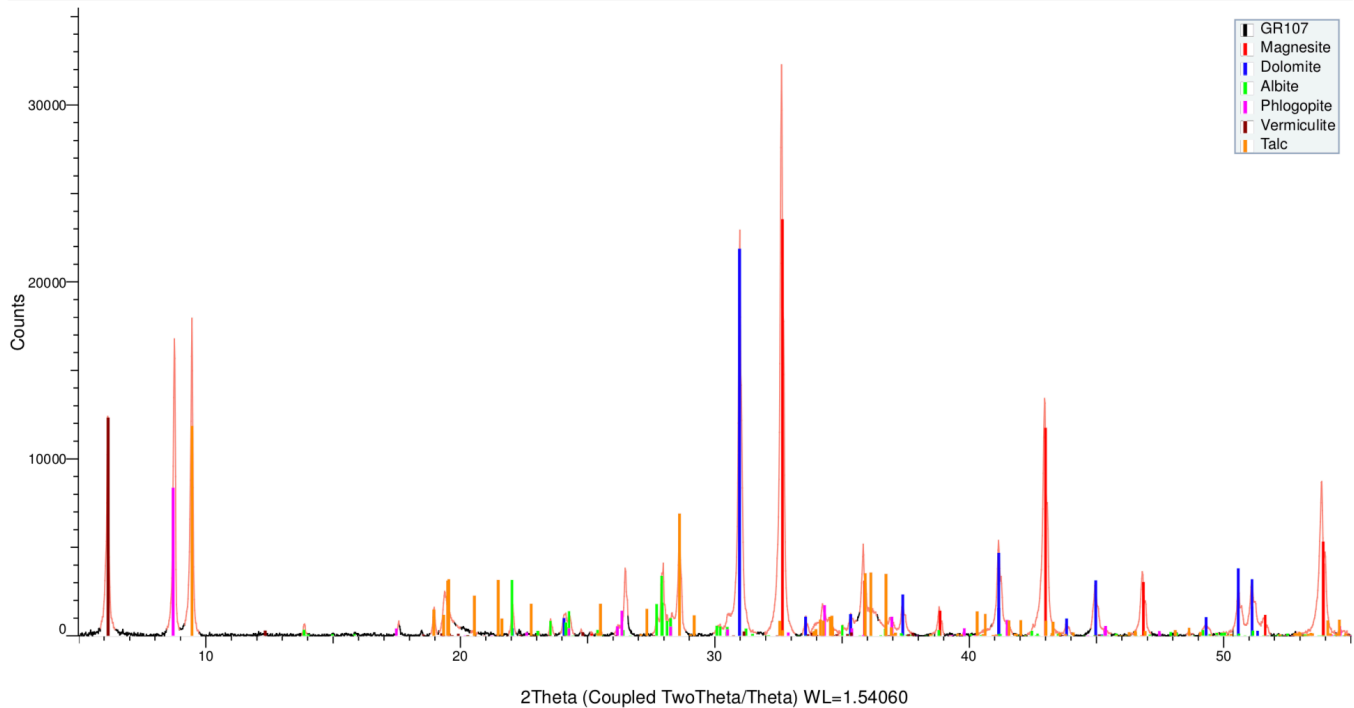


Figure 23: Termination Hill (blue), Gammon Ranges (red) and Copley (green). A lack of significant correlation implies minimal diagenetic alteration throughout these Burra Group sediments.

XRD spectra output for Skillogalee Formation – Gammon Ranges

(Coupled TwoTheta/Theta)



(Coupled TwoTheta/Theta)

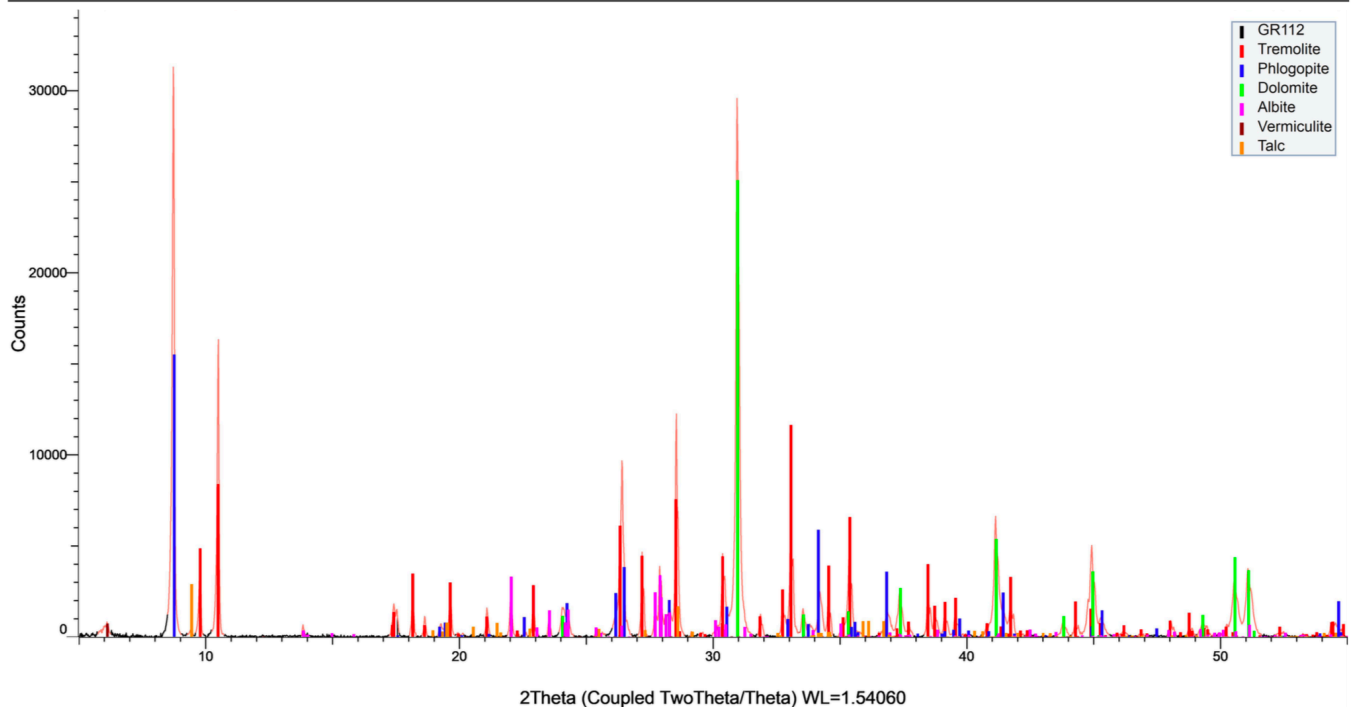
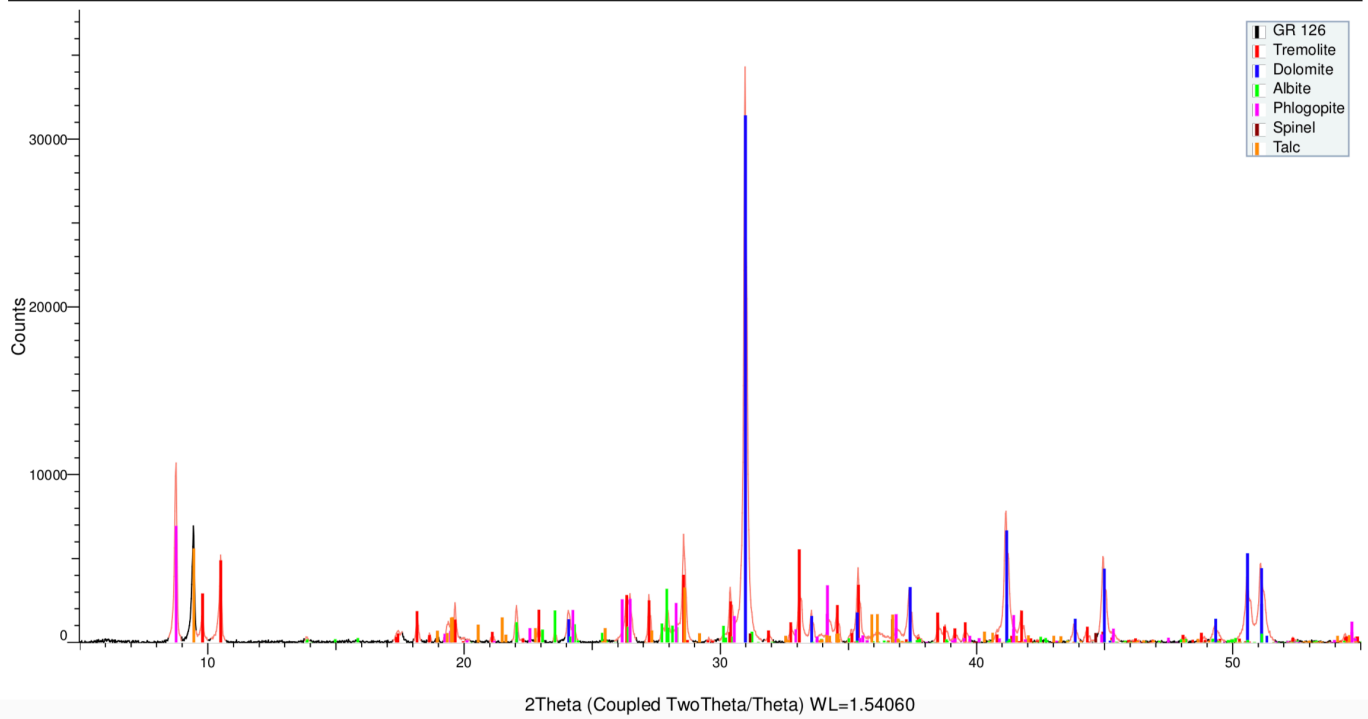


Figure 24: Top; XRD spectra output for sample GR107. Bottom; XRD spectra output for sample GR112

(Coupled TwoTheta/Theta)



(Coupled TwoTheta/Theta)

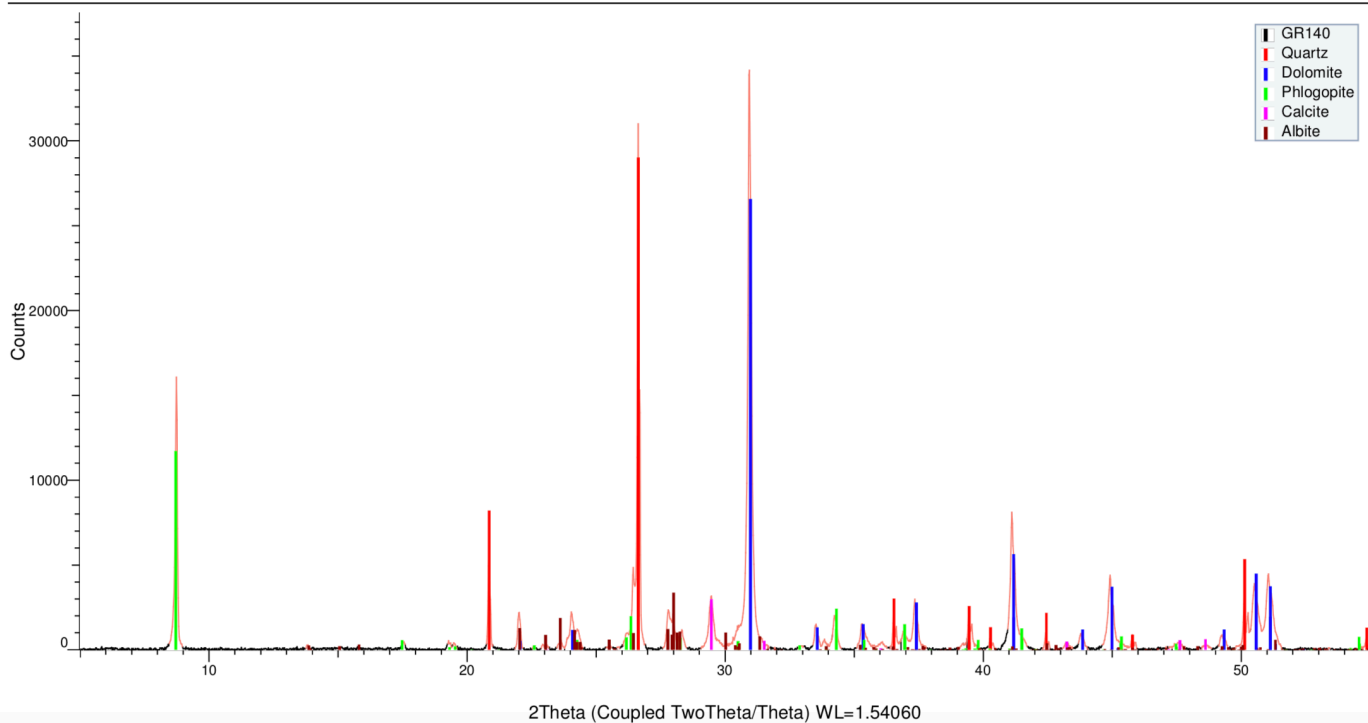
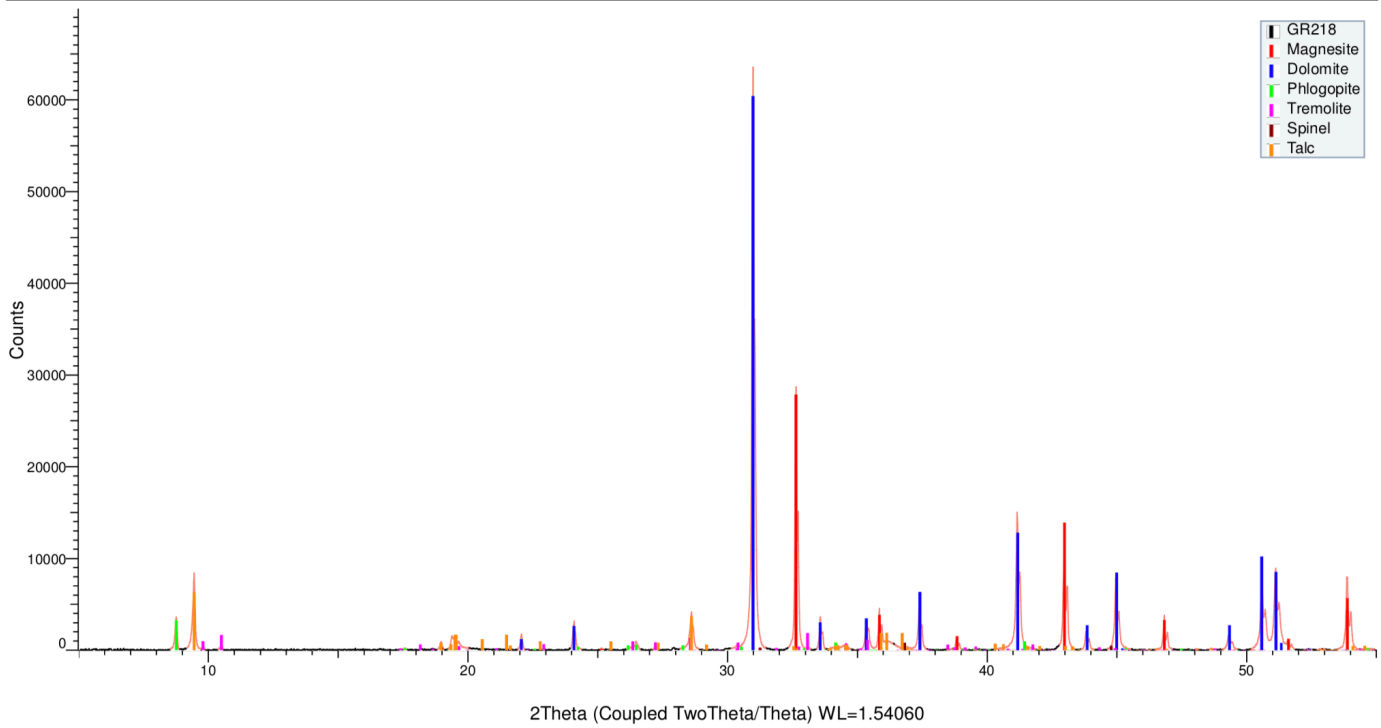


Figure 25: Top; XRD spectra output for sample GR126. Bottom; XRD spectra output for sample GR140

(Coupled TwoTheta/Theta)



(Coupled TwoTheta/Theta)

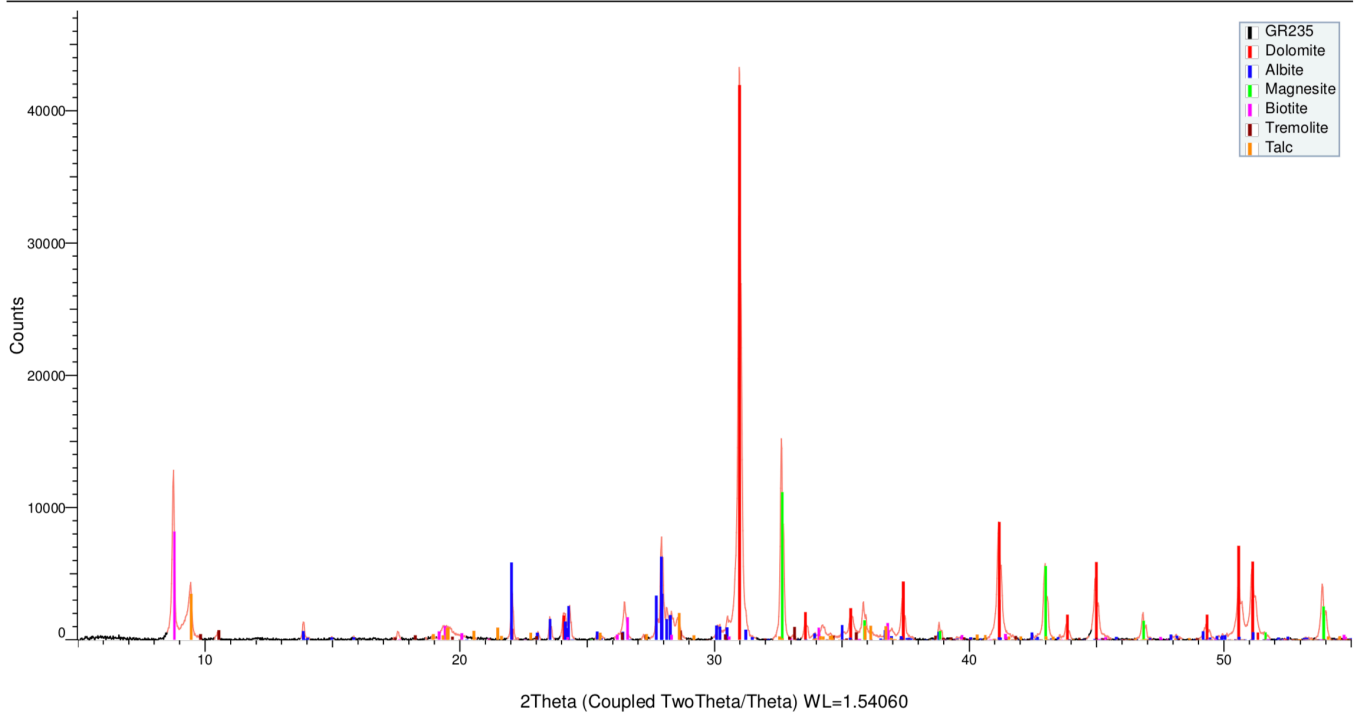


Figure 26: Top; XRD spectra output for sample GR218. Bottom; XRD spectra output for sample GR235.

7 REFERENCES

- Barovich, K. M., & Foden, J. (2000). A Neoproterozoic flood basalt province in southern-central Australia: geochemical and Nd isotope evidence from basin fill. *Precambrian Research*, 100(1), 213-234. doi:[https://doi.org/10.1016/S0301-9268\(99\)00075-3](https://doi.org/10.1016/S0301-9268(99)00075-3)
- Bau, M., & Dulski, P. (1996). Distribution of yttrium and rare-earth elements in the Penge and Kuruman iron-formations, Transvaal Supergroup, South Africa. *Precambrian Research*, 79(1), 37-55. doi:[https://doi.org/10.1016/0301-9268\(95\)00087-9](https://doi.org/10.1016/0301-9268(95)00087-9)
- Bau, M., Möller, P., & Dulski, P. (1997). Yttrium and lanthanides in eastern Mediterranean seawater and their fractionation during redox-cycling. *Marine Chemistry*, 56(1), 123-131. doi:[https://doi.org/10.1016/S0304-4203\(96\)00091-6](https://doi.org/10.1016/S0304-4203(96)00091-6)
- Belperio, A. (1990). Palaeoenvironmental interpretations of the Late Proterozoic Skillogalee Dolomite in the Willouran Ranges, South Australia. *The Evolution of a Late Precambrian-Early Palaeozoic Rift Complex: The Adelaide Geosyncline*. *Geol. Soc. Aust. Spec. Publ.*, 16, 85-104.
- Borch, C. C. V. D., & Lock, D. (1979). Geological significance of Coorong dolomites. *Sedimentology*, 26(6), 813-824. doi:10.1111/j.1365-3091.1979.tb00974.x
- Brand, U., & Veizer, J. (1980). Chemical diagenesis of a multicomponent carbonate system; 1, Trace elements. *Journal of Sedimentary Research*, 50(4), 1219-1236.
- Broecker, W. S. (1970). A boundary condition on the evolution of atmospheric oxygen. *Journal of Geophysical Research*, 75(18), 3553-3557. doi:10.1029/JC075i018p03553
- Brookins, D. (1989). Aqueous geochemistry of rare earth elements. *Reviews in Mineralogy and Geochemistry*, 21(1), 201-225.
- Byrne, R. H., & Kim, K.-H. (1990). Rare earth element scavenging in seawater. *Geochimica et Cosmochimica Acta*, 54(10), 2645-2656. doi:[https://doi.org/10.1016/0016-7037\(90\)90002-3](https://doi.org/10.1016/0016-7037(90)90002-3)
- Canfield, D. E., Poulton, S. W., & Narbonne, G. M. (2007). Late-Neoproterozoic deep-ocean oxygenation and the rise of animal life. *Science*, 315(5808), 92-95.
- Chen, J., & Jahn, B.-m. (1998). Crustal evolution of southeastern China: Nd and Sr isotopic evidence. *Tectonophysics*, 284(1-2), 101-133.
- Cole, D. B., Reinhard, C. T., Wang, X., Gueguen, B., Halverson, G. P., Gibson, T., . . . Planavsky, N. J. (2016). A shale-hosted Cr isotope record of low atmospheric oxygen during the Proterozoic. *Geology*, 44(7), 555-558.
- Compston, W., Crawford, A., & Bofinger, V. (1966). A radiometric estimate of the duration of sedimentation in the Adelaide Geosyncline, South Australia. *Journal of the Geological Society of Australia*, 13(1), 229-276.
- Cox, G. M., Halverson, G. P., Stevenson, R. K., Vokaty, M., Poirier, A., Kunzmann, M., . . . Macdonald, F. A. (2016). Continental flood basalt weathering as a trigger for Neoproterozoic Snowball Earth. *Earth and Planetary Science Letters*, 446, 89-99. doi:<https://doi.org/10.1016/j.epsl.2016.04.016>
- Crawford, A. J., & Hilyard, D. (1990). Geochemistry of Late Proterozoic tholeiitic flood basalts, Adelaide Geosyncline, South Australia. *The Evolution of a Late Precambrian-Early Paleozoic Rift Complex: The Adelaide Geosyncline*. *Geological Society of Australia, Special Publications*, 16, 49-67.
- De Baar, H. J., Bacon, M. P., Brewer, P. G., & Bruland, K. W. (1985). Rare earth elements in the Pacific and Atlantic Oceans. *Geochimica et Cosmochimica Acta*, 49(9), 1943-1959.

- De Baar, H. J. W., Brewer, P. G., & Bacon, M. P. (1985). Anomalies in rare earth distributions in seawater: Gd and Tb. *Geochimica et Cosmochimica Acta*, 49(9), 1961-1969. doi:[https://doi.org/10.1016/0016-7037\(85\)90090-0](https://doi.org/10.1016/0016-7037(85)90090-0)
- Derry, L. A., Kaufman, A. J., & Jacobsen, S. B. (1992). Sedimentary cycling and environmental change in the Late Proterozoic: Evidence from stable and radiogenic isotopes. *Geochimica et Cosmochimica Acta*, 56(3), 1317-1329. doi:[https://doi.org/10.1016/0016-7037\(92\)90064-P](https://doi.org/10.1016/0016-7037(92)90064-P)
- Dilek, Y., & Furnes, H. (2013). *Evolution of Archean crust and early life* (Vol. 7): Springer.
- Douville, E., Bienvenu, P., Charlou, J. L., Donval, J. P., Fouquet, Y., Appriou, P., & Gamo, T. (1999). Yttrium and rare earth elements in fluids from various deep-sea hydrothermal systems. *Geochimica et Cosmochimica Acta*, 63(5), 627-643. doi:[https://doi.org/10.1016/S0016-7037\(99\)00024-1](https://doi.org/10.1016/S0016-7037(99)00024-1)
- Elderfield, H., & Pagett, R. (1986). Rare earth elements in ichthyoliths: Variations with redox conditions and depositional environment. *Science of The Total Environment*, 49, 175-197. doi:[https://doi.org/10.1016/0048-9697\(86\)90239-1](https://doi.org/10.1016/0048-9697(86)90239-1)
- Elderfield, H., Upstill-Goddard, R., & Sholkovitz, E. R. (1990). The rare earth elements in rivers, estuaries, and coastal seas and their significance to the composition of ocean waters. *Geochimica et Cosmochimica Acta*, 54(4), 971-991. doi:[https://doi.org/10.1016/0016-7037\(90\)90432-K](https://doi.org/10.1016/0016-7037(90)90432-K)
- Ernst, R. E., & Buchan, K. L. (2001). *Mantle plumes: their identification through time* (Vol. 352): Geological Society of America.
- Ernst, R. E., Wingate, M. T. D., Buchan, K. L., & Li, Z. X. (2008). Global record of 1600–700Ma Large Igneous Provinces (LIPs): Implications for the reconstruction of the proposed Nuna (Columbia) and Rodinia supercontinents. *Precambrian Research*, 160(1), 159-178. doi:<https://doi.org/10.1016/j.precamres.2007.04.019>
- Eugster, H. P., & Hardie, L. A. (1978). Saline lakes. In *Lakes* (pp. 237-293): Springer.
- Fairchild, I., Sprio, B., Herrington, P., & Song, T. (2000). Controls on Sr and C isotope compositions of Neoproterozoic Sr-rich limestones of East Greenland and North China. *Society for Sedimentary Geology*, 67, 297-313.
- Fanning, C., Ludwig, K., Forbes, B., & Preiss, W. (1986). *Single and multiple grain U–Pb zircon analyses for the early Adelaidean Rook Tuff, Willouran Ranges, South Australia*. Paper presented at the Geological Society of Australia Abstracts.
- Foden, J.D., Turner, S.P., & Morrison, R.S. (1990). *Tectonic implications of Delamerian magmatism in South Australia and western Victoria* (Vol. 16, pp. 465-482). Geological Society of Australia.
- Forbes, B. (1960). Magnesite of the Adelaide System: petrography and descriptive stratigraphy. *Trans. R. Soc. S. Aust*, 83, 1-9.
- Forbes, B. G. (1977). *The Boucaut Volcanics*: Department of Mines, South Australia.
- Gehrels, G. E., Butler, R. F., & Bazard, D. R. (1996). Detrital zircon geochronology of the Alexander terrane, southeastern Alaska. *Geological Society of America Bulletin*, 108(6), 722-734.
- German, C. R., & Elderfield, H. (1990). Application of the Ce anomaly as a paleoredox indicator: The ground rules. *Paleoceanography*, 5(5), 823-833. doi:[10.1029/PA005i005p00823](https://doi.org/10.1029/PA005i005p00823)
- Goldstein, S. L., O'Nions, R. K., & Hamilton, P. J. (1984). A Sm-Nd isotopic study of atmospheric dusts and particulates from major river systems. *Earth and Planetary Science Letters*, 70(2), 221-236. doi:[https://doi.org/10.1016/0012-821X\(84\)90007-4](https://doi.org/10.1016/0012-821X(84)90007-4)
- Halverson, G. P. (2006). A Neoproterozoic chronology. In *Neoproterozoic geobiology and paleobiology* (pp. 231-271): Springer.

- Halverson, G. P., Dudás, F. Ö., Maloof, A. C., & Bowring, S. A. (2007). Evolution of the $^{87}\text{Sr}/^{86}\text{Sr}$ composition of Neoproterozoic seawater. *Palaeogeography, Palaeoclimatology, Palaeoecology*, 256(3), 103-129.
doi:<https://doi.org/10.1016/j.palaeo.2007.02.028>
- Halverson, G. P., Hoffman, P. F., Schrag, D. P., Maloof, A. C., & Rice, A. H. N. (2005). Toward a Neoproterozoic composite carbon-isotope record. *GSA Bulletin*, 117(9-10), 1181-1207. doi:10.1130/B25630.1
- Halverson, G. P., Maloof, A. C., Schrag, D. P., Dudás, F. Ö., & Hurtgen, M. (2007). Stratigraphy and geochemistry of a ca 800 Ma negative carbon isotope interval in northeastern Svalbard. *Chemical Geology*, 237(1-2), 5-27.
doi:10.1016/j.chemgeo.2006.06.013
- Halverson, G. P., Wade, B. P., Hurtgen, M. T., & Barovich, K. M. (2010). Neoproterozoic chemostratigraphy. *Precambrian Research*, 182(4), 337-350.
doi:<https://doi.org/10.1016/j.precamres.2010.04.007>
- Hardie, L. (1977). Layering: the origin and environmental significance of lamination and thin bedding. *Sedimentation on the modern carbonate tidal flats of Northwest Andros Island, Bahamas*.
- Hayes, J. M., Strauss, H., & Kaufman, A. J. (1999). The abundance of ^{13}C in marine organic matter and isotopic fractionation in the global biogeochemical cycle of carbon during the past 800 Ma. *Chemical Geology*, 161(1), 103-125.
doi:[https://doi.org/10.1016/S0009-2541\(99\)00083-2](https://doi.org/10.1016/S0009-2541(99)00083-2)
- Hill, A. C., & Walter, M. R. (2000). Mid-Neoproterozoic (~830–750 Ma) isotope stratigraphy of Australia and global correlation. *Precambrian Research*, 100(1), 181-211. doi:[https://doi.org/10.1016/S0301-9268\(99\)00074-1](https://doi.org/10.1016/S0301-9268(99)00074-1)
- Hilyard, D. (1990). Willouran Basic Province: stratigraphy of Late Proterozoic flood basalts, Adelaide Geosyncline, South Australia. *The evolution of a Late Precambrian-Early Palaeozoic rift complex: The Adelaide Geosyncline: Geological Society of Australia Special Publication*, 16, 34-48.
- Hoffman, P. F., Abbot, D. S., Ashkenazy, Y., Benn, D. I., Brocks, J. J., Cohen, P. A., . . . Erwin, D. H. (2017). Snowball Earth climate dynamics and Cryogenian geology-geobiology. *Science Advances*, 3(11), e1600983.
- Hoffman, P. F., Kaufman, A. J., Halverson, G. P., & Schrag, D. P. (1998). A Neoproterozoic snowball earth. *Science*, 281(5381), 1342-1346.
- Holser, W. T. (1997). Evaluation of the application of rare-earth elements to paleoceanography. *Palaeogeography, Palaeoclimatology, Palaeoecology*, 132(1), 309-323. doi:[https://doi.org/10.1016/S0031-0182\(97\)00069-2](https://doi.org/10.1016/S0031-0182(97)00069-2)
- Ireland, T., Flottmann, T., Fanning, C., Gibson, G., & Preiss, W. V. (1998). Development of the early Paleozoic Pacific margin of Gondwana from detrital-zircon ages across the Delamerian orogen. *Geology*, 26(3), 243-246.
- James, R. H., Elderfield, H., & Palmer, M. R. (1995). The chemistry of hydrothermal fluids from the Broken Spur site, 29°N Mid-Atlantic ridge. *Geochimica et Cosmochimica Acta*, 59(4), 651-659. doi:[https://doi.org/10.1016/0016-7037\(95\)00003-I](https://doi.org/10.1016/0016-7037(95)00003-I)
- Javoy, M., Pineau, F., & Delorm, H. (1986). Carbon and nitrogen isotopes in the mantle. *Chemical geology*, 57(1-2), 41-62.
- Jenkins, R. (1990). The Adelaide fold belt: tectonic reappraisal. *The evolution of a Late Precambrian-Early Palaeozoic Rift Complex: The Adelaide Geosyncline*, 16, 395-420.
- Kaufman, A. J., Hayes, J. M., Knoll, A. H., & Germs, G. J. B. (1991). Isotopic compositions of carbonates and organic carbon from upper Proterozoic successions in Namibia:

- stratigraphic variation and the effects of diagenesis and metamorphism. *Precambrian Research*, 49(3), 301-327. doi:[https://doi.org/10.1016/0301-9268\(91\)90039-D](https://doi.org/10.1016/0301-9268(91)90039-D)
- Kaufman, A. J., & Knoll, A. H. (1995). Neoproterozoic variations in the C-isotopic composition of seawater: stratigraphic and biogeochemical implications. *Precambrian Research*, 73(1), 27-49. doi:[https://doi.org/10.1016/0301-9268\(94\)00070-8](https://doi.org/10.1016/0301-9268(94)00070-8)
- Kirschvink, J. L. (1992). Late Proterozoic low-latitude global glaciation: the snowball Earth.
- Klaebe, R. M., Kennedy, M. J., Jarrett, A. J. M., & Brocks, J. J. (2016). Local paleoenvironmental controls on the carbon-isotope record defining the Bitter Springs Anomaly. *Geobiology*, 15(1), 65-80. doi:10.1111/gbi.12217
- Koeppenkastrop, D., & De Carlo, E. H. (1992). Sorption of rare-earth elements from seawater onto synthetic mineral particles: An experimental approach. *Chemical Geology*, 95(3), 251-263. doi:[https://doi.org/10.1016/0009-2541\(92\)90015-W](https://doi.org/10.1016/0009-2541(92)90015-W)
- Koeppenkastrop, D., & De Carlo, E. H. (1993). Uptake of rare earth elements from solution by metal oxides. *Environmental science & technology*, 27(9), 1796-1802.
- Krabbenhöft, A., Eisenhauer, A., Böhm, F., Vollstaedt, H., Fietzke, J., Liebetrau, V., . . . Horn, C. (2010). Constraining the marine strontium budget with natural strontium isotope fractionations ($^{87}\text{Sr}/^{86}\text{Sr}$, $\delta^{88/\text{Sr}}$) of carbonates, hydrothermal solutions and river waters. *Geochimica et Cosmochimica Acta*, 74(14), 4097-4109.
- Kraemer, D., Kopf, S., & Bau, M. (2015). Oxidative mobilization of cerium and uranium and enhanced release of “immobile” high field strength elements from igneous rocks in the presence of the biogenic siderophore desferrioxamine B. *Geochimica et Cosmochimica Acta*, 165, 263-279. doi:<https://doi.org/10.1016/j.gca.2015.05.046>
- Kump, L.R., Junium, C., Arthur, M.A., Brasier, A., Fallick, A., Melezhik, V., . . . & Luo, G. (2011). Isotopic evidence for massive oxidation of organic matter following the Great Oxidation Event. *Science*, 334(6063), 1694-1696.
- Lawrence, M. G., & Kamber, B. S. (2006). The behaviour of the rare earth elements during estuarine mixing—revisited. *Marine Chemistry*, 100(1), 147-161. doi:<https://doi.org/10.1016/j.marchem.2005.11.007>
- Lenton, T. M., Boyle, R. A., Poulton, S. W., Shields-Zhou, G. A., & Butterfield, N. J. (2014). Co-evolution of eukaryotes and ocean oxygenation in the Neoproterozoic era. *Nature Geoscience*, 7(4), 257.
- Li, X.-h., & McCulloch, M. T. (1996). Secular variation in the Nd isotopic composition of Neoproterozoic sediments from the southern margin of the Yangtze Block: evidence for a Proterozoic continental collision in southeast China. *Precambrian Research*, 76(1-2), 67-76.
- Liu, C., Wang, Z., Raub, T. D., Macdonald, F. A., & Evans, D. A. (2014). Neoproterozoic cap-dolostone deposition in stratified glacial meltwater plume. *Earth and Planetary Science Letters*, 404, 22-32.
- Liu, X., Hazen, R., Kah, L., Sverjensky, D., Cui, H., & Kaufmann, A. (2014). *Tracing Earth's O₂ Evolution Using Zn/Fe Systematics in Carbonates*. Paper presented at the AGU Fall Meeting Abstracts.
- Lyons, T. W., Reinhard, C. T., & Planavsky, N. J. (2014). The rise of oxygen in Earth's early ocean and atmosphere. *Nature*, 506(7488), 307-315. doi:10.1038/nature13068
- Meyer, E. E., Quicksall, A. N., Landis, J. D., Link, P. K., & Bostick, B. C. (2012). Trace and rare earth elemental investigation of a Sturtian cap carbonate, Pocatello, Idaho: Evidence for ocean redox conditions before and during carbonate deposition. *Precambrian Research*, 192-195, 89-106. doi:<https://doi.org/10.1016/j.precamres.2011.09.015>
- Miall, A. D. (1973). Markov chain analysis applied to an ancient alluvial plain succession. *Sedimentology*, 20(3), 347-364.

- Moffett, J. W. (1990). Microbially mediated cerium oxidation in sea water. *Nature*, 345, 421. doi:10.1038/345421a0
- Murrell, B. (1977). *Stratigraphy and tectonics across the Torrens Hinge Zone between Andamooka and Marree, South Australia*. University of Adelaide, Department of Geology,
- Nakada, R., Takahashi, Y., & Tanimizu, M. (2013). Isotopic and speciation study on cerium during its solid–water distribution with implication for Ce stable isotope as a paleo-redox proxy. *Geochimica et Cosmochimica Acta*, 103, 49-62. doi:<https://doi.org/10.1016/j.gca.2012.10.045>
- Nothdurft, L. D., Webb, G. E., & Kamber, B. S. (2004). Rare earth element geochemistry of Late Devonian reefal carbonates, Canning Basin, Western Australia: confirmation of a seawater REE proxy in ancient limestones. *Geochimica et Cosmochimica Acta*, 68(2), 263-283. doi:[https://doi.org/10.1016/S0016-7037\(03\)00422-8](https://doi.org/10.1016/S0016-7037(03)00422-8)
- Nozaki, Y., & Zhang, J. (1995). The rare earth elements and yttrium in the coastal/offshore mixing zone of Tokyo Bay waters and the Kuroshio. *Biogeochemical Processes and Ocean Flux in the Western Pacific*, 171-184.
- Och, L. M., & Shields-Zhou, G. A. (2012). The Neoproterozoic oxygenation event: Environmental perturbations and biogeochemical cycling. *Earth-Science Reviews*, 110(1-4), 26-57.
- Parker, A., Cowley, W., & Thomson, B. (1990). The Torrens Hinge Zone and Spencer Shelf with particular reference to early Adelaidean volcanism. *The evolution of a late Precambrian-early Palaeozoic rift complex*, 129-148.
- Paul, E., Flöttmann, T., & Sandiford, M. (1999). Structural geometry and controls on basement-involved deformation in the northern Flinders Ranges, Adelaide Fold Belt, South Australia. *Australian Journal of Earth Sciences*, 46(3), 343-354. doi:10.1046/j.1440-0952.1999.00711.x
- Piepgras, D. J., & Jacobsen, S. B. (1992). The behavior of rare earth elements in seawater: Precise determination of variations in the North Pacific water column. *Geochimica et Cosmochimica Acta*, 56(5), 1851-1862.
- Pourmand, A., Dauphas, N., & Ireland, T. J. (2012). A novel extraction chromatography and MC-ICP-MS technique for rapid analysis of REE, Sc and Y: Revising CI-chondrite and Post-Archean Australian Shale (PAAS) abundances. *Chemical Geology*, 291, 38-54. doi:<https://doi.org/10.1016/j.chemgeo.2011.08.011>
- Powell, C. M., Preiss, W. V., Gatehouse, C. G., Krapez, B., & Li, Z. X. (1994). South Australian record of a Rodinian epicontinental basin and its mid-neoproterozoic breakup (~700 Ma) to form the Palaeo-Pacific Ocean. *Tectonophysics*, 237(3), 113-140. doi:[https://doi.org/10.1016/0040-1951\(94\)90250-X](https://doi.org/10.1016/0040-1951(94)90250-X)
- Preiss, W., & Forbes, B. (1981). Stratigraphy, correlation and sedimentary history of Adelaidean (Late Proterozoic) basins in Australia. *Precambrian Research*, 15(3-4), 255-304.
- Preiss, W. V. (1973). Palaeoecological interpretations of South Australian Precambrian stromatolites. *Journal of the Geological Society of Australia*, 19(4), 501-532.
- Preiss, W. V. (1987). *The Adelaide Geosyncline: Late Proterozoic stratigraphy, sedimentation, palaeontology and tectonics*: Department of Mines and Energy.
- Preiss, W. V. (2000). The Adelaide Geosyncline of South Australia and its significance in Neoproterozoic continental reconstruction. *Precambrian Research*, 100(1), 21-63. doi:[https://doi.org/10.1016/S0301-9268\(99\)00068-6](https://doi.org/10.1016/S0301-9268(99)00068-6)
- Quinn, K. A., Byrne, R. H., & Schijf, J. (2004). Comparative Scavenging of Yttrium and the Rare Earth Elements in Seawater: Competitive Influences of Solution and Surface

Chemistry. *Aquatic Geochemistry*, 10(1), 59-80.
doi:10.1023/B:AQUA.0000038959.03886.60

Raiswell, R., Tranter, M., Benning, L. G., Siegert, M., De'ath, R., Huybrechts, P., & Payne, T. (2006). Contributions from glacially derived sediment to the global iron (oxyhydr)oxide cycle: Implications for iron delivery to the oceans. *Geochimica et Cosmochimica Acta*, 70(11), 2765-2780.
doi:<https://doi.org/10.1016/j.gca.2005.12.027>

Reinhard, C. T., Planavsky, N. J., Gill, B. C., Ozaki, K., Robbins, L. J., Lyons, T. W., . . . Konhauser, K. O. (2016). Evolution of the global phosphorus cycle. *Nature*, 541, 386.
doi:10.1038/nature20772

<https://www.nature.com/articles/nature20772#supplementary-information>

Rooney, A. D., Macdonald, F. A., Strauss, J. V., Dudás, F. Ö., Hallmann, C., & Selby, D. (2014). Re-Os geochronology and coupled Os-Sr isotope constraints on the Sturtian snowball Earth. *Proceedings of the National Academy of Sciences*, 111(1), 51-56.

Schier, K., Bau, M., Münker, C., Beukes, N., & Viehmann, S. (2018). Trace element and Nd isotope composition of shallow seawater prior to the Great Oxidation Event: Evidence from stromatolitic bioherms in the Paleoproterozoic Rooinekke and Nelani Formations, South Africa. *Precambrian Research*, 315, 92-102.
doi:<https://doi.org/10.1016/j.precamres.2018.07.014>

Schlünz, B., & Schneider, R. R. (2000). Transport of terrestrial organic carbon to the oceans by rivers: re-estimating flux- and burial rates. *International Journal of Earth Sciences*, 88(4), 599-606. doi:10.1007/s005310050290

Scott, C., Lyons, T. W., Bekker, A., Shen, Y., Poulton, S. W., Chu, X., & Anbar, A. D. (2008). Tracing the stepwise oxygenation of the Proterozoic ocean. *Nature*, 452, 456.
doi:10.1038/nature06811

<https://www.nature.com/articles/nature06811#supplementary-information>

Severmann, S., Lyons, T. W., Anbar, A., McManus, J., & Gordon, G. (2008). Modern iron isotope perspective on the benthic iron shuttle and the redox evolution of ancient oceans. *Geology*, 36(6), 487-490. doi:10.1130/G24670A.1

Shields, G., Stille, P., Brasier, M. D., & Atudorei, N. V. (1997). Stratified oceans and oxygenation of the late Precambrian environment: a post glacial geochemical record from the Neoproterozoic of W. Mongolia. *Terra Nova*, 9(5-6), 218-222.

Tanaka, T., Togashi, S., Kamioka, H., Amakawa, H., Kagami, H., Hamamoto, T., . . . Dragusanu, C. (2000). JNd-1: a neodymium isotopic reference in consistency with LaJolla neodymium. *Chemical Geology*, 168(3), 279-281.
doi:[https://doi.org/10.1016/S0009-2541\(00\)00198-4](https://doi.org/10.1016/S0009-2541(00)00198-4)

Tostevin, R., Shields, G. A., Tarbuck, G. M., He, T., Clarkson, M. O., & Wood, R. A. (2016). Effective use of cerium anomalies as a redox proxy in carbonate-dominated marine settings. *Chemical Geology*, 438, 146-162.
doi:<https://doi.org/10.1016/j.chemgeo.2016.06.027>

Turner, S., Foden, J., Sandiford, M., & Bruce, D. (1993). Sm-Nd isotopic evidence for the provenance of sediments from the Adelaide Fold Belt and southeastern Australia with implications for episodic crustal addition. *Geochimica et Cosmochimica Acta*, 57(8), 1837-1856. doi:[https://doi.org/10.1016/0016-7037\(93\)90116-E](https://doi.org/10.1016/0016-7037(93)90116-E)

Uppill, R. K. (1980). *Sedimentology of the late Precambrian Mundollo Subgroup: a clastic-carbonate (Dolomite, Magnesite) sequence in the Mt. Lofty and Flinders Ranges, South Australia*.

Uppill, R. K. (1990). Sedimentology of a dolomitemagnesite-sandstone sequence in the late Precambrian Mundollo Subgroup, South Australia. *The evolution of a late*

- Precambrian–early Paleozoic rift complex: The Adelaide geosyncline: Geological Society of Australia Special Publication, 16*, 105-128.
- Veizer, J., & Compston, W. (1976). $^{87}\text{Sr}/^{86}\text{Sr}$ in Precambrian carbonates as an index of crustal evolution. *Geochimica et Cosmochimica Acta*, 40(8), 905-914.
[doi:\[https://doi.org/10.1016/0016-7037\\(76\\)90139-3\]\(https://doi.org/10.1016/0016-7037\(76\)90139-3\)](https://doi.org/10.1016/0016-7037(76)90139-3)
- Von der Borch, C. (1980). Evolution of late proterozoic to early paleozoic Adelaide foldbelt, Australia: Comparisons with postpermian rifts and passive margins. *Tectonophysics*, 70(1-2), 115-134.
- Wade, B., Hand, M., & Barovich, K. (2005). Nd isotopic and geochemical constraints on provenance of sedimentary rocks in the eastern Officer Basin, Australia: implications for the duration of the intracratonic Petermann Orogeny. *Journal of the Geological Society*, 162(3), 513-530.
- Wang, X.-C., Li, X.-H., Li, Z.-X., Liu, Y., & Yang, Y.-H. (2010). The Willouran basic province of South Australia: Its relation to the Guibei large igneous province in South China and the breakup of Rodinia. *Lithos*, 119(3), 569-584.
[doi:<https://doi.org/10.1016/j.lithos.2010.08.011>](https://doi.org/10.1016/j.lithos.2010.08.011)
- Wang, X.-C., Li, Z.-X., Li, X.-H., Li, Q.-L., & Zhang, Q.-R. (2011). Geochemical and Hf–Nd isotope data of Nanhua rift sedimentary and volcaniclastic rocks indicate a Neoproterozoic continental flood basalt provenance. *Lithos*, 127(3-4), 427-440.
- Webb, G. E., & Kamber, B. S. (2000). Rare earth elements in Holocene reefal microbialites: a new shallow seawater proxy. *Geochimica et Cosmochimica Acta*, 64(9), 1557-1565.
[doi:\[https://doi.org/10.1016/S0016-7037\\(99\\)00400-7\]\(https://doi.org/10.1016/S0016-7037\(99\)00400-7\)](https://doi.org/10.1016/S0016-7037(99)00400-7)
- White, A. F., & Brantley, S. L. (1995). Chemical weathering rates of silicate minerals; an overview. *Reviews in Mineralogy and Geochemistry*, 31(1), 1-22.
- Zhao, J., McCulloch, M., & Bennett, V. (1992). Sm-Nd and U-Pb zircon isotopic constraints on the provenance of sediments from the Amadeus Basin, central Australia: Evidence for REE fractionation. *Geochimica et Cosmochimica Acta*, 56(3), 921-940.